Spring 2007

Central and peripheral autonomic influences : analysis of cardio-pulmonary dynamics using novel wavelet statistical methods

Anne Marie Petrock
New Jersey Institute of Technology

ABSTRACT

CENTRAL AND PERIPHERAL AUTONOMIC INFLUENCES: ANALYSIS OF CARDIO-PULMONARY DYNAMICS USING NOVEL WAVELET STATISTICAL METHODS

by
Anne Marie Petrock

The development and implementation of novel signal processing techniques, particularly with regard to applications in the clinical environment, is critical to bringing computer-aided diagnoses of disease to reality. One of the most confounding factors in the field of cardiac autonomic response (CAR) research is the influence of the coupling of respiratory oscillations with cardiac oscillations.

This research had three objectives. The first was the assessment of central autonomic influence over heart rate oscillations when the pulmonary system is damaged. The second was to assess the link between peripheral and central autonomic control schema by evaluating the heart rate variability (HRV) of people who were able or unable to adapt to the use of integrated lenses for vision, specifically accommodation, correction (adaptive and non-adaptive presbyopes). The third objective was the development of a wavelet-based toolset by which the first two objectives could be achieved. The first tool is a wavelet based entropy measure that quantifies the level of information by assessing not only the entropy levels, but also the distribution of the entropy across frequency bands. The second tool is a wavelet source separation (WavS) method used to separate the respiratory component from the cardiac component, thereby allowing for analysis of the dynamics of the cardiac signal without the confounding influence of the respiratory signal that occurs when the body is perturbed.

With regard to hypothesis one, the entropy method was used to separate the COPD study populations with 93% classification accuracy at rest, and with 100% accuracy during exercise. Changes in COPD and control autonomic markers were evident after respiration is removed. Specifically, the LF/HF ratio slightly decreased on average from pre to post reconstruction for controls, increased on average for COPD. In healthy controls, respiration frequency is distributed across multiple bandwidths, causing large decreases in both LF and HF when removed. With respiration effect removed from COPD population, LF dominates autonomic response, indicating that the frequency is concentrated in the HF autonomic region. Decrease in variance of data set increases probability that smaller changes can be detected in values.

The theory set forth in hypothesis two was validated by the quantification of a correlation between peripheral and central autonomic influences, as evidenced by differences in oculomotor adaptability correlating with differences in HRV. Standard Deviation varies with grouping, not with age. Increasing controlled respiration frequencies resulted in adaptive presbyopes and controls displaying similar sympathetic responses, diverging from non-adaptive group. WavS reduced frequency content in ranges concurrent with breathing rate, indicating a robust analysis.

The outcome of hypothesis three was the confirmation that wavelet statistical methods possess significant potential for applications in HRV. Entropy can be used in conjunction with cluster analysis to classify patient populations with high accuracy. Using the WavS analysis, the respiration effect can be removed from HRV data sets, providing new insights into autonomic alterations, both central and peripheral, in disease.

CENTRAL AND PERIPHERAL AUTONOMIC INFLUENCES: ANALYSIS OF CARDIO-PULMONARY DYNAMICS USING NOVEL WAVELET STATISTICAL METHODS

by
Anne Marie Petrock

A Dissertation
Submitted to the Faculty of
New Jersey Institute of Technology
in Partial Fulfillment of the Requirements for the Degree of
Doctor of Philosophy in Biomedical Engineering

Department of Biomedical Engineering

May 2007

APPROVAL PAGE

CENTRAL AND PERIPHERAL AUTONOMIC INFLUENCES: ANALYSIS OF CARDIO-PULMONARY DYNAMICS USING NOVEL WAVELET STATISTICAL METHODS

Dr. Stanley Reisman, Dissertation Advisor — Date
Professor, Department of Biomedical Engineering, NJIT
Professor, Department of Electrical and Computer Engineering, NJIT

Dr. Ronald Rockland, Committee Member — Date
Associate Professor, Department of Biomedical Engineering, NJIT
Associate Dean, Newark College of Engineering, NJIT

Dr. Richard Foulds, Committee Member — Date
Associate Professor, Department of Biomedical Engineering, NJIT

Dr. John Tavantzis, Committee Member — Date
Professor, Department of Mathematics, NJIT

Dr. Ronald DeMeersman, Committee Member — Date
Professor, College of Physicians and Surgeons, Columbia University

Dr. Matthew Bartels, Committee Member — Date
John A. Dewey Associate Professor of Clinical Rehabilitation Medicine
College of Physicians and Surgeons, Columbia University

BIOGRAPHICAL SKETCH

Author: Anne Marie Petrock

Degree: Doctor of Philosophy

Date: May 2007

Undergraduate and Graduate Education:

- Doctor of Philosophy in Biomedical Engineering, New Jersey Institute of Technology, Newark, NJ, 2007
- Master of Science in Biomedical Engineering, New Jersey Institute of Technology, Newark, NJ, 2002
- Bachelor of Science in Electrical Engineering, New Jersey Institute of Technology, Newark, NJ, 1999

Presentations and Publications:

A. M. Petrock.; S. Reisman; T. L. Alvarez. "Vergence Variability: A Key to Understanding Oculomotor Variability?" Proceedings of the International IEEE Engineering in Medicine and Biology Society Annual Meeting, New York, NY. August, 2006.

Anne Marie Petrock. "Biomedical Engineering: A Conduit for Attracting Women into Engineering." Women in Engineering Programs and Advocates Network (WEPAN) National Conference, Pittsburgh, PA. May, 2006.

A. M. Petrock.; Dr. S. Reisman; Dr. I. Dardik. "Total wavelet entropy analysis of cyclic exercise protocol on heart rate variability." Proceedings of the IEEE 30th Annual Northeast Bioengineering Conference. April, 2004.

A. M. Petrock, S. Reisman, I. Dardik. "24-Hour Total Wavelet Entropy Analysis of Cyclic Exercise Protocol." International BioMedical Engineering Society (BMES) Conference, Philadelphia, PA. 2004.

A. Petrock; S. Reisman. "Wavelet analysis of masseter muscle EMG during emotional provocation." Proceedings of IEEE 29th Annual Northeast Bioengineering Conference. 2003.

K. Jayaraman.; S. Reisman.; A. M. Petrock. "Preliminary assessment of the effectiveness of enhanced external counter pulsation on heart rate variability for heart failure

patients." Proceedings of IEEE 29th Annual Northeast Bioengineering Conference. 2003.

A. Petrock; S. Reisman; S. Weiner; A. Siegel. "Wavelet analysis of masseter muscle activity resulting from stimulation of hypothalamic behavioral sites." Proceedings of the IEEE 28th Annual Northeast Bioengineering Conference. 2002.

S. Reisman, I. Dardik, S. Hagberg, M. Rymer, A. Petrock, A. Stuckey. "Controlled Breathing in Parkinson's disease during Cyclic Exercise." 12th International Symposium on the Autonomic Nervous System of the AAS, Palm Springs, CA. October, 2001.

M. Rymer, I. Dardik, S. Reisman, S. Hagberg, A. Petrock. "Cyclic Activation / Relaxation Exercise: Effects on Cardiovascular Dynamics in Patients with Parkinson's Disease." 17th International Puijo Symposium, Kuopio, Finland. 2001.

To Chris and Charlie, who helped me to laugh and stay grounded, and kept me up to date with style and what was pretty while I buried my head in the books.

To Tony, my research assistant and best friend, who answered the phone during those wee hours in the morning when nothing was working, and kept me laughing even in the face of great adversity. You were my rock when I was in hard places and the pillow that I could rest my worried head upon.

To Marissa and Charlize, my little angels: You are my shining light and hope for the future. I can't wait to read *your* dissertation one day!

Most especially, to mom and dad: You supported me when I wanted to be the Easter bunny and the first lady president. From my silly goals to my wildest dreams, thank you for being the rock that I built my world upon. Quicquid laudis haec vitae mundum habet, laus tota tuae est.

ACKNOWLEDGMENT

Particular thanks go to Dr. Stanley Reisman, my advisor, for many years of advice, reassurance and exchange of ideas. The freedom that you gave me to explore my own academic paths, means more than you may ever know. I will always be thankful that BME (in a world of EE) brought me to your door those many years ago. Special thanks to Drs. Ronald Rockland and John Tavantzis for sharing so much of their time and insights with me. Particular thanks to Drs. Matthew Bartels and Ronald DeMeersman for sharing ideas and physiological insights. Finally, great appreciation is extended to Dr. Richard Foulds, who added his expertise and enthusiasm just when I needed it most.

I would like to thank Mrs. Trudy Morse for being such an inspiration. I will always be grateful for her unyielding support of biomedical research and, in particular, her enthusiasm and dedication to NJIT. This work was funded in part by the Malcolm Morse Fellowship, the Vincent DeCaprio Fellowship, the NJ Commission on Higher Education and the National Institutes of Health (NIH).

Thanks to Dr. Rosenberg for being so patient and encouraging as I finished this work. Thanks to Dr. Kane for his tenacity in helping the NJIT scholars get out into the world. Thanks to Mrs. Gonzalez-Lenahan for the knowledge and sanity breaks that she provided, and to Ms. Marlene Masi. Thank you to Ms. Knox at the Women's Center and Dr. Donahue, Mrs. Hulin and Ms. Massey at the Honors College, Ms. Raines and Ms. Clarke at Career Development, Ms. Naporano and Ms. Price in BME, and Ms. Osseiran-Hanna in University Development for supporting me from day one at NJIT. Thanks to my fellow graduate students, particularly my BFF, Bruno, Darnell, Jason and Amanda.

Thanks to my family and friends, particularly to Uncle Bill and Auntie Rose, and to Aunt Maddie, to my NJIT sisters and to Shawnee my forever friend. Thanks for always believing in me, especially when I didn't have the strength to do it for myself.

TABLE OF CONTENTS

TABLE OF CONTENTS
(Continued)

TABLE OF CONTENTS
(Continued)

LIST OF TABLES

LIST OF FIGURES

LIST OF FIGURES
(Continued)

LIST OF FIGURES
(Continued)

CHAPTER 1

INTRODUCTION

1.1 Objective

This research sought to understand how autonomic function changes as a result of disease. The systems investigated are influence by the autonomic nervous system. This chapter will discuss the systems under investigation, and the physiological background of the methods developed and described in chapter three.

This research seeks to clarify cardiac autonomic response in disease and aging by developing new statistical methods. These methods are validated in three ways. First, a model was created to simulate the IIBI signal as a summation of cardiac and respiratory oscillatory signals to test the separation technique at frequencies in the cardiac autonomic range. Once the method is verified in this way, it is applied to clinical data sets in an effort to understand the central autonomic changes in cardio-pulmonary interactions. The first clinical application of the methods was a data set consisting of ECG and respiration signals, for COPD subjects and controls. This application evaluated the *central* autonomic influence of pulmonary changes in disease. The next application was in the analysis of the cardiac autonomic response of a subject population with varying levels of visual adaptability, as measured from their ability to adapt to the use of progressive lenses for a condition called presbyopia. This application evaluated the *peripheral* autonomic influence over the oculomotor system, and how it changes with aging, and combined it with the *central* autonomic influence over heart rate variability to determine how, if at all, the two systems interacted.

There are two signal processing approaches taken in this research. The first aids in the classification of the level of health of Chronic Obstructive Pulmonary Disease patients clinically by the use of information contained within the IIBI signal. This method is a non-linear dynamics approach to quantifying variability via an entropy analysis at each scale in a wavelet analysis, and using that information in a k-means cluster separation. The second enables the assessment of cardiac autonomic response with the influence of the respiration, which confounds the analysis of the underlying neural control patterns, removed. The method is a wavelet based statistical source separation technique that employs the correlation between the respiration and IIBI signals at various frequencies to remove the influence of the respiration from the dynamic cardio-pulmonary signal. The foundation for the development of these methods will be discussed in more detail in Section 2.2.

1.2 Hypotheses

There are three hypotheses being tested in this research. The first is that the central autonomic influence over heart rate variability, as evidenced in cardio-pulmonary interactions, is modulated in pulmonary disease. It was hypothesized that lower levels of entropy and cardiac autonomic markers exist in the COPD population than in the control population.

The second hypothesis is that the peripheral autonomic influence over the visual system is linked to the central autonomic influence over cardio-pulmonary interactions. It was further hypothesized that changes in near vision that occur with age are not due solely to lens crystallization and weakening of the muscles. It was also hypothesized that

lowered visual adaptability would be linked with lowered heart rate variability.

The third hypothesis is that the validation of the first two theories would be facilitated by the development of methods that are based upon wavelet transforms. The third hypothesis consists of the development of two specific tools to aid in the analysis of the data sets described above. This hypothesis consists of two parts:

1) The difference in cardio-pulmonary activity between subject populations may be evidenced in the energy of the heart rate signal at different frequencies, which should be distributed differently for people with different levels of health. Further, this difference in energy can be employed to classify the level of cardio-pulmonary health in a clinical setting. Specifically, the development of a wavelet entropy analysis, coupled with the application of a k-means clustering algorithm, will aid in the computer based diagnosis of level of health in COPD. This method will be referred to as the Wavelet Entropy method.

2) Respiration artifact can be successfully removed from a dynamically changing heart rate variability signal to reveal the cardiac changes that occur with aging and disease. This separation can take place in the frequency domain by employing the correlation of coefficient sets generated by a wavelet transformation as a basis for the separation. The signal, now free from respiration artifact, can then be reconstructed into the time domain. This method will be referred to as the Wavelet Source Separation method.

1.3 Background

All human systems exhibit a certain amount of variability. Among other systems, it is evidenced in the cardiovascular system, in the activation/deactivation of neurotransmitters and receivers resulting in behavioral changes and even in the circadian (day/night) cycle of sleep and wake. Typically manifesting itself as a change in power in a specific frequency range, the level of variability has been observed to be associated with various states of health and disease, ranging from behavioral to neurological to physiological abnormalities. In recent years, there has been an increased effort at

understanding this variability in terms of the amount of information that it can provide [1, 2, 3].

1.3.1 Physiological Research Studies

The term information is used in many ways in engineering. With respect to this research, it is in reference to the level of variability of the system. The level of auto-correlation of the data points in a time series is indicative of the amount of information contained within the signal. At one end of the spectrum, when data are too correlated, they become periodic. This indicates a low level of information within the system, because there is little to no variation from one point to the next and therefore gaining one small sample of data is sufficient to understand the entire system. At the opposite end of the spectrum is data that are not correlated at all, a state that is commonly referred to as noise. Somewhere between these two extremes lies the "healthy level of variability." In this state, there are sufficient interactions occurring within the system being investigated which preclude it from being described by one linear, time-invariant equation, but not enough interactions to preclude the system from being defined by one or a set of equations. While there is still disagreement about the level of correlation at which the signal becomes noise, there is agreement that in any system, a lower level of correlation is indicative of a higher level of variability, and thus, a higher level of information that is available to the researcher regarding the system status. The level of information contained within a signal is directly proportional to the level of complexity within the signal.

Research on physiological systems has begun to acknowledge that although it is

easier to model a system using linear parameters and models, it is not accurate and it is often not appropriate to assume that a physiological system behaves in a linear, stationary manner [4, 5, 6]. The reason for this is that biological systems vary with time. This is an adaptive mechanism which serves to protect the system from damage when environmental conditions change and place stress upon the system. An inability of the system to respond to stress, either real or perceived, is detrimental to the long-term survival of the organism. This inability to adapt is evidenced by depressed or exaggerated variability and complexity in a system [5, 7, 8, 9, 10, 11]. When the variability is too low, the system cannot respond effectively to the perturbation and will fail to provide an adequate level of physiological response over an extended period of time. When the variability is too high, the system overreacts to stresses and cannot recover properly. The problem that exists is that currently, there is little understanding of what is too low and what is too high, only that those states exist. Perhaps if more was known regarding the underlying neural processes that create this variability, it would become more apparent how to use this information as a tool to classify levels of health of a system.

The objective of this work was to investigate autonomic behavior at the system level as evidenced in the coupling of the cardiovascular and pulmonary systems in control and diseased populations, as well as the cardiac autonomic response to ANS stimulation via respiratory changes in an aging population that displayed varying levels of ability to adapt to the use of corrective lenses. Both populations displayed alterations in variability and control scheme at rest as well as with altered input from the respiratory system.

The manner in which this objective was accomplished was twofold. First, a toolset was developed with the express intent of deciphering underlying neural control processes for biological signals. This includes wavelet based entropy analysis combined with a data clustering technique for distinguishing between subject populations which can be employed in a clinical setting. The toolset also includes a wavelet based source separation (WavS) technique that extracts neural response information from stimuli signals, providing control system information that can be compared across subject populations.

The second step is to employ this toolset on clinically relevant data to delineate physiological changes in neural processes that occur during aging and disease. Specifically, it is of interest to understand how cardio-pulmonary interactions are altered with Chronic Obstructive Pulmonry Disease (COPD), a class of lung disease that incorporates emphysema, chronic bronchitis, or a combination of both. Further, it is of interest to determine how the cardiac neural control scheme is altered in the aging visual tracking system before and after the onset of the condition typically referred to as presbyopia, a stiffening of the lens of the eye or a weakening of the muscles that control the curvature of the lens or a combination of both. Presbyopia affects all people as they age, with the onset typically starting at the age of forty.

Traditional signal processing techniques are not appropriate in the analysis of biological signals because they are based upon the assumption that the signal being analyzed is stationary and/or linear, for ease of analysis. In reality the systems generating the signals, in addition to the signals that are generated, are often non-linear, time-varying signals. To account for this, efforts at investigating physiological systems can make the

assumption that the system is a black box [12], an assumption which can often lead to confounding and contradictory results. This research helps to open this box and investigate the activity of the systems within by using time-varying, non-linear analysis methods.

The tools that were developed in this research involve the use of wavelets, either through the analysis of the resultant time series generated as a result of performing a wavelet analysis, or via the use of a wavelet series as the basis of separation in a source separation and subsequent reconstruction technique. The methods were developed based upon a combination of non-linear techniques published in the literature and knowledge of the parameters of the systems to which they will be applied. Calculated wavelet coefficients were be used to determine the amount of information within the system via a Wavelet Entropy study. A cluster analysis of the data was then employed because it was hypothesized that it is possible to separate subjects according to various levels of health and age, based upon the information content, or variability, displayed by the system. This method proved able to classify subjects with greater than 90% accuracy.

The tools developed were used to analyze the neural underpinnings of two physiological systems that are both innervated by the autonomic nervous system. It is well known that cardio-pulmonary interactions are heavily interdependent. The typical measure of interdependence, also believed to be indicative of the level of activity of the parasympathetic nervous system, is respiratory sinus arrhythmia (RSA), which looks at the connection between variations in the heart rate and the respiration cycle. Currently, the gold standard method used in research of this phenomenon is limited to a Fourier analysis of power in the frequency range of 0.14 – 0.4 Hz [5, 13].

The neural control mechanisms that determine how the two systems are coupled and the control signal of the cardiac system remain unclear, as the gold standard seeks only to quantify, not specify, the level of activity resulting from stimulation. This research employs respiratory and cardiac data from populations that are healthy and also populations suffering from various degrees of Chronic Obstructive Pulmonary Disease (COPD). Using these data, the methods proposed in this research will attempt to remove the respiratory signal from heart beat fluctuations using a blind source separation technique. This should enable fuller analysis of the neural control signal that is present, since it is believed that the fluctuations in the heart rate signal are a result of the interaction of the branches of the autonomic nervous system and the respiratory system. It is proposed that this technique will enable investigation of changes that occur in disease and aging, particularly with regard to the neural input to the heart when the lungs are damaged and with respect to populations with decreased adaptability evidenced in other systems influenced by the autonomic nervous system. As will be seen, the signals change in amplitude, phase and frequency with various stimulations and levels of health.

The results of the information analysis were effectively implemented to objectively categorize varying levels of health within the disease population. It also validates variability theory by setting different levels of variability for health and disease. In an effort to investigate the influence of the autonomic nervous system (ANS) on the body, activity in the cardio-pulmonary system, known to be influenced by the activity of the two branches of the ANS, will be investigated simultaneously. It was hypothesized that the two systems will display similar changes in disease. The method employed to investigate whether there are cardiac differences in apparently healthy subjects who are

able to adapt to visual tasks is a standard controlled breathing task. This experiment is significant because there have not been experiments that specifically examine system level interactions of the ANS. Studies of the ANS input to the visual system are not reported in the literature, although ANS input to the cardiovascular system has been reported extensively. This study builds upon a vast pool of knowledge of autonomic activity in one physiological area to understand farther reaching implications of the system to indicate that the physiological variability that has been observed and attributed to the interacting branches of the ANS may influence the levels of adaptability in systems other than the cardio-pulmonary system. The findings of this study suggest that cardiac autonomic response differences may be measurable, even in apparently healthy individuals, when investigating adaptability in other systems influenced by the autonomic nervous system.

Controlled breathing was performed by having the subjects follow a light emitting diode (LED) display placed in a dark room, such that the LEDs were placed parallel to their line of sight. The subjects were instructed to control their breathing to match inspiration to the lights on the LED display when they illuminate in the direction toward the subjects, and expiration to match the outward travel of the LED display. The electrocardiogram (ECG) and respiration signals were be recorded to investigate the cardio-pulmonary interactions. In order to appreciate why this work is important, it is necessary to understand what is known about the physiological systems discussed above, as well as the changes that are known to occur in the systems with disease and aging. There is a vast amount of knowledge of the system and diseases that affect it that exists, and yet neural influence remains largely a mystery. Chapter two discusses the systems,

changes that occur in them with aging and disease, and the methods that are proposed to investigate the ANS activity.

1.3.2 Signal Processing Research Studies

The wavelet entropy analysis applied in this research was applied by Kowalski, et al., in an effort to determine the classical and quantum interface of particles. As the system consists of coupled oscillations, the wavelet entropy method was employed to determine if the change from classical to quantum particle behavior could be detected using the information level contained within specific bandwidths [54]. This application was significant because it attempted to quantify non-linear coupled interactions using wavelet entropy, and was the basis for the application of the method in this research.

The wavelet entropy approach has also been employed in physiological applications such as scalp electroencephalogram (EEG) analysis for detection and analysis of seizures, event-related potential derived from the EEG (ERP), using the electrocardiogram (ECG) to differentiate normal from ischemic episodes, and cardiac valve disease analysis [96, 98, 99, 100]. It has not been used to classify patient populations in an effort to augment clinical toolsets, as is done in this research.

Some of the earliest applications of wavelets were for denoising and compression of data, and those applications continue to be prevalent in the literature [111, 110]. This research employed the theory of wavelet denoising with a priori knowledge of the noise signal, which in this case is the respiration influence in the interbeat interval. The influence of respiration on the HRV signal has been a confound in research and has been investigated [104, 105, 108, 109]. Barbieri's group investigated the use of time-varying spectral analysis to quantify continuous respiration and baroreflex influences of heart

rate. This group was able to model the influence of respiration, but not to quantify the underlying dynamics of the physiology. Byrne, et al. quantified RSA using a peak-valley estimator, which did not have good time resolution. This resulted in errors in the analysis when short time-periods were being investigated, or if analysis of transient episodes was required. Of note is the finding by Min that the LF and LF/HF ratios were elevated in subjects with hypoxia. The finding is in agreement with the findings regarding the COPD population in this research, which found that after removal of respiration the LF content was higher in COPD than control subjects, driving the LF/HF ratio higher after the analysis. Further, in healthy subjects, LF/HF ratio was lower after removal of respiration due to the removal of low frequency content as well as high frequency content. Nagata, et al. used neural networks to observe that sympathetic activity dominates during vigorous conditions, while 19 markers of general autonomic activity declined during fatigue. The question remains, however, whether the increase in sympathetic activity was respiration mediated.

Methods to derive and quantify the respiration signal based upon ECG and/or blood pressure waveforms have been presented, but methods to remove the influence of respiration from the IIBI signal are limited [103, 106, 107, 112]. DeMeersman et al. derived a method of estimating respiratory information from the pulse signal. This method quantified, rather than using as a basis for extraction, the respiration signal. As a first phase of analysis, when only the pulse information is available but not the respiration data, this method may be used in conjunction with the separation method developed in this research. Yildiz et al. developed a model that assessed respiratory influence on HRV. Significantly, as with Min's finding, the model analysis derived

significant influence of respiration over the HF peak, but also plays an important role in the genesis of the LF activity. The group also suggests that LF/HF ratio may not be a suiTable measurement of sympatho-vagal tone unless there is first a respiration correction performed in the HRV data.

Time-frequency methods have successfully been employed to perform blind-source separation of signals [115, 116]. Belouchrani and Amin developed an algorithm to remove noise from signals. The basis for their work was to employ the distribution of noise in the time-frequency domain, and the local frequency activity the source signal to remove the noise from the signal. In the case of HRV analyses, the "noise" is a continuous signal throughout the course of the entire signal, with spectral power in the same region as the signal of interest. Zhang and Amin use time-frequency distributions to whiten the signals and for subsequent separation of the source signals. The limitation is that the time-frequency distributions of each of the signals must have disjoint distributions. In the WavS method, the similarity of the time-frequency distributions is exploited to separate the two sources.

1.4 Significant Contributions of this Research

With regard to central autonomic pathways, evidence was presented that the removal of respiration does not remove the entire variability from the signal. Further, cardio-pulmonary correlation in controls is measurably different from that of COPD subjects, evidenced by different minimum requirements for correlation required to effectively separate the respiration from the heart rate variability signal. The level of complexity in the HRV signal is also distributed differently in COPD than in the control population.

The distribution of the complexity in specific frequencies is significant during exercise, while the actual entropy values are the significant components employed to distinguish between COPD and control populations at rest.

With regard to the peripheral and central autonomic link, several key findings of this research goal exist. First, the presbyopic group unable to adapt to the use of lenses exhibited different HF content than the adaptive presbyopic and control groups. In addition, the non-adaptive presbyopic group exhibited lowered levels of heart rate variability, as evidenced by standard deviation and HRV markers of HF, LF and LF/HF ratio, in comparison to the control and adaptive presbyopic groups.

Finally, wavelet statistical methods possess significant potential in applications to cardiac autonomic function. The wavelet entropy method was able to classify patient populations with classification rates of 93% and 100% for resting and exercising populations, respectively. With regard to wavelet source separation, the potential of this method to delineate autonomic modification with disease is very significant. The model indicated a 0.9988 correlation between the original subcomponent of interest and the signal that the WavS program extracted. The presbyopic data, which were controlled to three different breathing rates, resulted in decreased low frequency HRV marker when breathing at 8 breaths/min, and decreased high frequency HRV markers when breathing at 12 and 16 breaths. This validates the method clinically due to the removal of spectral content relative to the breathing influence that was created. The COPD study yielded interesting results, which point to other mechanisms underlying the variability in the

timing of successive heart beats. This information was confounded previously by respiration. The WavS holds significant potential for future research, in cases where the influence of respiration is unclear.

CHAPTER 2

BACKGROUND

This research seeks to understand how autonomic function changes as a result of disease. The systems investigated are influence by the autonomic nervous system. This chapter will discuss the systems under investigation, and the physiological background of the methods developed and described in chapter three.

This research seeks to clarify cardiac autonomic response in disease and aging by developing new statistical methods. These methods are tested in three ways. First, a model was created to simulate the IIBI signal as a summation of cardiac and respiratory oscillatory signals to test the separation technique at frequencies in the cardiac autonomic range. Next, the methods were applied to the clinically obtained data, consisting of ECG and respiration signals, for COPD subjects and controls. Finally, the methods were applied to analyze the cardiac autonomic response of a subject population with varying levels of visual adaptability, as measured from their ability to adapt to the use of progressive lenses for a condition called presbyopia, which will be discussed more fully in Section 2.1.

There are two signal processing approaches taken in this research. The first aids in the classification of the level of health of Chronic Obstructive Pulmonary Disease patients clinically by the use of information contained within the IIBI signal. This method is a non-linear dynamics approach to quantifying variability via an entropy analysis at each scale in a wavelet analysis, and using that information in a cluster separation. The second enables the assessment of cardiac autonomic response with the influence of the respiration, which confounds the analysis of the underlying neural

control patterns, removed. It does this by the development of wavelet-based statistical measures. The next method is a wavelet based source separation technique that employs the correlation between the respiration and IIBI signals at various frequencies to remove the influence of the respiration from the cardiac autonomic signal. The foundation for the development of these methods will be discussed in more detail in Section 2.2.

2.1 Physiological Background

2.1.1 The Nervous System

The nervous system is affected by environmental conditions, both real and perceived, and affects all physiological and emotional systems of the body. There are two branches of the nervous system that are interdependent. One branch, the Central Nervous System (CNS), is composed of the brain and the spinal cord. The other branch is called the Peripheral Nervous System (PNS). This branch is composed of electrically conductive cells (nerves) that connect the CNS to the remaining organs and tissues of the body.

The PNS consists of 43 pairs of nerves, distinguished as twelve pairs of cranial nerves and 31 pairs of spinal nerves. The scope of this research is interested in the neuromotor signals carried on two cranial nerves: the Oculomotor (III) and Vagus (X). As the name might suggest, the Oculomotor nerve influences the motor control of the muscles that move the eye. The Vagus nerve has an influence over the activity of the heart, among other organs, although for the scope of this research, the Vagal influence over the cardio-pulmonary activity is of significance. The influence of both cranial nerves with reference to specific systems under investigation is discussed later in this chapter.

The PNS is comprised of two parts: the afferent division and the efferent division. The nerves leaving the CNS are part of the efferent division. They carry the commands from the CNS to the target, or effector, organs. The afferent division carries sensory information from the effector organs back to the CNS for processing and resultant adjustment of systems to maintain homeostasis, the relative equilibrium of the internal environment. Table 2.1 illustrates the role of the afferent and efferent nerve fibers of the cranial nerves mentioned above.

Table 2.1 Afferent and Efferent branches of Cranial Nerves III and X

III. Oculomotor Nerve		X. Vagus Nerve	
Afferent	Efferent	Afferent	Efferent
Transmit information from receptors in muscles	Innervate muscles that move eyeball up, down, medially, as well as muscles that constrict pupil & alter lens for near/far vision	Transmit information from receptors in thorax and abdomen	Innervate muscles of pharynx and larynx, as well as muscle and glands of thorax and abdomen

The efferent division of the PNS is composed of two systems: the Somatic Nervous System and the Autonomic Nervous System (ANS). The primary difference between the two types of systems in this division is based upon the type of tissue that they innervate and how they innervate it. The somatic nervous system innervates skeletal muscle and can only perform excitatory stimulation. The ANS innervates smooth and cardiac muscle cells, glands and GI neurons and can carry either an inhibitory or an excitatory stimulus. Efferent innervation of most tissue other than skeletal muscle is carried out by the ANS. The ANS is further subdivided into three parts: the Sympathetic

branch, the Parasympathetic branch and the Enteric branch. Figure 2.1 reflects the sympathetic and parasympathetic branches of the ANS and identifies effector organs. Note the difference in exit points for the nerves in both branches of the ANS as they leave from the CNS. The parasympathetic branch leaves from the brainstem and sacral Section of the spinal cord, while the sympathetic branch exits from the CNS in the remaining Sections. Although the two branches innervate many of the same systems, they receive their commands from very different locations within the central nervous system. In addition, the physiological roles of the two branches are dramatically different.

The sympathetic nervous system serves as an excitatory pathway for the response to a stressful situation while the parasympathetic branch acts as an inhibitory pathway to return the system to normal operation after the stress has passed. The interaction of the two branches creates quite a bit of variability within the system and results in what has been termed "tone." It is this interaction of both branches that enables the body to respond to quickly changing environmental conditions. Research has shown that the more these two systems interact, generating larger variations in activity, the better able the system is to respond to changing external conditions. In essence, the research has indicated that the stronger the give and take interaction is between the two systems, the stronger the ability to adapt to changing conditions. Note that the cardiac, respiratory and visual systems are innervated by both branches of the ANS (refer to Figure 2.1 and Table 2.2).

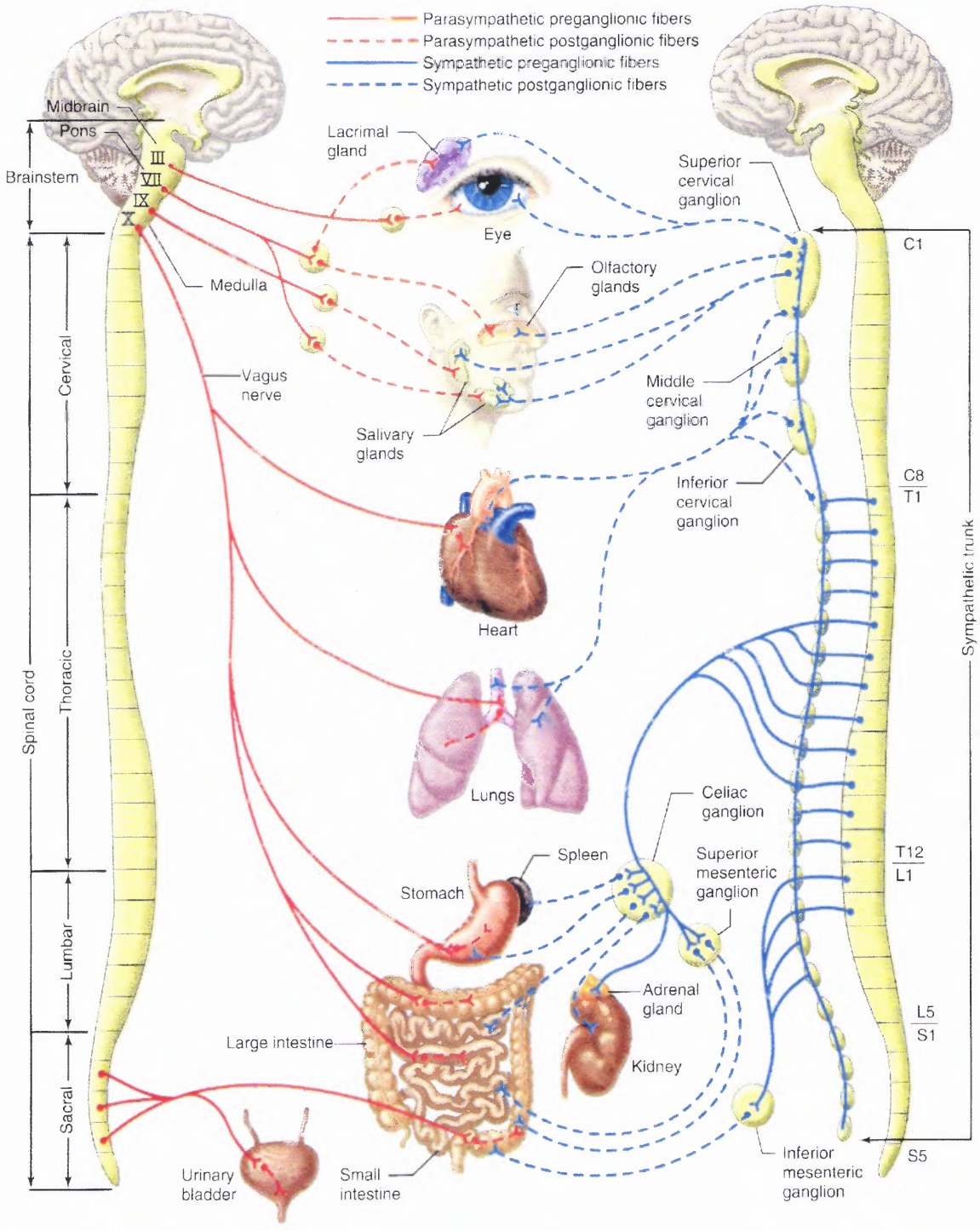

Figure 2.1 Parasympathetic (left) and Sympathetic (right) branches of the ANS, and effector organs.

Source: Vander, Human Physiology, 8th ed. 2001

The scope of this research involves both the Sympathetic and Parasympathetic branches of the ANS. It is hypothesized that the proposed methods will provide a deeper understanding of the specific control schemes of the aforementioned two branches of the ANS by building upon the currently accepted theories of ANS impact on cardio-pulmonary dynamics of healthy and diseased subject populations, which will be discussed in further detail later in this chapter. In addition, the research will seek to identify neuromotor control schemes from Cranial Nerve III and how it is impacted by aging. Table 2.2 outlines the sympathetic and parasympathetic influences on the effector organs of the eyes, heart and lungs. Although the proposed methods will be applied to

Table 2.2 ANS Interaction with Specific Organs Relative to Research

Effector organ	**Receptor Type**	**Sympathetic Effect**	**Parasympathetic Effect**
Eyes			
Iris Muscles	Alpha	Contracts Radial muscle (dilates pupil)	Contracts sphincter muscle (contracts pupil)
Cilliary Muscle	Beta	Relaxes muscle (flattens lens for far vision)	Contracts muscle (increases lens curvature for near vision)
Heart			
SA Node	Beta	Increase heart rate	Decrease heart rate
Atria	Beta	Increase contractility	Decrease contractility
AV Node	Beta	Increase conduction velocity	Decrease conduction velocity
Ventricles	Beta	Increase contractility	Slightly decrease contractility
Lungs			
Bronchial Muscle	Beta	Relaxes	Contracts
Bronchial Glands	Alpha	Inhibits secretion	Stimulates Contraction
	Beta	Stimulates Secretion	

Source: Vander, Human Physiology, 2001

two distinct physiological systems, it is hypothesized that the tools will be able to delineate heretofore unknown neural control processes and their alteration with disease and aging.

2.1.2 Cardiovascular System

The cardiovascular system is composed of the heart, an electro-mechnical pumping device, and its associated periphery. The periphery, or systemic circulation, consists of a closed system of conduits of various sizes, which serve different purposes. It consists of three components: the arteries, the veins and the capillaries. The lungs have a separate system in which gas exchanges occur. This system is termed the pulmonary circulation, and also consists of arteries, capillaries and veins.

The arteries in the systemic system serve as the pathway through which oxygenated blood is passed from the heart to the body. This system is composed of arteries, which are large diameter highly elastic structures, and arterioles, which are smaller in diameter but are also highly elastic structures. Running parallel to the arteries are the veins. The two systems are connected via capillaries, thin walled structures that are only wide enough to allow one cell to pass through at any given time. Oxygen saturated blood travels through the arterial system and passes through the capillaries. Gas transfer occurs in these structures, which allow the surrounding tissue access to oxygen while absorbing waste products. The waste laden blood then passes to the veins and is returned to the heart to get pumped to the pulmonary system for re-oxygenation via the capillaries in the pulmonary circulation. The heart, then, is the pump that drives the exchange of gasses within the body.

The heart is composed of four chambers, two atria and two ventricles. The left side of the heart is responsible for passing the blood into the periphery. The periphery is composed of the vascular structures that transport the blood through all of the systems of the body, except the lungs. The right chambers of the heart pump the blood into the pulmonary system to be oxygenated in the lungs. The blood enters the respective sides of the heart via the atria and exits via the ventricles. Unoxygenated blood from the periphery enters the right atrium via the superior and inferior vena cavae and is passed into the right ventricle. From the right ventricle, the blood passes to the lungs via the pulmonary arteries. From the lungs, oxygenated blood returns to the heart via the pulmonary veins to the left atrium. The blood then passes to the left ventricle and out to the periphery via the aorta. Figure 2.2 illustrates the anatomical location of these structures within the heart. In a healthy heart, there is a septum which prevents the blood from passing between the left and right sides of the heart. The passage of blood in a healthy heart from the atria to the ventricles occurs in a unidirectional, pulsatile manner.

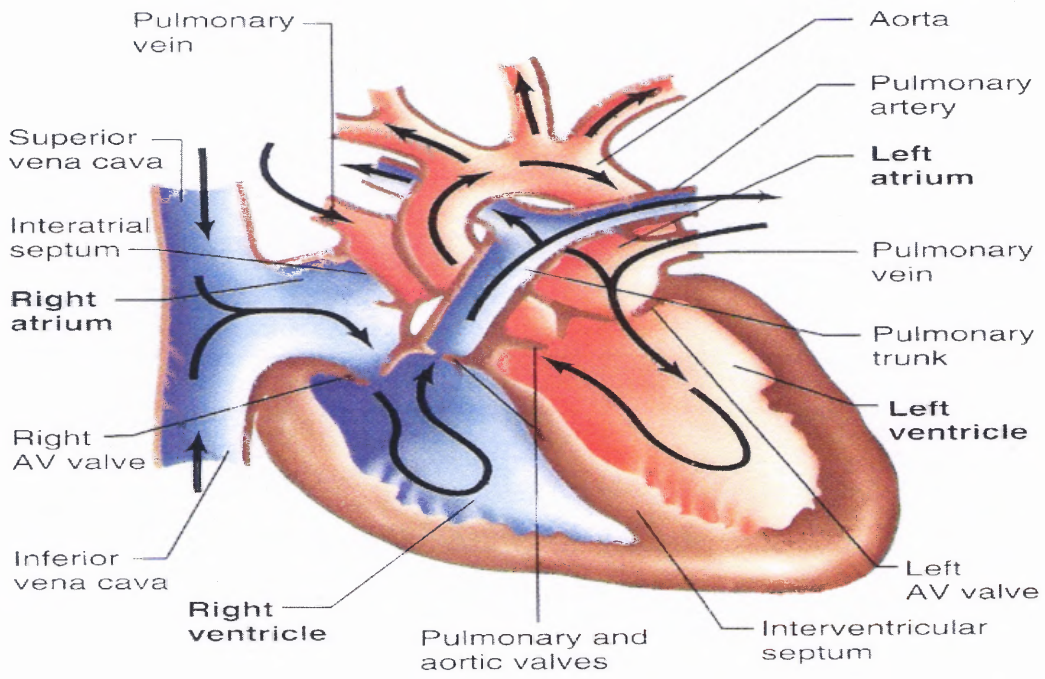

Figure 2.2 The heart.
Source: Vander, et al., Human Physiology, 8th ed. New York: McGraw-Hill, 2001

The heart is capable of acting as an entirely autonomous organ. If necessary, it is capable of spontaneously generate heart beats, assuming that it is in a solution that contains the proper chemical properties. Figure 2.3 illustrates the electrical conduction pathways of the heart. The electrical aspect of the heart beat begins at the sinoatrial (SA) node, the heart's internal pacemaker. This small cluster of cells in the right atrium generates the action potential in the heart that ultimately results in the contraction of the heart. The electrical impulse passes from the SA node to the atrioventricular (AV) node, located at the bottom of the right atrium, just above the tricuspid valve. The AV node serves as a delay mechanism in the conduction of the electrical signal from the atria to the ventricles. This enables the atria to completely empty into the ventricles before the signal is passed to the ventricles, causing them to contract. From the AV node, the signal passes

from the atria to the ventricles via the Bundle of His, located in the Inter-ventricular septum and down through the left and right bundle branches. The bundle branches spread to their respective ventricles, and ultimately terminate at the Purkinje Fibers of each ventricle. It is the action potential on the Fibers that cause the contraction of the ventricles and the subsequent coordinated ejection of blood to the systemic and pulmonary circulation systems that is commonly referred to as the "heartbeat."

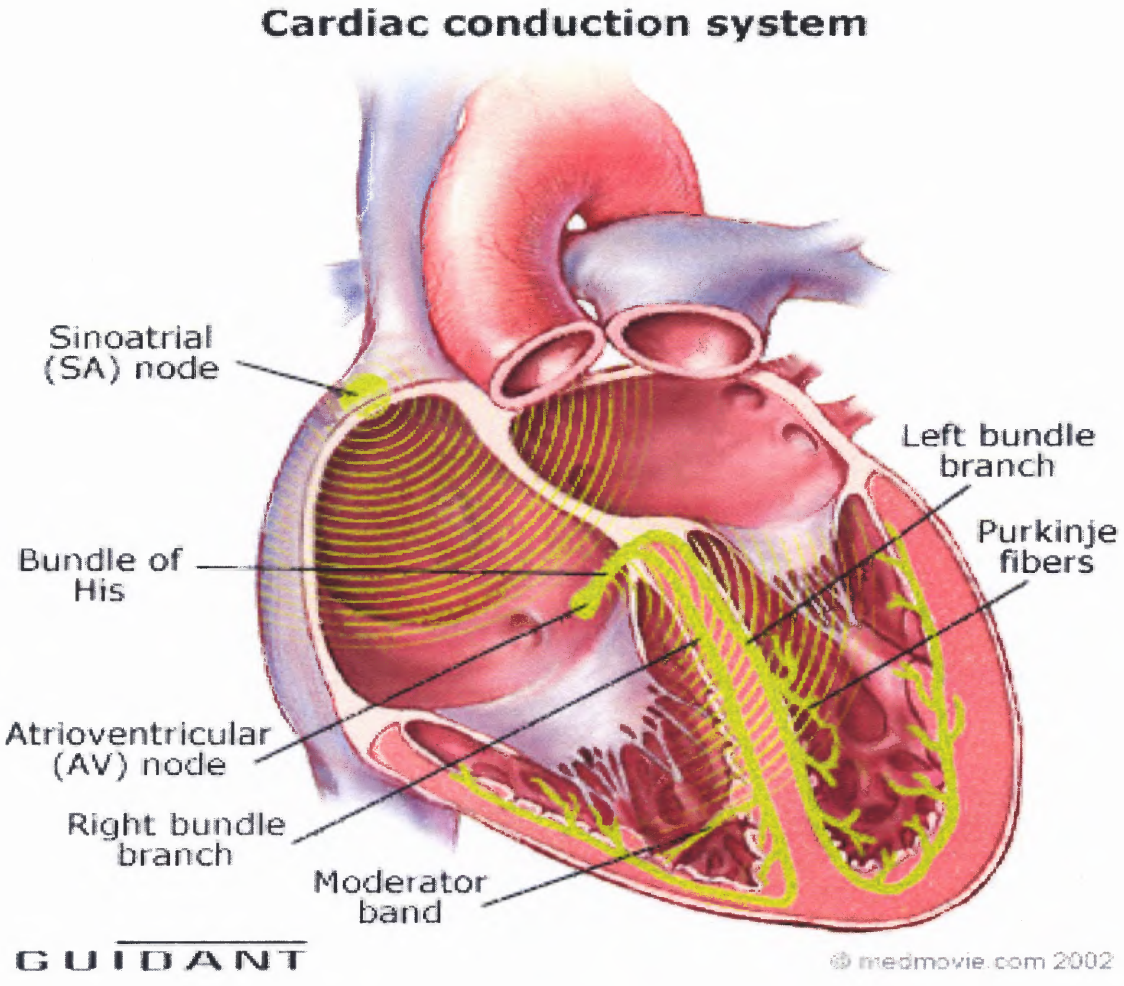

Figure 2.3 Intrinsic conduction system of the heart and associated conduction pathways from the SA node to the ventricles.
Source: http://www.guidant.com/webapp/emarketing/compass/comp.jsp?lev1=resourc&lev2=glossary
Printed 12/1/2005.

However, in addition to internal pacemaking and feedback mechanisms, it is known that the heart is innervated by the sympathetic and parasympathetic branches of the autonomic nervous system. Figure 2.4 indicates the pathways that are employed by the body to control the arterial pressure generated by the heart in a loop that is commonly referred to as the arterial baroreflex. The direct sympathetic inputs (see Figure 2.5) to the cardiac vasculature serve to control the aterial and venal tone, which in turn impacts the blood pressure. This type of control mechanism is generated electrically rather than using mechanoreceptors, as are used in the baroreceptor control loop.

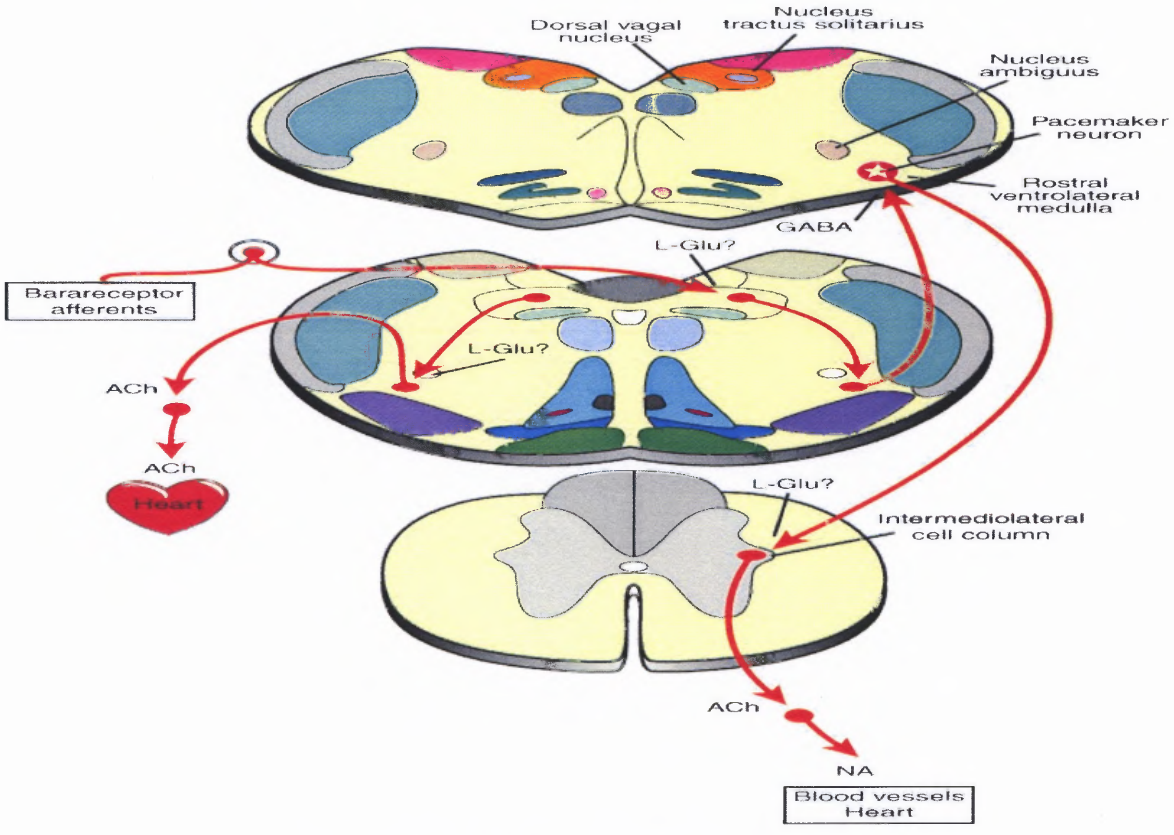

Figure 2.4 Neural pathways for the arterial baroreflex. Primary afferents in the IX and X cranial nerves project to the nucleus tractus solitarii (NTS). As shown on the right, interneurons form sympathetic pathways between the NTS and caudal ventrolateral medulla. Pathways from the NTS to the nucleus ambiguus form the major parasympathetic arm of the reflex.
Source: Guyenet, 1990

The vagus nerve (Nerve X, see Section 2.1.1) acts as the main parasympathetic input to the heart. The Vagus also innervates pulmonary vasculature, aiding in the coordination that is inherent between the cardiac and pulmonary systems. The interaction between mechanoreceptors, chemoreceptors and electrical stimuli from both the sympathetic and parasympathetic branches of the ANS serve to counteract each other to maintain a healthy level of activity, as well as ensuring a healthy response to stressors. When one of the mechanisms does not function properly, it impacts this interchange and lessens the give and take between relaxation and stress responses within the cardiopulmonary system. This, in turn, results in lowered levels of variability that can be recorded non-invasively via the continuous electrocardiogram (ECG) or blood pressure signals.

The heart rate is controlled in many ways. Ways in which it is affected include changes in mechanoreceptor and electrical stimulation. The interaction of respiratory and cardiac pathways is illustrated in Figure 2.5. Note the proximity of cardiac and pulmonary afferents. Changes in oxygen demand result in increased lung volume, which

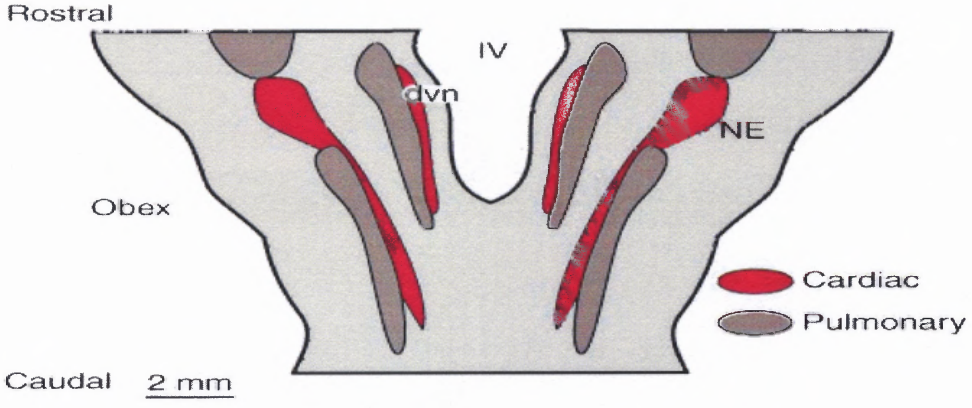

Figure 2.5 Horizontal View of Preganglionic parasympathetic cardiac and pulmonary motoneurons in the nucleus ambiguus (nA) and dorsal motor nucleus of the vagus (dvn)
Source: Jordan, 1995

in turn actives the cardiopulmonary stretch receptors. Changes in the perceived or real states of stress result in sympathetic stimulation of the vasculature, which results in the stimulation of carotid sinus baroreceptors as a result of the changing vascular resistance as part of the baroreceptor control loop. Figure 2.6 displays the inverse relationship that these types of receptors display in terms of changes in mean arterial pressure.

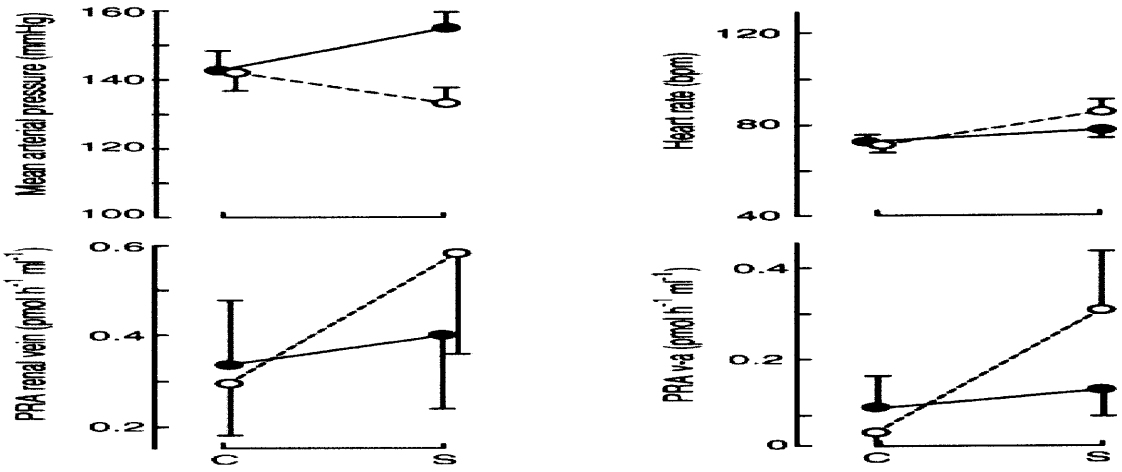

Figure 2.6 Contrasting responses of mean arterial pressure, heart rate, **renal** vein, and renal venous–arterial (v-a) plasma renin activity (PRA) to 5 min of head-up tilt to unload cardiopulmonary stretch receptors (open circles, dashed lines) or positive neck pressure to unload carotid sinus baroreceptors (closed circles, solid lines). Compared to the control state (C), unloading low-pressure cardiopulmonary receptors (S) decreased arterial pressure and reflexly increased heart rate and PRA. Conversely, reduced stimulation of high-pressure arterial baroreceptors reflexly increased blood pressure and heart rate but did not significantly influence PRA.
Source: Mancia et al. 1978

2.1.3 Heart Rate Variability

The rate at which the heart contracts to pump blood (heart rate, or HR) is influenced by many factors. The most significant influence over the timing between successive heart beats is the innervation of the heart by the two branches of the autonomic nervous system

(ANS). The opposing interaction of the two branches of the ANS, the sympathetic and parasympathetic branches, causes the heart rate to increase and decrease, respectively (see Table 2.2). If the heart was allowed to self pace, the sino-atrial (SA) node would cause the heart to beat at a rate of approximately 100 beats/minute at rest. Dominant innervation from the parasympathetic nervous system via the Vagus nerve lowers the resting HR to approximately 60-70 beats/minute. Due to sympathetic innervation, however, the heart rate is the result of constantly interacting branches of the ANS, and constantly increases and decreases, depending on which branch of the ANS dominates the control schema at any given time. Measurement of the variations in heart rate called heart rate variability (HRV) can yield information about the health of the ANS and ultimately, about the overall health of the person [14, 15, 16]. HRV has been called an all-cause mortality indicator due to the absence or depression of the variations present during various classifications of disease, such as chronic obstructive pulmonary disease (COPD), bipolar behavioral disorder, depression, myocardial infarction, AIDS, Parkinson's Disease, diabetes, various types of cancer and more. It typically decreases with age.

The role of respiration in the modulation of heart rate cannot be overlooked. Akselrod, et al. [17] investigated the relationship of the activity in various frequency ranges with the activity of specific branches of the autonomic system. This landmark HRV study found that fluctuations at the respiratory frequency, today referred to as the high frequency content (0.14 through 0.4 Hz), were almost entirely attribuTable to centrally mediated input to the heart rate. In addition, they found that the low frequency content (0.04 through 0.14 Hz) was directly correlated with changes in the musculature

that controls the constriction and dilation of the vasculature 17, 18]. Malliani, et al. later found that sympatho-vagal balance is reflected by the ratio of the power in the low to high frequency ranges. Further, they found that low frequency oscillations increased during sympathetic stimulation and high frequency power increased during parasympathetic, or vagal, stimulation [19, 20]. In 2003, Pyetan, et al. described via a model of cardiac vagal response the small range of values into which heart rate variability and resting sinus arrhythmia fall and suggested that it may be possible to clinically quantify levels of cardiac and or neural disease with great accuracy using the variability parameters [21].

2.1.4 Pulmonary System

The primary function of the pulmonary system is to maintain proper levels of gas in the bloodstream and tissues. The system provides oxygen, eliminates carbon dioxide, regulates the levels of hydrogen ions (i.e., the pH level of the blood), defends against microbes and traps and dissolves blood clots [22]. The pulmonary system is dependant upon several types of receptors to ensure healthy control of the amount of oxygen entering the bloodstream, and the amount of carbon dioxide leaving the body. It does this via a complex set of interacting neural pathways, as shown in Figure 2.7, Ramon Y Cajal's neural model of respiratory control. Respiratory neurons in the solitary tract (C) process signals from pulmonary afferents [K; cell bodies in nodose ganglion (J)] and some blood factor present in local capillaries (A). Descending control signals go to spinal motor neurons (D), innervating the diaphragm (E) or intercostal muscles (F). The diaphragm and intercostal muscles will not contract unless stimulated to do so neurally.

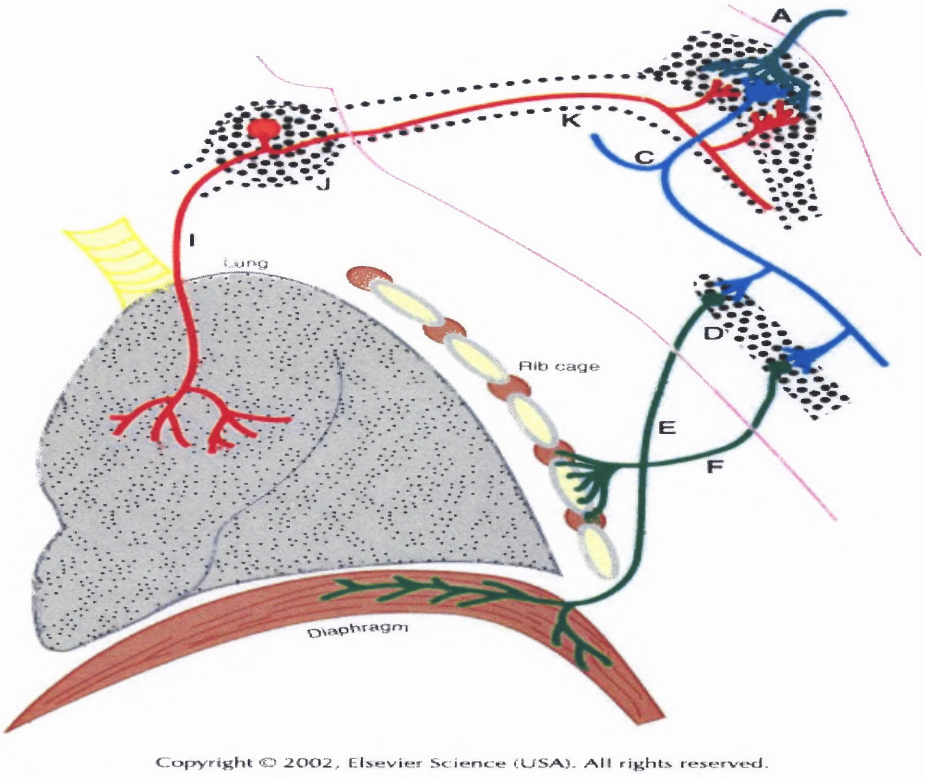

Figure 2.7 Ramon Y Cajal's model for respiratory control.
Source: Squire, 2003.

The control of the inspiration-expiration cycle is mainly organized in the medulla oblongata, which also is the main control center for cardiovascular activity [22]. Expiration is frequently the result of the cessation of motor neuron stimulation of the inspiratory muscles. Neurons called the medullary inspiration neurons discharge during inspiration and are quiescent during expiration. It is this pattern of activation and silence that causes the inspiratory muscles to contract during inspiration and to be at rest during expiration. The inspiratory neurons possess internal pacemakers, not unlike cardiac tissue, which also influence the breathing pattern. The majority of the stimulation of the inspiratory neurons arrives at the medulla from the pons, part of the brain stem located

above the medulla. It is believed that the pons influences the respiratory pattern by inhibiting the action potential received at the medulla.

In addition to input from the pons, pulmonary stretch receptors, located in the smooth-muscle layer of the airway, send inhibitory signals to the medulla via the Hering-Breur inflation reflex (see Figure 2.8). Slowly adapting pulmonary stretch receptor afferents (SAR) arise from receptors located in airway smooth muscle (pulmonary stretch receptors) and cells in the nucleus of the solitary tract (NTS). These neurons are believed to activate E-Dec neurons in the ventral respiratory group (VRG) that inhibit inspiratory neurons, thereby prolonging expiration. The stretch receptors send signals via afferent pulmonary fibers to the medulla when large levels of lung inflation occur. These action potentials received from the mechanical receptors inhibit the medullary inspiratory neurons, and as a result, cause the cessation of inspiration.

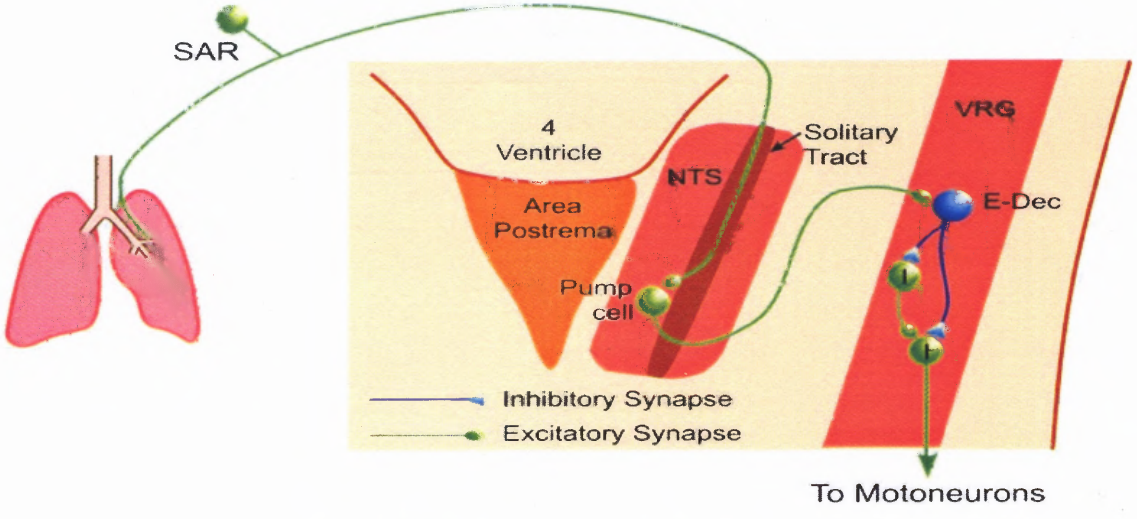

Figure 2.8 Dorsal view of rat brain stem showing hypothesized central pathway for producing reflex termination of inspiration and prolongation of expiration (the Breuer–Hering reflex).
Source: Squire, 2003

Chemoreceptors play a significant role in the formation of a respiratory pattern. Because it is the role of the pulmonary system to maintain proper gas concentrations, it is critical that the system has a means of monitoring the concentrations of P_{O_2}, P_{CO_2} and H^+ in the blood. There exist both central and peripheral chemoreceptors within the pulmonary system.

Central chemoreceptors are located within the medulla. Stimulated by a change in the pH level of the extracellular fluid in that region of the brain, they provide excitatory stimulation of the medullary inspiratory neurons to increase the level of inspiration in an effort to remove excess H^+ ions from the bloodstream. It is believed that the change in pH is the result of elevated P_{CO_2}. The primary means of removing excess concentrations of CO_2 from the bloodstream is via increased exhalation, and small increases in the amount of CO_2 in the bloodstream result in marked increases in inspiration. Pathologies of the respiratory system result in abnormal levels of CO_2 in the bloodstream. A retention of excess CO_2 results in increased ventilation while low concentrations of CO_2 result in inhibition of inspiratory action potentials [23].

Peripheral chemoreceptors are located in either side of the neck at the branches of the carotid artery (carotid bodies) and in the thorax on the aortic arch (aortic bodies). Figure 2.9 illustrates the location of these receptors. The role of these receptors is to monitor arterial blood for increases in arterial H^+ and, conversely, decreases in the concentration of arterial O_2. Either of these conditions trigger an excitatory response on the afferent neurons to the medullary inspiratory neurons.

Figure 2.9 displays the interaction of pathways that influence the respiratory pattern. This pattern, however, can also be controlled voluntarily and can influence the cardiovascular system. Vascular resistance is part of the pulmonary control loop and can be instrumental in altering the cardiovascular response. Figure 2.10 illustrates pathways of the interactions of chemo- and mechano-receptors in terms of the origination of changes in airway resistance and external stimuli.

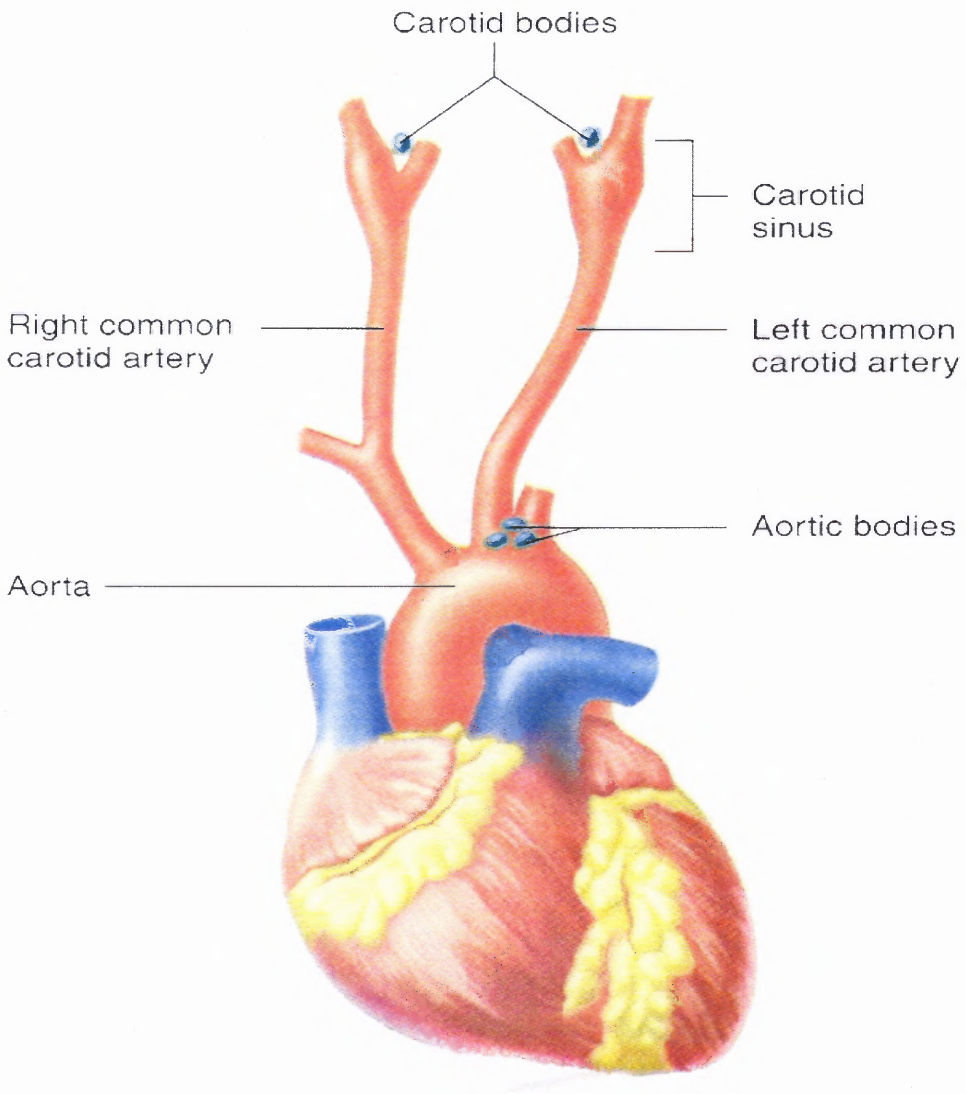

Figure 2.9 Location of Peripheral chemoreceptors, **the** Carotid and Aortic bodies.
Source: Vander, Sherman, Luciano. Human Physiology, 8th ed. 2001

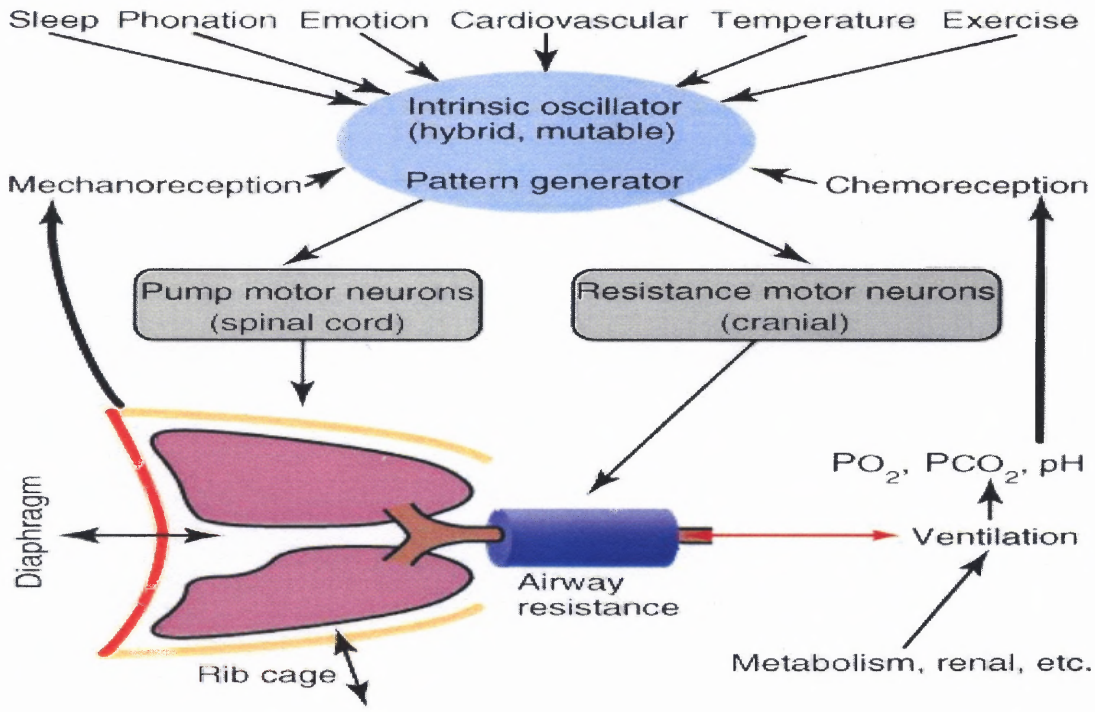

Figure 2.10 Functional organization of CNS control of breathing.

2.1.5 Cardio-Pulmonary Interactions

The cardiac system responds to an increased demand for oxygen by increasing the heart rate to provide the appropriate amount of oxygenated blood to the muscle, coupled with pumping more blood to the lungs for oxygenation. This increase is thought to be triggered in several ways. Figure 2.11 illustrates the response of the cardiac and pulmonary systems to the detection of a low P_{O_2} at the peripheral chemoreceptors. Opening of the veins, or vasodilation, occurs to pass more blood through the vasculature in an attempt to allow more oxygen to pass from the lungs to the tissues. This results in a

drop in blood pressure. Note that the heart rate increases in conjunction with the vasodilation.

Conversely, the Central Nervous System works to increase the blood pressure via vasoconstriction and an increase in heart rate (HR). The responses are a composite of the influence of low arterial P_{O2} on the peripheral chemoreceptors, and their subsequent influence on both respiratory and cardiovascular centers in the brain stem (solid arrows), as well as direct effects of low P_{O2} on the central nervous system (CNS) and effector organs, including the heart and blood vessels (dotted arrows). Note the conflict between the responses of the cardiovascular and respiratory centers in the brain stem, and the CNS response [23].

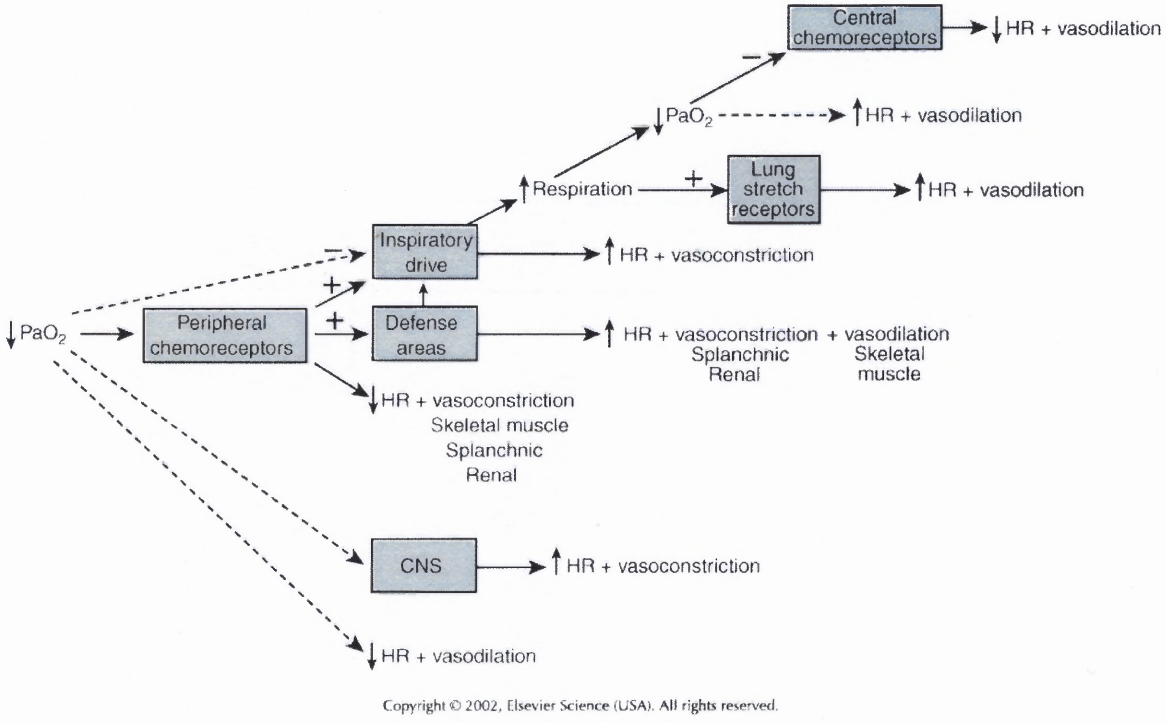

Figure 2.11 Cardiovascular and respiratory responses induced by systemic hypoxia. Note that peripheral chemoreceptors are at the start of the mechanism driving respiration, which ultimately affects central chemoreceptors and baroreceptors to influence HR and vasodilation.

The interaction of heart rate variability (HRV) and respiration is commonly referred to as Respiratory Sinus Arrythmia (RSA) [24]. Varying schools of thought apply to the physiological necessity for the coupling of the two systems, which research suggests "disappears" the farther from rest the systems move. Recent research by Grossman, et al. [25] suggests that normalization for respiratory alterations when the body moves away from a restful state can improve recognition of RSA coupling. A problem with the current methods of detection of the coupling phenomenon is that it is based upon the power of the spectral content in the high frequency range. It is believed that the respiratory rate is the primary influence in the high frequency range. It is further believed that the stimulation of the sympathetic nervous system removes the influence of this system [26]. It is hypothesized that the proposed research will account for changes in respiratory amplitude and frequency by identifying the respiratory signal in the heart rate variability signal and allow for fuller investigation of the signal(s) that link the two systems. This will aid in the understanding of the complex neural activity controlling the RSA. It is further hypothesized that the interaction of the two systems does not "disappear" as the literature suggests, but rather that it changes state and is obscured by larger influences of increased oxygen demand and increased amplitude and frequency of the heart beat.

2.1.6 Chronic Obstructive Pulmonary Disease (COPD)

According to the American Lung Association, COPD is a term used to describe two specific lung diseases: chronic bronchitis, which leads to scar tissue of the respiratory tract, and emphysema. The diseases are characterized by the restriction of normal airflow

due to an obstruction. The two diseases commonly coexist. It is estimated that nearly 16 million Americans suffer from COPD, with another 14 million undiagnosed because they are in the early stages of the disease. Beginning in 2000, the percentage of deaths of women with the disease surpassed the percentage of male mortality as a result of this disease. The main risk factor of COPD is smoking, whether first or second-hand. Additional risk factors include air pollution, second-hand smoke, history of childhood respiratory infections and heredity. Occupational exposure to certain industrial pollutants also increases the odds for COPD. A recent study found that the fraction of COPD attributed to work was estimated as 19.2% overall and 31.1% among never smokers.

Chronic bronchitis is the inflammation and eventual scarring of the lining of the bronchial tubes. When the bronchi are inflamed and/or infected, less air is able to flow to and from the lungs and a heavy mucus or phlegm is coughed up. The condition is defined by the presence of a mucus-producing cough most days of the month, three months of a year for two successive years without other underlying disease to explain the cough.

This inflammation eventually leads to scarring of the lining of the bronchial tubes. Once the bronchial tubes have been irritated over a long period of time, excessive mucus is produced constantly, the lining of the bronchial tubes becomes thickened, an irritating cough develops, and air flow may be hampered, the lungs become scarred. The bronchial tubes then make an ideal breeding place for bacterial infections within the airways, which eventually impedes airflow.

Emphysema begins with the destruction of air sacs (alveoli) in the lungs where oxygen from the air is exchanged for carbon dioxide in the blood. The walls of alveoli are thin and fragile. Damage to them is irreversible and results in permanent "holes" in the

tissues of the lower lungs. As air sacs are destroyed, the lungs are able to transfer less and less oxygen to the bloodstream, causing shortness of breath. The lungs also lose their elasticity, which is important to keep airways open. This results in the patient experiencing great difficulty exhaling.

Emphysema doesn't develop suddenly. It comes on very gradually. Years of exposure to the irritation of tobacco smoke usually precede the development of emphysema. Of the estimated 3.1 million Americans ever diagnosed with emphysema, 95 percent were 45 or older.

The quality of life for a person suffering from COPD diminishes as the disease progresses. At the onset, there is minimal shortness of breath. People with COPD may eventually require supplemental oxygen and may have to rely on mechanical respiratory assistance. A recent American Lung Association survey revealed that half of all COPD patients (51%) say their condition limits their ability to work. It also limits them in normal physical exertion (70%), household chores (56%), social activities (53%), sleeping (50%) and family activities (46%).

None of the existing medications for COPD has been shown to modify the long-term decline in lung function that is the hallmark of this disease. Therefore, the goal of pharmacotherapy for COPD is to provide relief of symptoms and prevent complications and/or progression of the disease with a minimum of side effects. Bronchodilator medications (prescription drugs that relax and open air passages in the lungs) are central to the symptomatic management of COPD. They can be inhaled as aerosol sprays or taken orally. Additional treatment includes antibiotics, oxygen therapy, and systemic glucocorticosteroids. The efficacy of inhaled glucocorticosteroids continues to be under

study, however short-term benefit has been demonstrated. Chronic treatment with systemic steroids involves the risk of serious side effects; therefore these are used mostly for acute exacerbations. Lung volume reduction surgery (LVRS) is recommended in acute cases of COPD to reduce the workload on the lungs [27].

2.1.7 The Visual System

There are two distinct classes of eye movements. These are conjugate and disjunctive. The focus of this research is on the class of movements called vergence eye movements, which are classified as disjunctive because during these movements, the eyes move in either a convergent or divergent manner. This means that they mirror each other in movement, consisting of both eyes either both moving inward in a convergent movement

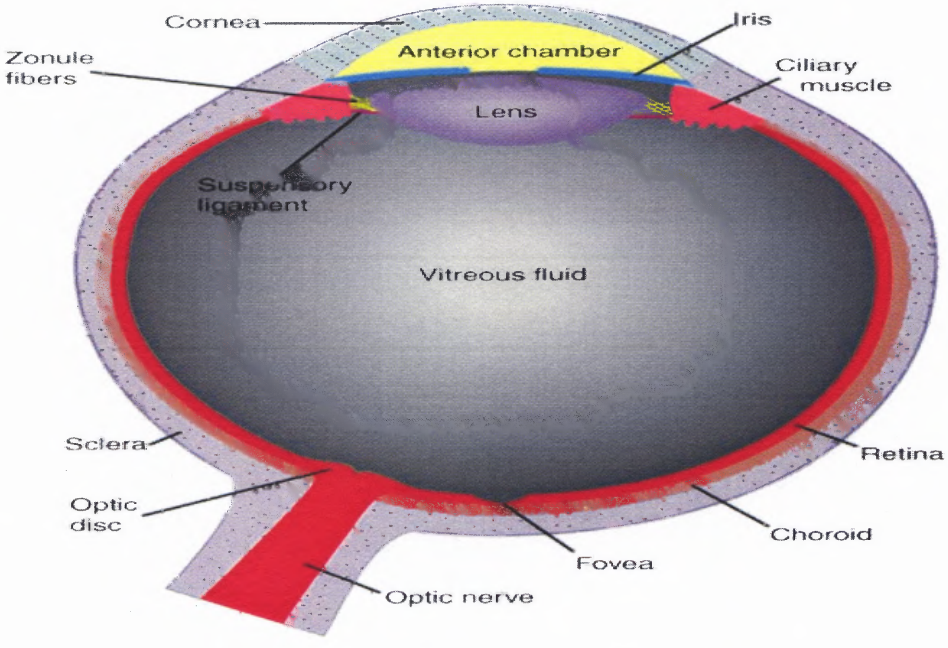

Figure 2.12 Schematic diagram of the human eye. Note the location of the fovea at the opposing side of the eye from the lens and cornea.
Source: Squrie, 2003.

or both moving outward in a divergent movement. The physiology underlying such movements is examined in this Section.

The eye consists of several components which are instrumental in the scheme that determines whether a conjunctive or disjunctive eye movement is initiated. The initiation of a vergence eye movement happens as a result of the interaction of several parts of the eye and brain. The structures are shown in the image of the eye in Figure 2.12, below. An inverted image is focused through the curvature of the cornea and lens and passes through the vitreous fluid and travels to the retina, which is the 0.5 mm thick multi-layered bundle of nerves that surrounds the back of the eye. The retina contains three layers of neural cell bodies and two layers of synapses. The most densely packed region of color receptors, or cones, in the retina occurs in a circular region that is approximately 200 microns in diameter and is referred to as the fovea. The fovea is located in the macula, which is located approximately in the center of the retina near the optic nerve and is responsible for central vision in the human.

The objectives of the cornea, which possesses a curvature that is not pliable, and of the lens, which can adjust its curvature, are to focus the image on the fovea. The lens continuously adjusts the focus of the image by employing the suspensory ligaments, cilliary muscles and zonule fibers to flatten or compress its curvature. When the cilliary muscles contract, the lens flattens and enables the eye to focus on objects that are farther away from the resting position of the eye. The optic disc contains no photoreceptors and thus is not the region of the retina that the lens focuses the image upon. Because of this, the optic disc is described as a blind spot in the eye, but is the beginning of the optic nerve. [23]

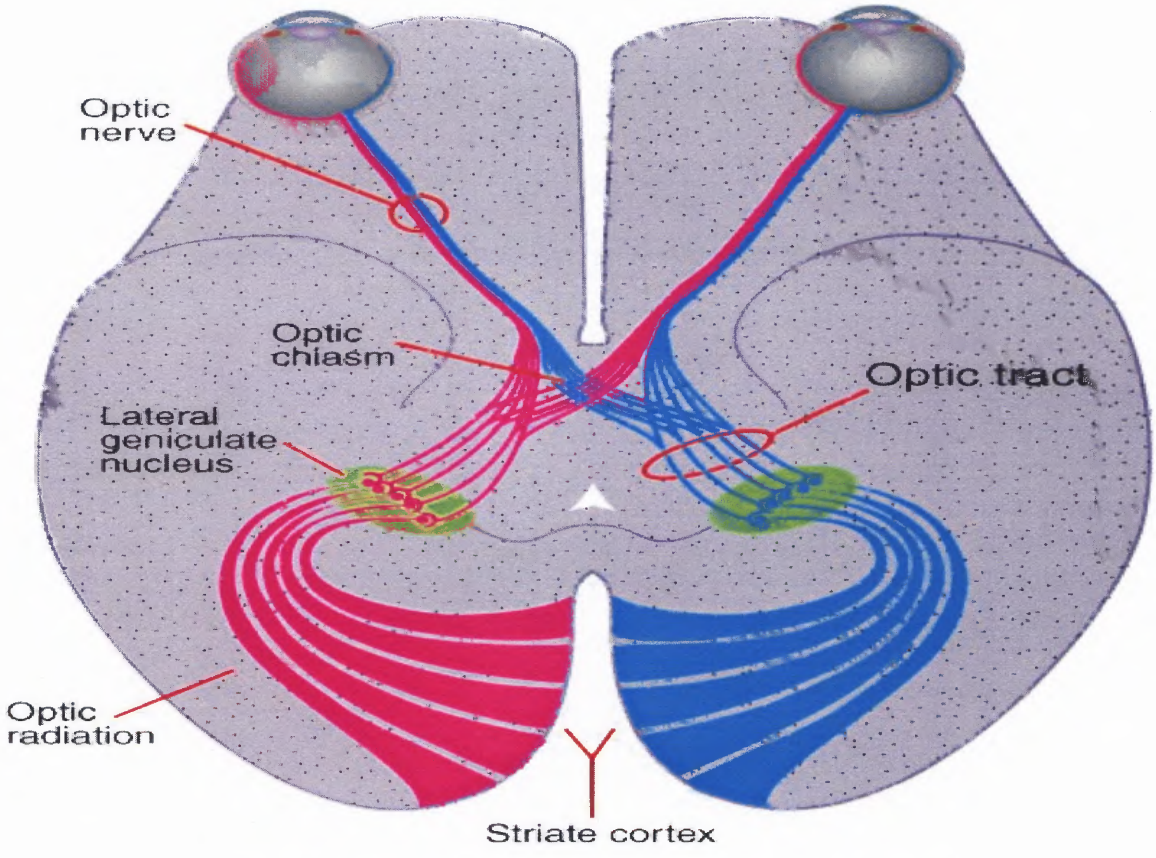

Figure 2.13 The retino-geniculo-cortical pathway in the human. Optic nerve axons from the nasal retina cross at the optic chiasm and join axons from the temporal retina of the other eye. Together, these contralateral and ipsilateral axons make up the optic tract, which projects to the LGN. Each of the six layers of the LGN receives input from only one eye. Axons from the LGN make up the optic radiations, which project to the striate cortex.
Source: Squire, 2003

When the image reaches the retina, the signal travels through the retinal ganglia up the optic nerve to the primary visual cortex, V1, for further processing via the optic nerve, as can be seen in Figure 2.13, below. The image travels to the Lateral Geniculate Nucleus (LGN) via the optic tract once the post-ganglion retinal efferents pass through the optic chiasm.

The component of the visual system that is of relevance in this research involves the control mechanism that determines direction, amplitude and velocity of eye movements in an effort to focus an image on the fovea. This motion is called foveating, and it serves to remove the disparity between what the image actually is and what the eye and brain perceive it to be. There are different directions in which the eye can move. These include left and right, up and down, and torsionally counter-clockwise and clockwise, as shown in Figure 2.14.

A pair of muscles is assigned to facilitate each type of movement, with each member in a pair acting to move the eye in specific opposing directions. The muscle groups are illustrated in Figure 2.15, a cutaway profile view of the eye in its socket. The muscles attach to the eyeball at the sclera, the white outer layer of the eye (refer to Figure 2.12). The muscles differ from skeletal muscles because they are not classified into fast or slow twitch and are not subjected to varying recruitment rules. All muscles actively participate in the initiation and sustaining stages of eye movements.

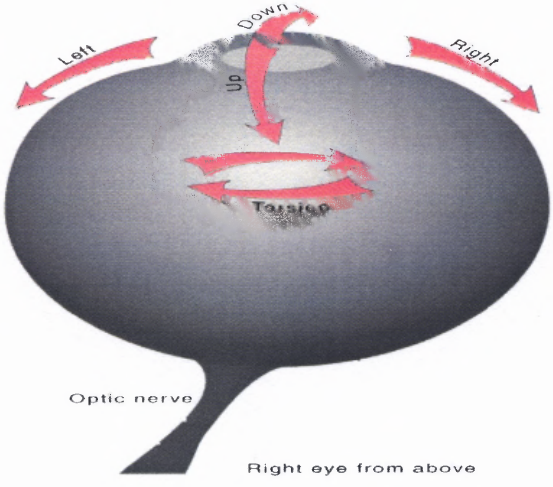

Figure 2.14 Axes of eye rotations. The eye muscles can rotate the eye along three axes; horizontal, vertical, and torsional.
Source: Squire, 2003.

The extraocular muscle pairs are named the medial and lateral rectus muscles, the superior and inferior rectus muscles, and the superior and inferior oblique muscles. The medial and lateral retci are the only pair of extraocular muscles that perform specific inward (adduction) and outward (abduction) movements of the eye. The two other pairs each influence the movement of the eye in combinatorial manners. Because of their location on the eye, the two remaining muscle pairs can influence in a small way movements that are not intuitively part of their function. For example, the oblique eye muscles can influence the upward and the downward movement of the eye, while the superior and inferior recti can influence the torsional movement of the eye.

The muscles which surround the eye, also referred to as the extraocular muscles, are moved according to control signals that are sent from the brain to the eye via three

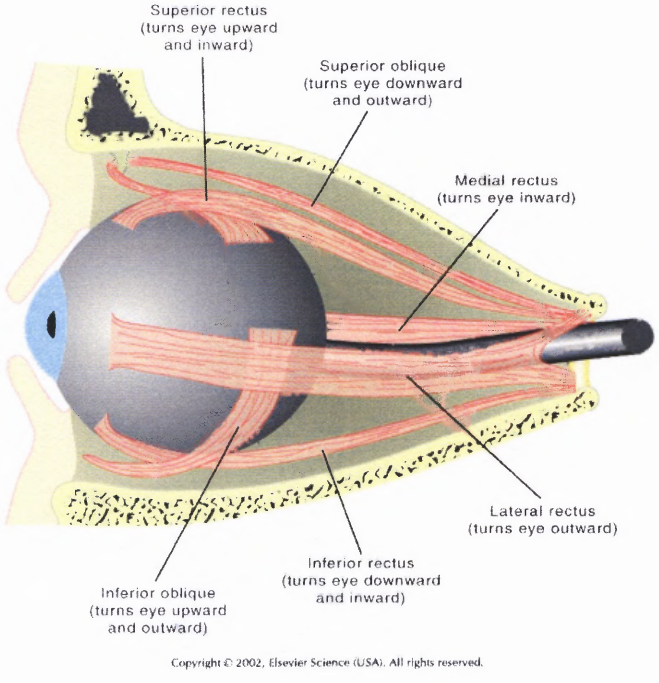

Figure 2.15 Muscles of the eye. Six muscles, arranged in three pairs, control the movements of the eye as shown here in a cutaway view of the eye in its socket, or orbit. The grey chord exiting the back of the eye socket is the optic nerve.
Source: Squire, 2003.

nerves which innervate the three muscle pairs. The nerves have their origin in the brainstem. The nerves are referred to as the oculomotor nerves due to their influence over the movement of the ocular system. Gray's Anatomy depicts the dissected eye, with the Section of the eye muscle and relevant nerves shown as they exist in the human eye socket. Figure 2.16, the dissected eye, is shown below. As can be seen, the oculomotor nerve, which is also referred to as cranial nerve number III, has two branches, the

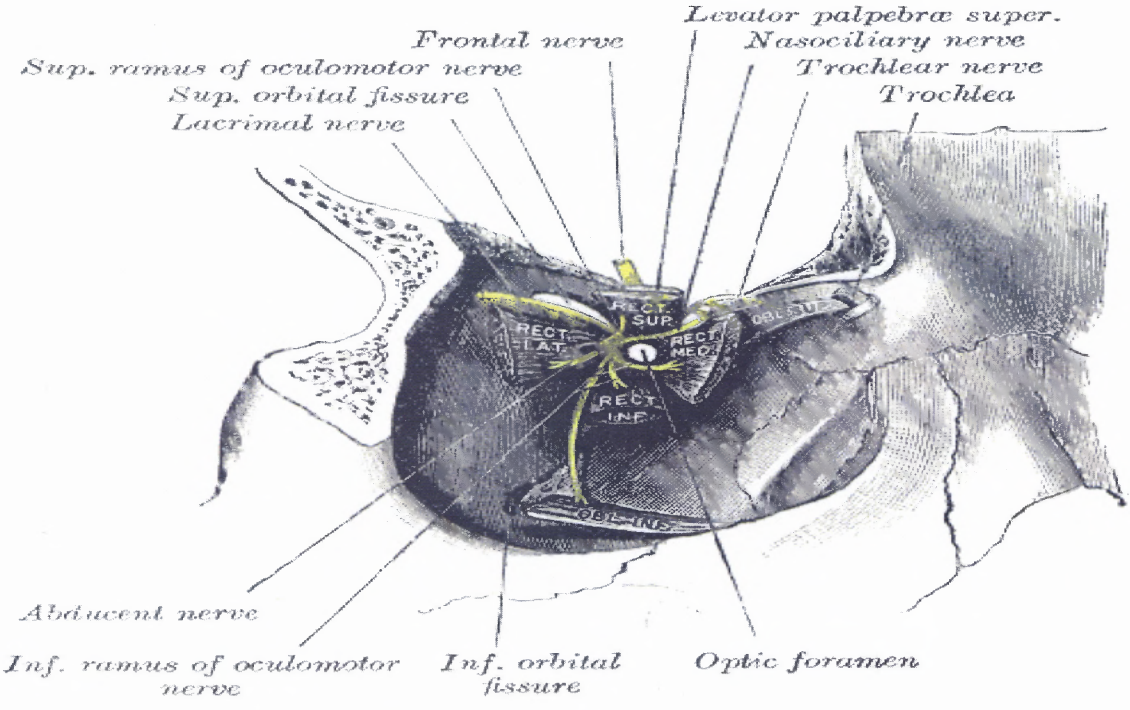

Figure 2.16 Gray's Anatomy *Dissection of Eye Muscles and Nerves* to display interconnection of each.
Source: education.yahoo.com, printed Dec. 2005.

superior and inferior rami, which innervate the eye muscles. Of all three oculomotor nerves, this nerve innervates the largest number of extraocular muscles, in addition to exerting control over the muscles that raise the eyelid, muscles that constrict the pupil and alter the curvature of the lens via parasympathetic fibers contained in the oculomotor

nerve bundle. This nerve controls the inferior oblique, the inferior and superior recti, and the medial rectus extraocular muscles. The oculomotor nerve has its root in the superior colliculus of the midbrain. The trochlear nerve, also referred to as the IV cranial nerve, innervates the superior oblique, which has its origin in the inferior colliculus of the midbrain. Cranial nerve VI, the abducens nerve, innervates the lateral rectus and originates from the fourth ventricle, in the pons.

Vergence eye movements are the only eye movements in which the two eyes are not yoked together. This special circumstance requires that special neural circuitry be employed to control this type of movement. German scientist Ewald Hering proposed that there are in fact two physiologically distinct neural pathways that are responsible for smooth pursuit and saccadic eye movements versus the pathway of vergence movements.

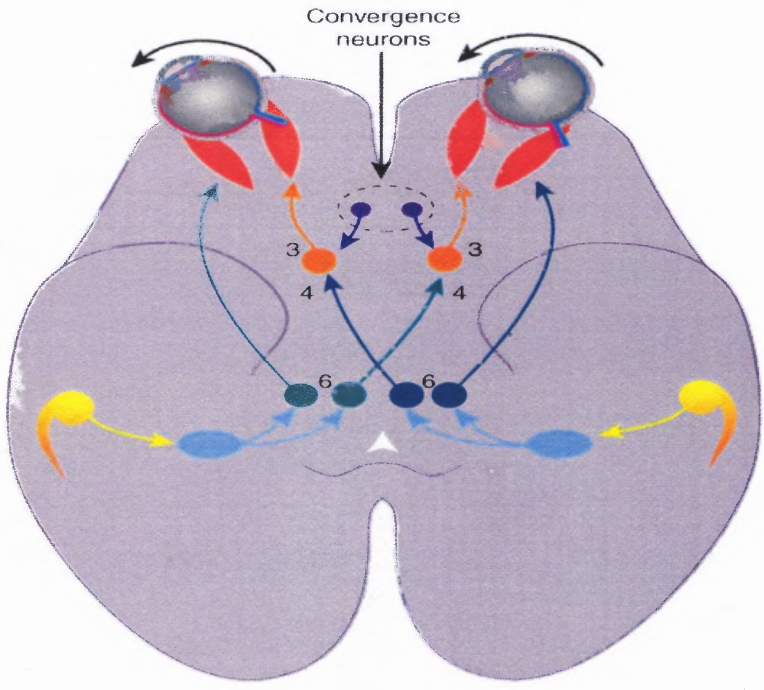

Figure 2.17 Oculomotor, trochlear and abducens illustrated by cranial nerve number (3, 4 and 6, respectively).
Source: Squire, 2003.

It is the intent of this research to better understand the neural underpinnings of such movements. Figure 2.17 illustrates the neural pathways involved in vergence eye movements. Note the locations in the brain of the oculomotor neurons, cranial nerves three, four and six. There exists an additional pathway in the neural processing of vergence movements, indicated by the blue arrows in the center of the image, which is under investigation. There are theories and research that have shown that there exist standard control system processing pathways between the eye and the brain which dictate eye movements.

As with any feedback control system, the brain generates error signals upon which the eye movement is based. The eye is then moved to minimize the error signal. There are four known types of vergence motor error signals. These are accomodation, binocular or retinal disparity, proximal vergence and tonic errors.

The accommodation error occurs when the eye tries to accommodate for, or adapt to, differences in distance to an image, resulting in a blur effect. This occurs when the eye must shift the gaze to adapt to a different location of the target, either nearer or farther. To adjust, the cilliary muscles either contract or relax to change the shape of the lens (refer to Figure 2.12), which in turn focuses the light image that enters the eye and reaches the fovea. This information is then used to compute the proximal vergence error.

The human visual system is binocular. This means that there are two eyes that work in conjunction as the sensors that send the image that reaches the brain for further processing. When a target appears in a location that causes it to strike the retina differently in each eye, there is a binocular disparity, or a difference between the position of each eye relative to the other. This stimulates one or both eyes to foveate, or move to

a new position in which the target strikes the fovea of each eye and is referred to as binocular disparity. It is the error that accounts for depth perception and is responsible for the majority of disjunctive eye movements.

Proximal vergence errors are generated when accommodation errors occur that force the brain to reposition the eye to adjust for modified distances to targets. This error uses as its sensor a monocular system in which the depth sensing is based upon cognitive activity. The image is pre-processed, in a sense, to determine if the perceived depth is correct. This type of error is not based purely upon what is detected, but rather what is interpreted to exist.

Tonic error is the position of the human eye at optical infinity. This means that if the subject is in complete darkness, with no target to gaze upon, the eye would converge inactively at a certain angle. In humans, this position is located at about three degrees of convergence.

Angle of convergence is depicted in Figure 2.18. This term refers to the angle to which the eye is turned inward to focus upon an image. Note that in near convergence, the angle is more acute than it is in far convergence eye positioning. When moving from a closer target to a farther target, the eyes move outward and the resultant angle is more acute than the original. This movement is referred to as a divergent movement. When the eyes change focus from a far target to a near target, the eyes move inward causing the angle to increase. This movement results in what is termed a convergent movement.

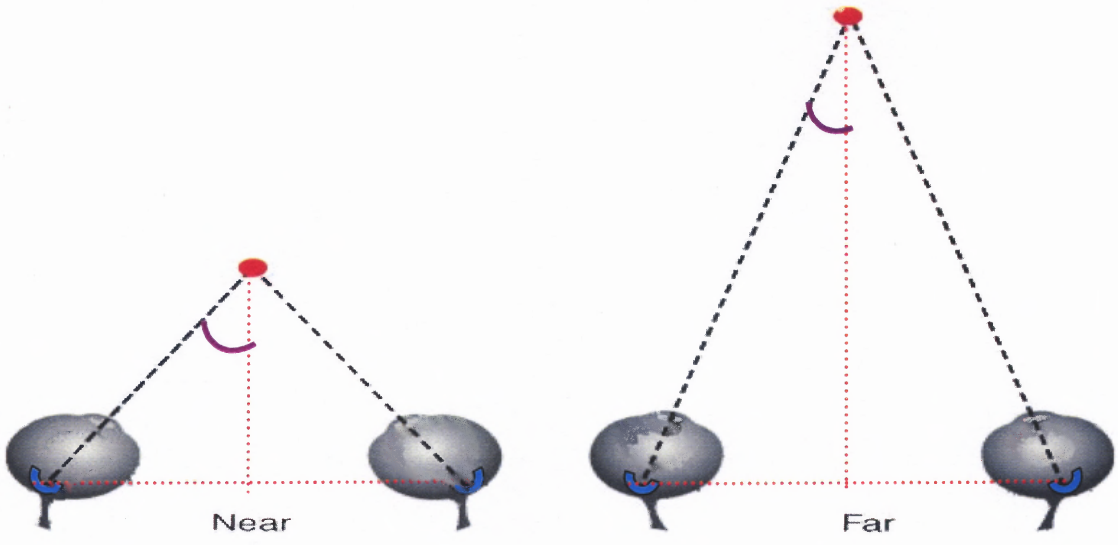

Figure 2.18 Convergence angle relationship to target distance in vergence eye movements. Note that the fovea, shown in blue, is the location at the posterior of the eye, in the retina, upon which the image strikes, and the angle in purple is the angle of convergence.
Source: Squire, 2003.

The neural circuitry underlying vergence eye movements remains a topic for debate. However, there is evidence from landmark neurophysiology studies performed by Mays [28, 29] that suggests that there is specific neural circuitry involved with convergence and specific circuitry involved with divergence. He and his colleagues discovered the existence of a small group of neurons in the region of the brain stem referred to as the mesencephalic reticular formation (MRF). These neurons are broken down into two types: vergence burst and vergence burst-tonic cells. The former cell type generate high frequency impulse trains that occur prior to the onset of a vergence movement. Mays and Gamlin [29] suggested that these cells are limited by the activity of saccadic omnipause neurons, which control conjunctive eye movements called saccades. They also suggested that because the firing frequency of the vergence burst cells is inhibited by the saccadic omnipause neurons, the velocity of the vergence movement can

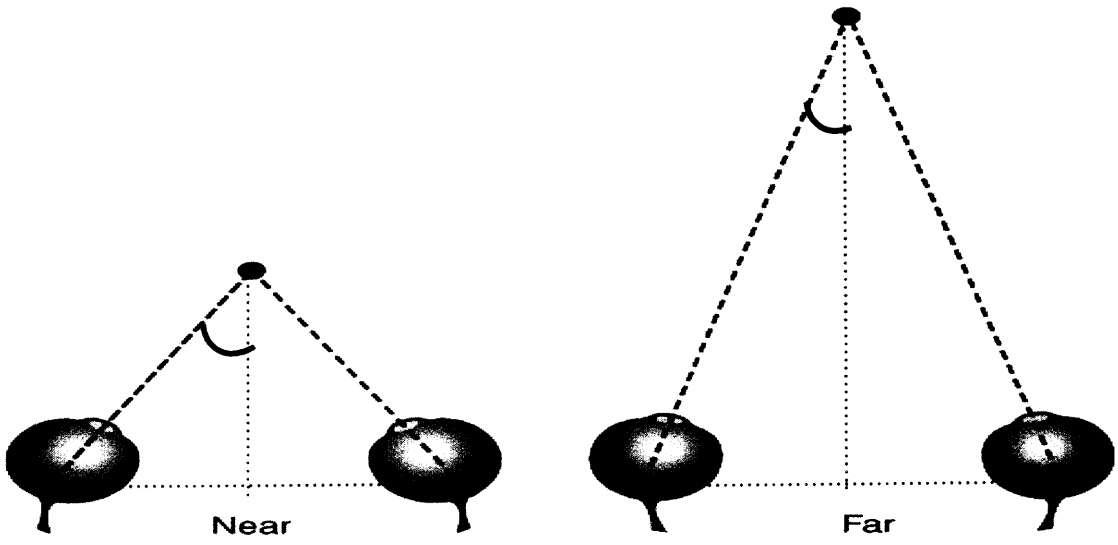

Figure 2.18 Convergence angle relationship to target distance in vergence eye movements. Note that the fovea, shown in blue, is the location at the posterior of the eye, in the retina, upon which the image strikes, and the angle in purple is the angle of convergence.
Source: Squire, 2003.

The neural circuitry underlying vergence eye movements remains a topic for debate. However, there is evidence from landmark neurophysiology studies performed by Mays [28, 29] that suggests that there is specific neural circuitry involved with convergence and specific circuitry involved with divergence. He and his colleagues discovered the existence of a small group of neurons in the region of the brain stem referred to as the mesencephalic reticular formation (MRF). These neurons are broken down into two types: vergence burst and vergence burst-tonic cells. The former cell type generate high frequency impulse trains that occur prior to the onset of a vergence movement. Mays and Gamlin [29] suggested that these cells are limited by the activity of saccadic omnipause neurons, which control conjunctive eye movements called saccades. They also suggested that because the firing frequency of the vergence burst cells is inhibited by the saccadic omnipause neurons, the velocity of the vergence movement can

be altered by the activity of saccadic omnipause neurons, because the velocity of the vergence movement is dependant upon the firing rate of the burst neurons. It is further suggested that during a saccadic movement the saccadic pause neurons are silenced to allow for the vergence movement to occur. When the saccadic movement is finished, the omnipause neurons reactivate and cause the velocity of the remaining vergence movement to slow.

This work is the strongest physiological basis of support for a theory called the Dual Mode theory. This theory hypothesizes that there are two systems, or modes, at work in a vergence eye movement. These two systems are called the initiating and sustaining components. It is believed that the initiating component is the faster and coarser response of the brain during three dimensional tracking. It is theorized that this is a pre-programmed response that is open loop and occurs as an impulse response. It is further theorized that a sustaining component then takes control of the movement. The proposed purpose of this portion of the movement is to focus on the target in finer increments. This portion of control implements a slower, feedback controlled movement. It is theorized that this aspect of the movement is a step response. It remains unclear how, if at all, the accommodation system influences the vergence movement. It is hypothesized that the influence of the accommodative system will occur in the movement signal as a delayed, low amplitude step response. This research will attempt to distinguish between types of movements and control schemes in vergence eye movements to clarify how the accommodation system interacts with the vergence system, and how this affects the dual mode theory. In addition, it will seek to provide a simple method of quantification of motor neuron control schema changes with aging.

2.1.8 Presbyopia

Presbyopia is a progressive inability to focus on near images. It is an age-related far-sightedness condition. It is not congenital. It is estimated that approximately 90 million people in the United States have this condition today or will develop it by 2014. The National Institute of Health (NIH) suggests that the onset of the condition begins between the ages of 40 and 50, with full onset occurring by the age of 65.

The mechanism underlying the onset and subsequent progression of presbyopia is unknown. It is known that all people will develop this condition, with the likelihood of occurrence increasing as the eyes age. It is unknown whether the condition is caused by a loss of plasticity within the lens of the eye, or whether this change occurs within the musculature that surrounds the lens and is instrumental in changing the shape of the lens. Figure 2.19-A illustrates the focus of objects in an eye that is presbyopic. Note that the focal point is behind the eye. Figure 2.19-B illustrates the refocusing of the image onto the retina via the use of a corrective lens. This subject population is of interest to this research to determine if an autonomically influenced system that shows signs of reduced adaptability would have cardiovascular autonomic correlates. This was investigated by collecting cardiac autonomic information from three groups of people: young controls, adapTable presbyopes and non-adapTable presbyopes.

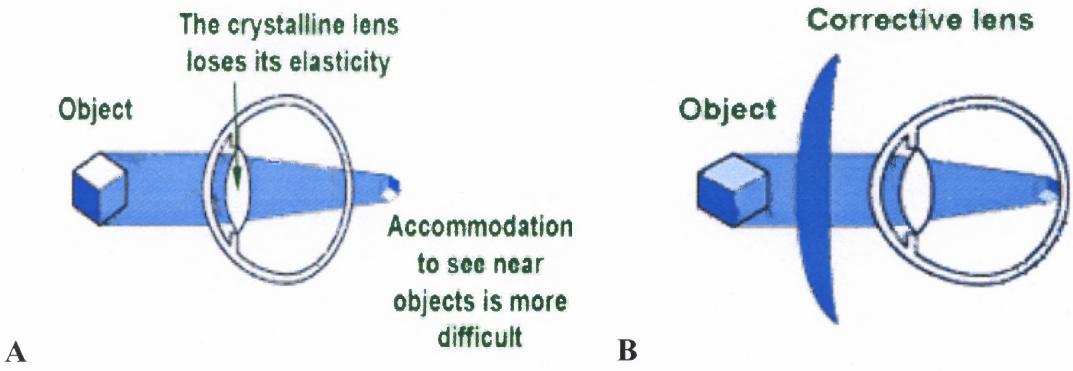

Figure 2.19 Lens alterations with aging. ***A*** - Theoretical underlying cause of presbyopia is the loss of near vision due to loss of lens elasticity or weakening of the muscles that adjust the curvature of the lens. ***B*** – Corrective lenses help focus the image on the fovea. *(http://www.essilor.com/Products/VisionAndVisionDefects/presbyopia.htm)*

2.2 Engineering Background

Engineering terms used in this research are explained in this Section. Wavelet techniques are discussed in this Section in some detail because it the third hypothesis of this work relies upon wavelet theory as the basis for the tools that were developed. Improvements over standard time or frequency techniques using wavelets are discussed in this Section. In addition, terms such as stationarity, regularity, linearity and independence are defined and discussed with reference to their role in the analysis of biological systems. A discussion of non-linear variability measures follows and builds upon the discussion of the wavelet analysis technique. The importance of wavelet decomposition in time series variability analyses is discussed, specifically in the form of Total Wavelet Entropy. A comparison of blind source separation techniques follows that discussion to clarify the utility of a wavelet-based source separation technique in the analysis of autonomic control systems in comparison to other methods that are currently employed to delineate input and control signals.

2.2.1 Wavelet Time-Frequency Distribution

A method of combining the two attributes of time and frequency without losing critical time or Fourier parameter information is through the implementation of a time-frequency, or multi-resolution, decomposition. This method of evaluating non-stationary signals that contain transient components has been gaining increasing popularity, with the first implications for applications to signal analysis in the 1940s. Recently, a time-frequency method has come to the forefront as a powerful method of analyzing transients and allowing the researcher to investigate frequency components over the length of the signal.

This method, known as the Wavelet Time-Frequency Multi-Resolution analysis, makes it possible to have good time and frequency resolution due to a shape that is other than a sinusoid and is applied to the signal using a scalable window. It is a form of adaptive filtering technique that can be applied to non-stationary signals and be used to generate independent time series.

A shortcoming of time-frequency decompositions based upon the Fourier transform is the inability to use a scalable window, which results in the loss of time resolution. Fourier transform based methods of time frequency analysis are based upon scaling and shifting a sinusoid and convolving it with signal to be analyzed, using a fixed window of time for all frequencies. Another shortcoming of this method is that because sinusoids are infinite signals, they are not contained completely in the window that is chosen for the analysis. For this reason, the use of a sinusoid introduces artifact into the analysis due to the fact that the window captures different quantities of periods of the sinusoid at different frequencies, depending on window size being used.

The wavelet transform uses the theory of time-frequency decomposition and employs an adaptive window size that changes based upon the frequency being examined. It also employs signals other than sinusoids in the analysis, called wavelets. The signals employed in the wavelet analysis decay to zero exponentially outside of the frequency of interest, reducing the problem of the base extending outside of the window and the associated introduction of artifact. They also oscillate about zero in the time domain and therefore possess a zero mean value. Translated to the frequency domain, the Fourier transform of the wavelet must approach zero at the zero frequency, which forces a band-pass behavior of the wavelet. This time and frequency characteristic of the

wavelet is referred to as the *admissibility condition*, which must be met in order for reconstruction of the signal using wavelet coefficients [30]. The requirements for wavelet construction and implementation are discussed in detail in 2.2.3.

The Fourier transform utilizes the infinitely bound sine wave as the basis for analysis. This increases the likelihood of missing small transients in signals that the wavelet would detect due to its limited duration. The wavelet, then, is well suited to analyze a local area of a signal that would otherwise be missed by the traditional Fourier analysis. The shape of the wavelet is typically asymmetrical as compared to the Fourier transform, which utilizes the uniformly shaped sinusoid. The shape of the wavelet renders it well suited to detection in signals that contain sharp changes in frequency content.

Another quality of certain wavelets which makes them a useful technique in non-stationary signal analysis is orthogonality (refer to Section 2.2.5). This attribute causes the wavelet coefficients generated from the analysis to be orthogonal. In turn, this causes each wavelet coefficient series to be representative of independent signal components [31, 32].

The wavelet method is unlike other time-frequency decomposition methods because it is not based upon the traditional Fourier base of sinusoids and does not use fixed windows of time to analyze the signal at all frequencies. The window size varies depending upon the scale, or frequency, that is being investigated. In addition, the wavelet method convolves a "mother wavelet," of shape and duration varied by the class of wavelet and the scale being assessed, with the signal to be analyzed. This mother wavelet is scaled and shifted based upon the frequency band of interest. This scaling and

shifting allows for the detection of small transients as well as larger trends within the data. It also allows for better time and frequency resolution than traditional methods have provided. A wavelet analysis is the method employed as the basis for the statistical measures of this work. The construction and implementation of the Continuous Wavelet Transform (CWT) as well as differences between that and the Discrete Wavelet Transform (DWT), will be discussed in this chapter.

2.2.2 Brief Background of the Wavelet Transform

The wavelet time frequency decomposition is a mathematical theory that has been in development since the early 1900s. Alfred Haar, in 1909, is credited with the first written description of the theory that has since become referred to as wavelet analysis. Since then, the theory has gained increasing popularity. In 1988, Stephane Mallat derived the algorithm that is the basis for this approach to time-frequency analysis [33]. Since then, engineers have embraced this method in various fields of research, including but not limited to acoustic emission [34, 35], transmission line fault detection and protection [36] and detection and classification of material attributes [32]. In 1995, biomedical applications of the wavelet analysis, such as the analysis of motor unit action potentials [37] and the use of electromyography for the detection of back muscle fatigue [38], began to appear in the literature.

The theory of wavelet based decomposition of signals is founded upon the nineteenth century theory presented by Joseph Fourier, which has come to be known as the Fourier analysis or Fourier transform, whereby a signal is decomposed into its frequency components via the use of sinusoids. The wavelet transform replaces the time information lost in the Fourier transform. Wavelet analysis performs a frequency

analysis that assesses frequency band activity over time, rather than calculating the sum of all frequency activity during the life of the signal of interest. Today, United States mathematicians, such as Daubechies and Coiflet, lead the advancement of wavelet theory [33].

2.2.3 Properties and Implementation of the Wavelet Transform

The Continuous Wavelet Transform (CWT) uses a main signal, referred to as the "mother wavelet" and convolves a shifted and scaled version of this signal with the signal to be analyzed. Mathematically, this approach is represented by the equation

$$C(a,p) = \int_{-\infty}^{\infty} f(t)\psi^{*}(a,p,t)dt \tag{2.1}$$

where C represents the coefficients that are a result of the product of the original function and the conjugate of the mother wavelet, ψ^*. The scaling factor, a, of the mother wavelet, p is the shifting factor of the mother wavelet, $f(t)$ is the original signal and $\psi^*(a, p, t)$ is the conjugate time-dependant mother wavelet, scaled and shifted by a and p, respectively. The mother wavelet is decomposed via scaling and translation, into a set of smaller basis functions, represented by $\psi^*_{ap}(t)$, where

$$\psi^*_{ap}(t) = \frac{1}{\sqrt{a}}\psi\left(\frac{t-p}{a}\right), \tag{2.2}$$

and $a^{-1/2}$ provides unity energy normalization across scales. Consider $\psi^*_{ap}(t) = \psi^*(a,p,t)$ as a function of time. Then, $\Psi(\omega) = F\{\psi(t)\}$. The Coiflet family, order 3 wavelet (coif3) was employed in this research. The Coiflet mother wavelet in time is represented in Figure 2.20, below.

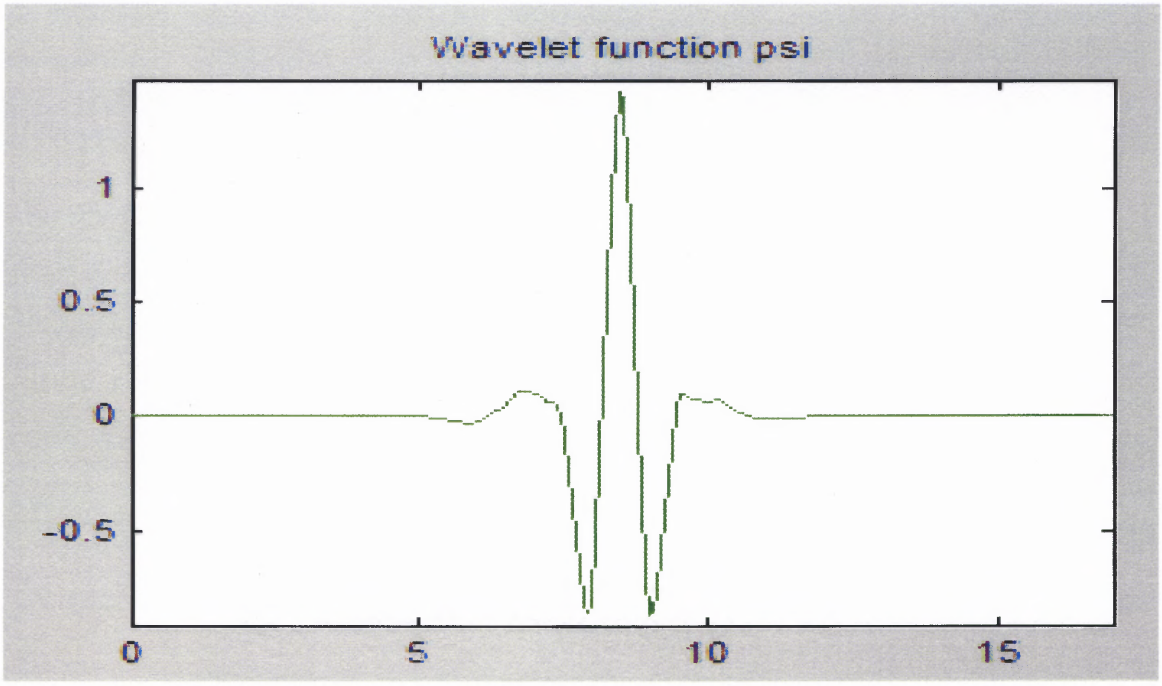

Figure 2.20. Time representation of $\psi^*(a,p,t)$, for the ciof3 wavelet.
(*from Matlab* ***wavemenu*** *function*)

Scaling is the process by which the wavelet is stretched or compressed at a certain level, as seen in Figure 2.21. This scaling or compressing enables the wavelet to capture frequency information at various frequency levels. Higher frequency content is captured at lower scales and conversely, lower frequency content is captured with higher scales.

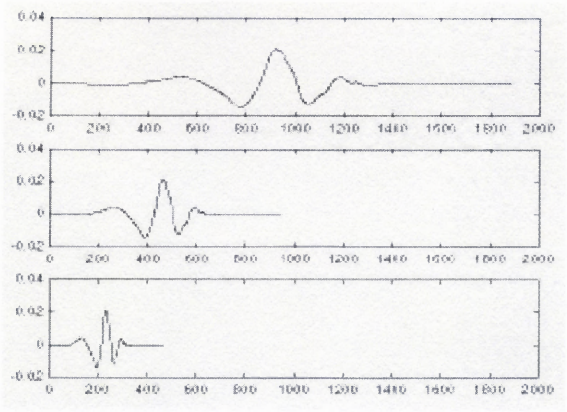

$$\psi^*(1,0,t), \omega_0 = 1/a = 1$$

$$\psi^*\left(\frac{1}{2},0,t\right), \omega_0 = 1/(1/2) = 2$$

$$\psi^*\left(\frac{1}{4},0,t\right), \omega_0 = 1/(1/4) = 4$$

Figure 2.21. Scaling the mother wavelet. Note that the signal becomes increasingly short in duration at smaller scales. This yields information about quickly changing, or the high frequency content, of signals.
Source: www.mathworks.com, 2005.

Scales are in powers of 2. For example, a scale factor of 9 corresponds to a level of 2^9, or 512, wavelet coefficients. At higher scale levels the wavelet analysis possesses greater frequency resolution, whereas lower scale levels yield better time resolution because decreasing the scale parameter increases the bandwidth of the wavelets, as shown in Figure 2.21 [39]. Therefore, it is useful to describe the wavelet transform as a bank of band-pass filters, with a pass frequency defined by the scaling and central frequencies of the mother wavelet. The bandwidth, ω_0, decreases by half at every scale, and $\omega_0 \propto \frac{2\pi}{a}$.

Wavelet representations are typically referred to as time-scale decompositions due to the fact that the mother wavelet is compared to the original signal in scales, not frequency.

However, frequency roughly correlates to the inverse of the scale value and is related to the scale in the following way:

$$F_a = \frac{F_c}{F_s a}, \tag{2.3}$$

where F_a is the frequency correlating to a specific scale, F_s is the sampling frequency, F_c is the center frequency of the specific mother wavelet at the scale being analyzed and a is the scale being analyzed.

Shifting is the process by which the onset of the application of the mother wavelet is delayed or hastened, as can be seen in Figure 2.22 [39]. This allows for the time component in the wavelet analysis. Rather than looking at specific windows of time, the

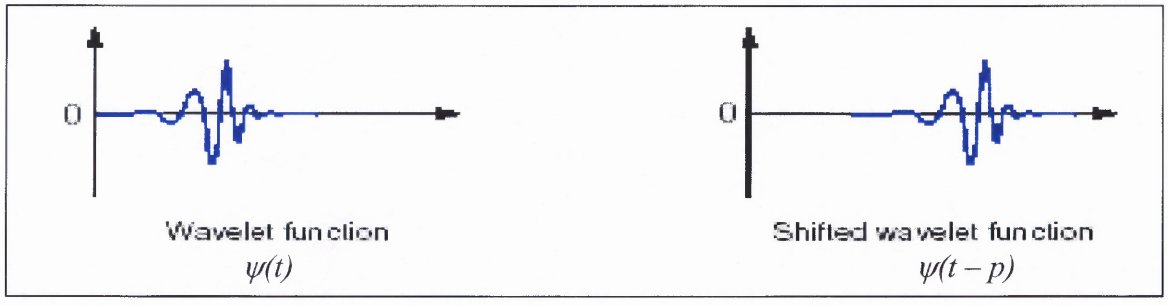

Figure 2.22 Shifting the mother wavelet. In this case, k is the shifting factor, or the length of time by by which to delay the onset of the application of the wavelet.

wavelet analysis looks at all time in the duration of the signal being analyzed, at varying scales. Higher scales will yield larger shifts in time in order to capture the activity at lower frequencies. Likewise, lower scales will yield smaller shifts in time, which will capture the higher frequency, or rapidly changing, content of the signal.

2.2.4 Properties of a Signal Required to be Considered a Wavelet

Wavelets address problems with inaccuracies of representation of the frequency content of a signal as a result of Fourier analysis based time-frequency analyses. It does this by convolving the signal to be analyzed with a signal that meets two specific properties: the

admissibility and the *regularity* conditions. The admissibility condition requires that the wavelet decays quickly to zero outside of the time and frequency of interest. This property of wavelets is known as the *localization property* of the wavelet. In the time domain, this is equivalent to saying that the wavelet must oscillate about zero and have a mean value of zero. In the frequency domain, this is equivalent to the statement that the wavelet is *compactly supported,* or *band limited*, and must decay quickly to zero outside of the frequency of interest. The concept of localization in both time and frequency is represented mathematically in equations 2.4 and 2.5.

$$\int \psi(t)dt = 0 \tag{2.4}$$

$$\left|\Psi(\omega)\right|^2_{\omega \neq \omega_0} = 0 \tag{2.5}$$

$$\left\|\psi^*_{a,p}\right\|^2 := \int \left|\psi^*_{a,p}(t)\right|^2 dt = 1 \tag{2.6}$$

Equation (2.4) indicates that the mean value of the signal must be zero. In addition, the signal must possess unity area, which controls the height of the signal, as shown in (2.6). Equation (2.5) indicates that the frequency content when $\omega \neq \omega_0$ is equal to zero, or that the signal is contained within a specific bandwidth in the frequency domain. Collectively, this means the mother wavelet signal exists only in the local region of the signal. These two combined attributes of the wavelet transform are collectively referred to as the *admissibility condition*, which is part of the requirement that must be met for the signal to be considered a wavelet.

The fact that wavelets decay in both the time and frequency domains results in an analysis that possesses very good time and frequency localization. However, it is impossible to have perfect accuracy of analysis due to Heisenberg's uncertainty principle. In the application of this theory to signal analysis, the principle states that it is impossible to obtain information about an exact frequency and exact time at which that frequency occurs. That is, it is impossible to get exact information about both time and frequency for any given time or frequency [40].

This research employs the wavelet coefficient sets, *C(a,p)*, as the basis for separation and analysis of the neural components of the cardio-pulmonary signals of the COPD and presbyope populations. As a requirement to perform this type of analysis, the coefficient sets must be orthogonal to, and therefore independent of, each other. Orthonormality is discussed and proved in the proceeding Section using the Haar wavelet for simplicity. The orthonormal wavelet families are the Haar, Meyer, DauBechies, Coiflet, Symlet, and biorthogonal wavelets.

2.2.5 Haar Wavelet as Illustration of Orthonormality

Certain wavelets are orthonormal. An inherent property of wavelets is that they possess unity area. This means that for each given scale, the amplitude is adjusted to ensure that the area under the curve is equivalent to 1, as in (2.6). This further means that for specific wavelet kernels, the wavelet basis is orthonormal. Using the simple example of the Haar wavelet, the orthonormal basis can be illustrated. The Haar wavelet is defined as follows, and is illustrated in Figure 2.23:

$$\psi_{haar}(x) \equiv \begin{cases} 1 & \left(0 \le x < 1/2\right) \\ -1 & \left(1/2 \le x < 1\right) \\ 0 & otherwise \end{cases} \tag{3.4}$$

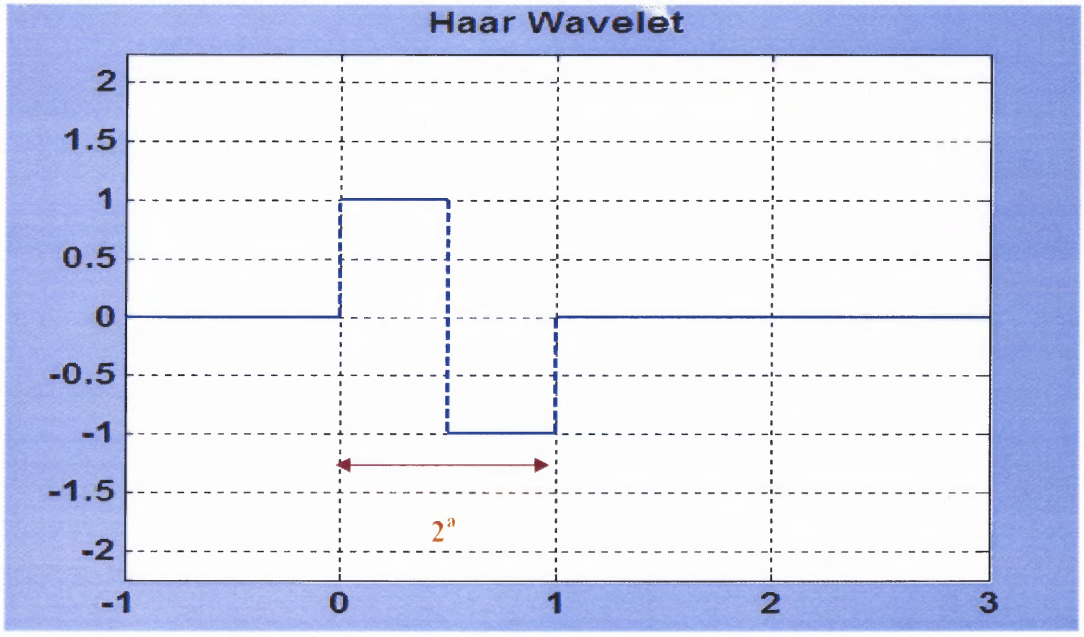

Figure 2.23. HAAR Wavelet.

Note that the area under the wavelet is 1. For larger time bases, the amplitude will be smaller. For smaller time bases, the amplitude increases, as shown below, to ensure that this remains true over the course of the analysis, as shown in Figure 2.24.

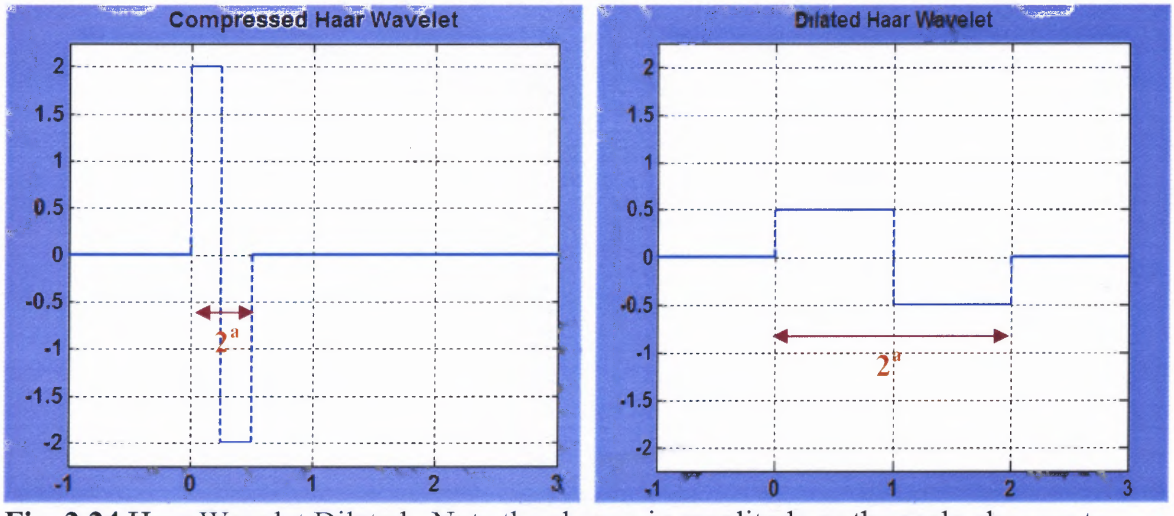

Fig. 2.24 Haar Wavelet Dilated. Note the change in amplitude as the scale changes to ensure unity area. Amplitude is equivalent to $1/2^a$ and support width is 2^a.

The support width is 2^a, where $\boldsymbol{a}$ is the scaling, or dilation, factor from (2.1). Let the signal start at $p*2^a$ and end at $(p+1)*2^a$, where p is the shifting factor from (2.1). If

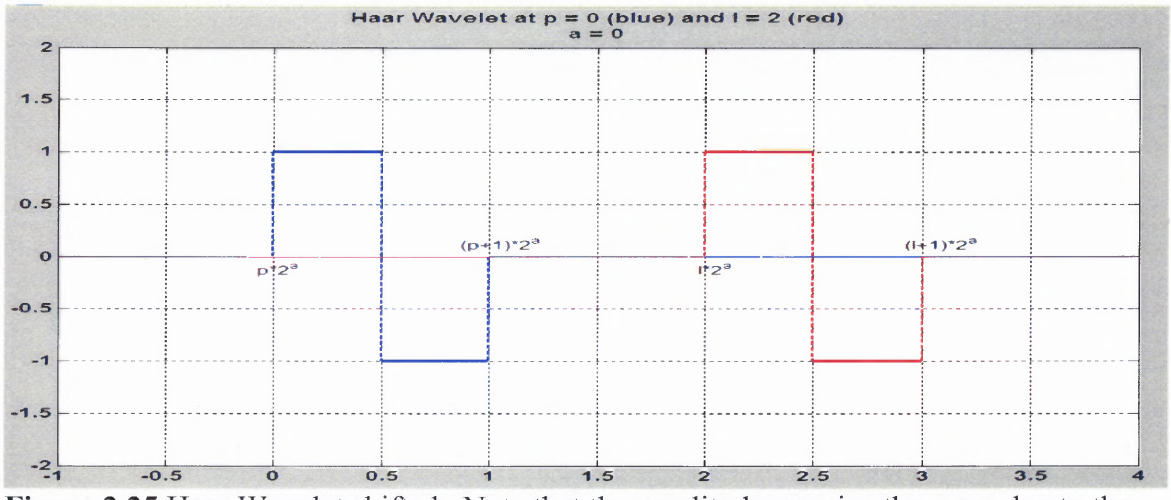

Figure 2.25 Haar Wavelet shifted. Note that the amplitude remains the same due to the scale, a, remaining fixed, with the shifting factor changing from p to l.

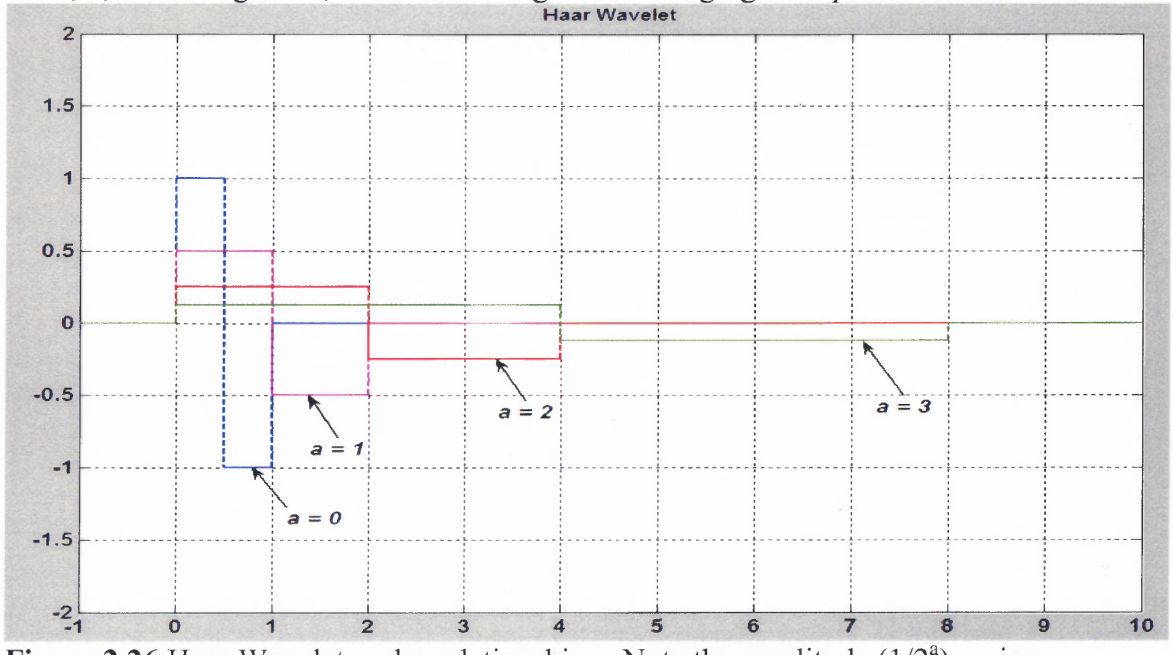

Figure 2.26 Haar Wavelet scalar relationships. Note the amplitude ($1/2^a$) varies according to the scale, a. Note also that with each successive scale, the signal is increasing in duration. This is a display of the inverse relationship between scale and frequency. As the scale increases, the frequency that is evaluated at that scale decreases.

the system is truly orthonormal, then $\langle \psi_{a,p}, \psi_{a,l} \rangle = 0$ for $p \neq l$, and $\langle \psi_{a,p}, \psi_{s,l} \rangle = 0$ for $a \neq s$.

Revisit Figure 2.24 and shift the Haar function for unequal p and l, as shown in Figure 2.25, below. The signal in blue is Haar at $p = 0$, while the red signal is Haar at $l = 2$, with $a = 0$ held constant for both signals. It can be seen in Figure 2.25 that for a held constant, the two systems are disjoint for given start times, and their resultant dot product is zero for all points. Figure 2.26 displays the scaling aspect of the wavelet orthonormality, $\langle \psi_{a,p}, \psi_{s,l} \rangle = 0$. Note that for all points of the two signals, the dot product is zero. Note also that the amplitude, per (2.6), must equal $\frac{1}{2^a}$. Also note that at it is impossible for the start of $\psi_{s,l}$ to be within $\psi_{a,p}$ and the end of $\psi_{s,l}$ to be outside of $\psi_{a,p}$, forcing $\psi_{s,l}$ to be completely contained within, or completely outside of, $\psi_{a,p}$, as shown in Figure 2.26 [93].

In summary, the wavelet should meet the conditions of admissibility and orthonormality for the purposes of this research. The admissibility condition allows the wavelet to be used in applications where perfect reconstruction of the original signal is necessary. The admissibility condition also enables the signals to be orthonormal, as per the above discussion. Orthonormality allows the coefficient sets generated by the wavelet analysis to be treated as independent signals, which enables the individual treatment of the coefficient sets for the purposes of source separation and entropy at specific frequencies.

2.2.6 Heart Rate Variability (HRV) Analysis and Wavelets

The wavelet analysis will be performed using Matlab version 6.5, with the Wavelet toolbox. The data files will be created from continuous blood pressure signals and filtered in a Labview version 7.0 program. The HRV data are square wave signals created by the timing between successive heart beats. As a result, the mother wavelet that will be employed in the analysis of these data will need to be simply shaped and have high frequency resolution to capture the sharp changes in the time signal. It has been suggested that the Morlet mother wavelet [41] is the most appropriate for this application. However, because the coefficients generated from the wavelet decomposition may be used for reconstruction and each time series will be used as an independent component of the HRV signal, it is inappropriate for this research to use the Morlet wavelet. The wavelet is not orthogonal, is not compactly supported, and the coefficient set that it generates cannot be used to reconstruct the signal. The appropriate wavelet basis for this research is the coiflet family of wavelets, due to their orthogonality and compact support, as well as the center frequency of the wavelet, which allows for better frequency resolution in the bands of interest for autonomic studies. The coefficient time series' can also be used to reconstruct the signal and are orthonormal.

The coiflet family of wavelets can also be used in continuous or discrete transformations. This is an important aspect to consider, depending upon the desired application. The Discrete Wavelet Transform (DWT) is necessary for the reconstruction of the wavelet coefficients into the original signal. This is true because the discrete wavelet transform down-samples the signal by a factor of two per scale during the signal decomposition. Down Sampling is necessary because in the wavelet analysis, both the

details (low frequency component of the signal at a given scale) and approximations (high frequency content of the signal at a given scale) create a signal that is the same length as the original signal. The difference in numbers of coefficients between the discrete and continuous analyses is illustrated in Figures 3.4a and b. The images illustrate the filtering of the original signal, ***S***. The signal is low passed to create the Approximations set of coefficients. ***S*** is also high passed to create the details set of coefficients.

Notice that in **Figure 2.27 a**, the continuous wavelet transform (CWT), the details and approximations values are not down-sampled. This results in approximation and detail signals that are each the length of the original signal. If the two sets of coefficients from the CWT are combined, the resultant signal contains twice the amount of data as is contained in the original signal.

In **Figure 2.27 b**, the discrete wavelet transform (DWT), the details and approximations are down-sampled by two. The discrete wavelet decomposition removes every other point from the details and approximations, yielding decomposition signals that are each half the length of the original signal. The signal integrity is not lost.

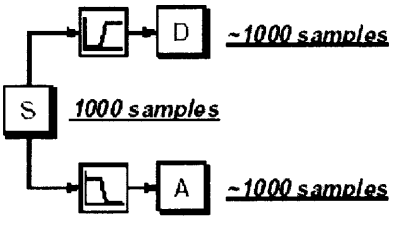

Figure 2.27a CWT Filtering. Techniques involved with the continuous wavelet transform (CWT).

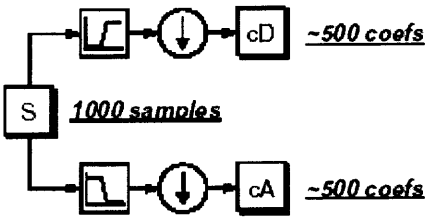

Figure 2.27b DWT Filtering. Techniques involved with the discrete wavelet transform (DWT).

During reconstruction of the signal, the algorithm needs to upsample the details and approximations signals by a factor of two, as illustrated in Figure 2.28, which can only be done if the original decomposition was done discretely. Upsampling involves placing a

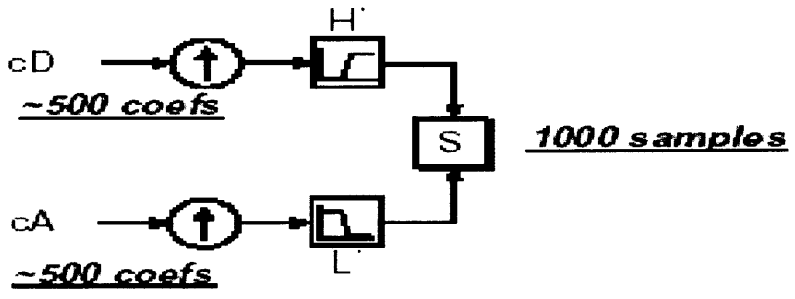

Figure 2.28 Reconstructing the original signal using the DWT coefficients.

zero between discrete points in the details and approximations signals, as shown in Figure 2.29. The resulting reconstructed signal is equal in length to the original signal.

The CWT does not provide a signal that can have a zero inserted at every other point and not lose the signal integrity. The CWT yields a smoother frequency analysis and ultimately yields a more complete picture of the frequency activity in the original signal. However, the DWT ability to remove noise from a signal and to reconstruct a denoised signal may be useful when trying to assess finer points in the signal. The Blind Source Separation that will be performed using a wavelet kernel will be performed on a denoised signal, which may be provided using a wavelet denoising algorithm that will be developed in Matlab v6.5.

The use of time-frequency distributions in biomedical signal processing has become increasingly popular due to the quantity of information that it can provide, as well as the ability to use this information to quantify health in a clinical setting. The search for the appropriate time-frequency distribution for biological signal processing is still underway.

In 1998, Keselbrener and Akselrod developed a time-frequency analysis method that detected cardiac transients, but in 2001, Akselrod, et al. suggested that independent time scales were an appropriate method of analyzing cardiac activity, using the standard

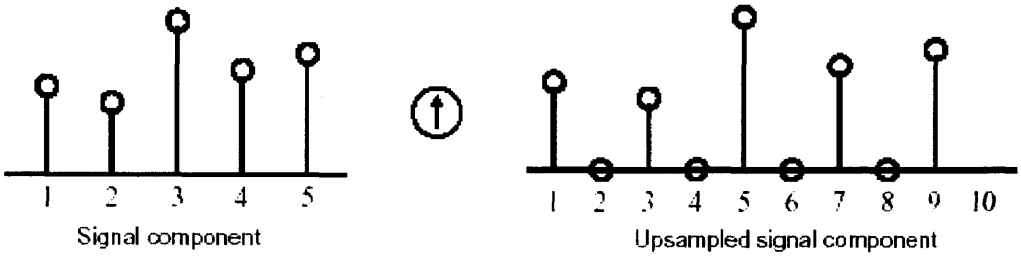

Figure 2.29 Zero insertion between coefficients during reconstruction. The arrow pointing upwards indicates that the upsampling has taken place. Note that the same arrow is present in Figure 3.5, which displays the filtering that takes place during reconstruction.

Wigner-Ville time-frequency distribution to first separate the data into various time series' based upon frequency activity and then using a varying time scale to investigate frequency activity according to specific events. That is, they investigated the utility of an adaptive time scale for the analysis of heart rate variability [42, 43]. The significance of investigating cardio-pulmonary activity at various time scales, using wavelets and other time-frequency distributions is presented increasingly in the literature [18, 44, 45, 46].

2.2.7 Measurement of Non-Linear Variability with Wavelet Entropy

In biological recordings, it has been observed that a bounded level of variability is present in healthy systems. Contrary to intuitive thinking, which would suggest that a sTable system would exhibit "sTable" dynamics, research has shown that the higher a system's variability, the higher a system's state of health. The boundaries for healthy levels of variability are still being defined. It is believed that at one end of the spectrum,

too high of a variability level, the signal becomes random and contains little information about the system. It is believed that the variability must be deterministic for the level of variability to continue to be considered "healthy." Uncorrelated variability, which would yield the highest non-linear variability parameter values, suggests a lack of coherent function within the system which is a result of a disturbance within the system. When variability becomes too low, the system becomes almost periodic in nature, and is indicative of a system that cannot adapt to changing conditions.

In physiological terms, examine cardiac health. Uncorrelated variability equates to a state of fibrillation, where the cardiomyocytes are firing in an uncontrolled, uncoordinated manner, and the cardiac cells, as well as the resultant signal obtained from the heart, are in a state of uncorrelated randomness (see Figure 2.30) . The heart must be stopped to allow for the cells to return to a cohesive contraction/relaxation relationship. This healthy relationship displays a level of coordinated variability. It is believed that the interaction of the sympatho-vagal branches of the nervous system contribute to this robust modulation of heart rate and pressure. It is this variability which allows the system to adapt and react quickly and safely to perturbations in the system. When the level of variability falls, the level of health has been shown to fall. In cardiac terms, conditions such as Tachycardia present an almost periodic signal that varies very little with time, and becomes a "single scale" signal, which in terms of a wavelet analysis, can be represented by a single scale, or frequency (see Figure 2.30). A low level of variability is evidence of an inability of a system to respond to stressors placed upon it [47, 48]. People with congestive heart failure (CHF), sleep apnea, hypertension, affective

mood disorder and chronic obstructive pulmonary disease (COPD), among others, have shown

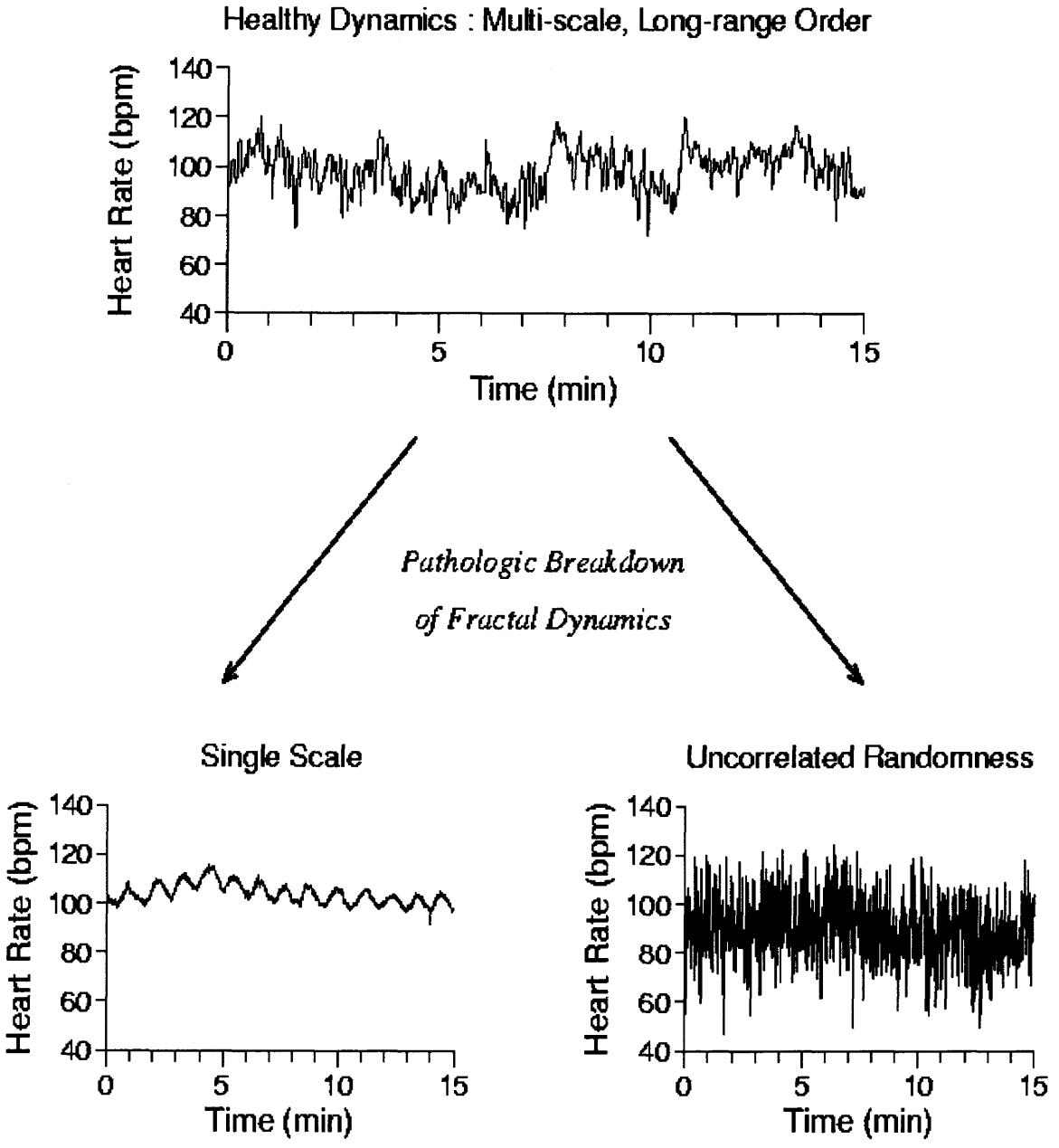

Figure 2.30 Representation of periodic versus random signals, the two sides of the spectrum of variability.

Source: Goldberger AL, Amaral LAN, Glass L, Hausdorff JM, Ivanov PCh, Mark RG, Mietus JE, Moody GB, Peng C-K, Stanley HE. PhysioBank, PhysioToolkit, and PhysioNet: Components of a New Research Resource for Complex Physiologic Signals. Circulation 101(23):e215-e220.

decreased levels of cardiac variability. Decreased Heart Rate Variability has been identified as an all-cause mortality indicator [49, 50, 51, 52, 53].

The research also investigated something as apparently different from cardiac activity as the visual tracking system. It was hypothesized that, not unlike the cardiovascular system, the visual tracking system adaptability is dependant upon the level of health of the visual control system. Cardiac autonomic function of people with adaptive versus more rigid tracking patterns in presbyopic individuals was also investigated in this research.

The method developed to assess autonomic function of the heart and lungs in aged and diseased populations is based upon the creation of several independent time series using a wavelet transform. The level of entropy, or information content, of each individual time series was investigated for physiological relevance. It is theorized that levels of entropy for healthy subjects will be statistically higher than the subject populations in the cardiac and visual systems. Total Wavelet Entropy (TWE) was developed in mechanics to analyze the classical limit of particles [54]. It was not used in cardiac or visual health assessments, beyond work published by the author of this research [55]. Related work includes a multiscale entropy analysis proposed by Costa, et al. in 2002, in which a time series is repeatedly decimated to obtain varying coarseness of a signal in time [56,57] and Shannon entropy measure of the Instantaneous Frequency [58]. In 1994, Wessel et al. [59] proposed a renormalized entropy measure that calculates the Shannon entropy of a normalized frequency distribution, and other variants of information analyses have since been proposed [60, 61, 62]. It was hypothesized that the separation of signals into independent, orthogonal components before performing a non-

linear analysis would provide a greater level of insight into the dynamics of the systems than traditional non-linear analysis methods because the frequency and time information will be assessed independently, thus avoiding the cloaking of the dynamics that results from analyzing the combined signals. It is also conceivable that further analysis can be performed based upon the wavelet time series.

2.2.8 Wavelet Source Separation

Blind Source Separation (BSS) is a method of processing data from systems that are a mixture of signals from various sources. The objective of such an analysis is to separate the sources of the signal for discrete processing and analysis using various statistical measures [63, 64, 65, 66]. The analysis is called a "blind" separation because it is assumed that no a priori knowledge of the system generating the mixed signal is present because the source signals are not being directly observed and because there is no information present about the manner in which the source signals are being mixed [67]. There exist several types of commonly used BSS techniques, the most prominent of which is Independent Component Analysis (ICA). ICA is a linear transformation technique that attempts source separation based upon a minimization of statistical dependence of the sources, and can only impose up to second order statistical independence [68, 69]. Most BSS methods are based upon statistical measures that typically go beyond second order measures, although some simpler separation techniques exist which are based upon second order statistics [67,70, 71, 72]. The method developed in this research is not a blind source separation, as the respiration provides a priori knowledge of one part of the system dynamics and is used as a template for the separation of the cardiac and respiratory source signals.

One popular method of source separation is Independent Component Analysis (ICA). This analysis requires a level of independence of the signal components and a level of stationarity that often does not exist, or is often not practical to obtain non-invasively, in most physiological signals. A new method of source separation employing a wavelet kernel provides a platform for analysis that can compensate for both stationarity and independence requirements of ICA which are unrealistic in physiological applications. A wavelet based analysis will have greater success in separating sources from a combined output signal because it can distinguish signals that are Gaussian in time and/or frequency, rather than basing the separation upon variance within the time series only, which is how ICA performs the separation.

The method of using Cohen class time frequency distributions as discriminators has been used successfully to separate speech signals directly recorded and those that are frequency modulated [75]. Wavelet transforms produce fewer cross-terms than traditional Cohen class time-frequency distributions and have good time and frequency localization. Thus, they are better suited for separation of multi-component physiological signals. Also, as proven in Section 2.2.3, the wavelet bases chosen for this analysis are orthonormal, which means that they are independent in time and scale. This property results in independent time series being generated from the wavelet analysis at all scales, which may each be independently analyzed for content.

In terms of heart rate variability and respiratory interaction, literature is unavailable on the concept of separating the interbeat interval into several components. There is a defined control mechanism from both the sympathetic and vagal branches of the autonomic nervous system. The wavelet-based Source Separation (WavS) technique

enhances the understanding of the neural control of the cardiovascular system by pinpointing the separate mechanisms contained within the signal. This is in contrast to the current state-of-the art methods of quantifying HRV information into specific clusters of levels of health, which the use of wavelets also enhances. While the respiratory and cardiac oscillations are intertwined, the frequency activity is a result of the neural control. The individual ANS control signals are now discernable, rather than assuming that activity in a specific frequency range is representative of the control schema. This method may be considered a deconvolution method, as it divides the frequency content of one signal by the frequency content of another. This is equivalent of a deconvolution in the time domain. To remove the input signal from a system that operates based upon non-linear interactions of the system is no trivial task. There are methods that are being developed in the cellular communications industry that may fit this application [76, 77]. This method is essentially an adaptive filtering method which employs time-scale decompositions that are not sensitive to the non-linear nature of the signals being analyzed. Other adaptive filtering methods are also being developed for the purpose of separating source signals [78].

In terms of cardio-respiratory interactions, the respiratory signal can be considered the input because modulation of this signal results in modulation of the output signal, which in this case is the interbeat interval signal. The resultant output signal that will be used for the system is the interbeat interval signal, derived from the electrocardiogram (ECG) as the time between successive heartbeats. Research has shown that there is a frequency dependence of heart rate variability on the frequency of the respiration signal [79]. This research distinguishes the control signal by which this

interdependence occurs, and in the process provides clinical indicators for varying states of health.

CHAPTER 3

METHODS

In chapter 2, background information was presented on the physiological systems and engineering methods used in the research. Chapter 3 presents information about the data collection methods employed to sample those systems, as well as signal processing methods developed to analyze those data. In addition, a simple model of the cardio-pulmonary oscillations is presented as a validation of the mathematical methods.

3.1 Cardio-Respiratory Coupling Simple Model

The objective of this dissertation is to develop novel time-frequency methods for the assessment of changes that occur in the cardio-pulmonary coupling circuitry as a result of disease and aging. To validate the wavelet source separation method, a model was developed that roughly approximated the Interpolated Inter-Beat-Interval (IIBI) signal as a sum of sinusoids. The sampling frequency of the signal was 200 Hz, to approximate the sampling rate of the clinical IIBI signals. In addition, the signals were decimated to 40 Hz, as was done with the clinical signals. The sinusoids represented the oscillations of the respiration and the cardiac cycles at frequencies of 0.2 and 1.0 Hz, respectively. The two signals and their sum are shown in Figure 3.1. The left two images are the respiration and cardiac cycles, and the image on the right is the combination of the two signals resulting in the simulated basic IIBI signal.

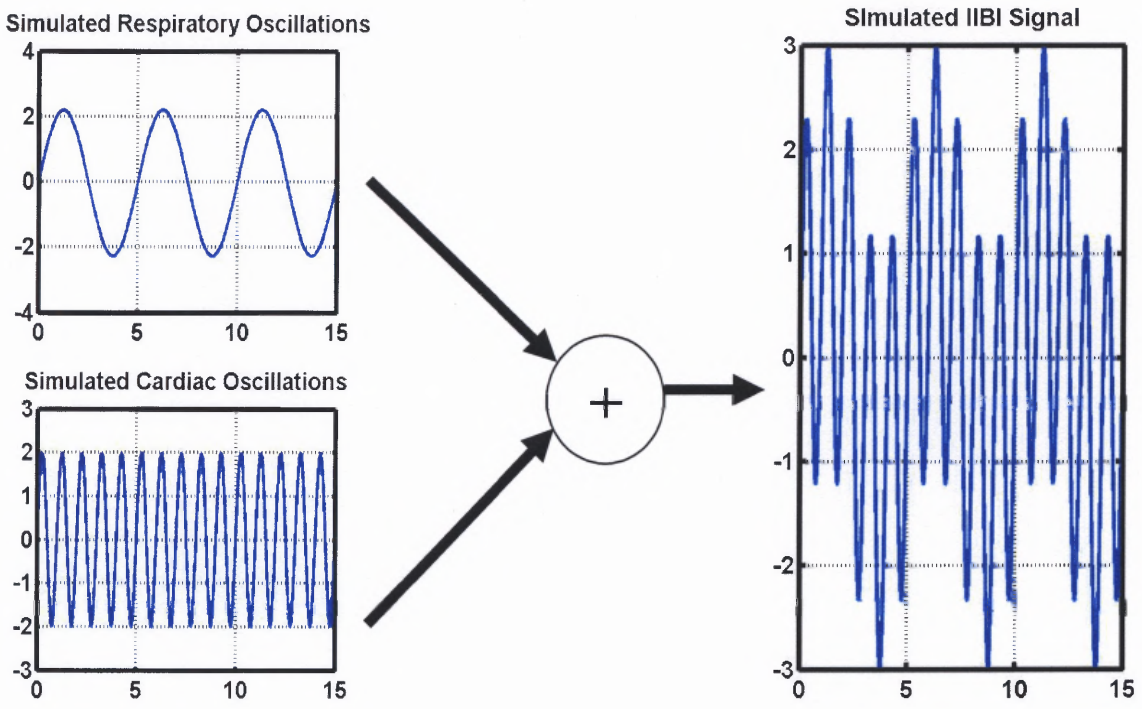

Figure 3.1. Individual and summed output of the model simulations.

The equations defining the signals are as follows:

$$y_1(t) = A_1 \sin(2\pi F_{RESP} t) \tag{3.1}$$

$$y_2(t) = A_2 \sin(2\pi F_{HRV} t) \tag{3.2}$$

$$y_3(t) = A_2 \sin(2\pi F_{HRV} t) + A_1 \sin(2\pi F_{RESP} t) \tag{3.3}$$

In addition to a steady state model, it is important to understand how the program would perform under dynamic situations, for example during exercise. The model was altered to include a steady state of five minutes followed by a transition to exercise state for another five minutes. As a result, the model output was a sum of sinusoids for two

specific conditions, rest and exercise, composed of four sinusoids, as shown in Figure 3.2. Seconds 290 through 300 are the rest simulation, and seconds 300 through 310 are the exercise simulation.

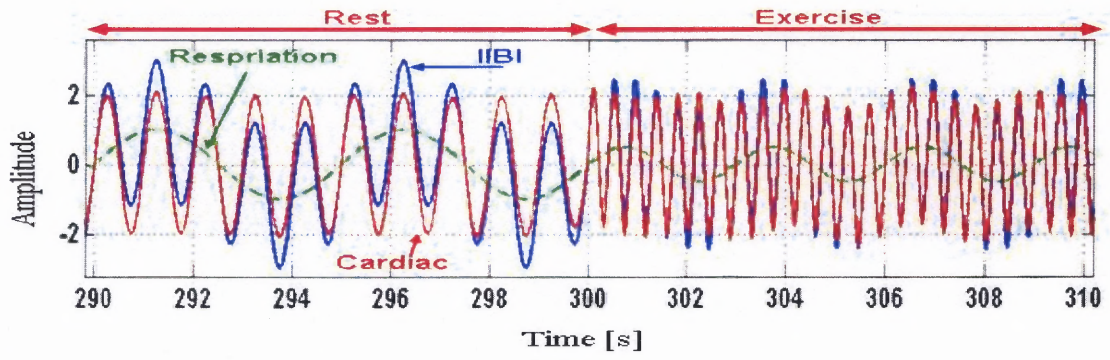

Figure 3.2 Rest and exercise simulations.
Note the change in frequency and amplitude at point 300.

For the simulated exercise model, a range of frequencies were employed to create a series of rest/exercise coupings to test the program. For example, Fresp_ex = 1.5*Fresp, Aresp_ex = 0.5 * Aresp, Fhrv_ex = 2.25*Fhrv, Ahrv_ex = Ahrv_ex. As in (3), the system during exercise is modeled by the sum of the two sinusoids, with frequencies altered as listed, with Fresp replaced by Fresp_ex, Aresp replaced by Aresp_ex, Fhrv replaced by Fhrv_ex and Ahrv replaced by Ahrv_ex. Model resting heart rate (HR) is 60 beats/min, with the exercise heart rate = 2.4 * 60, or 144 beats/min. The amplitude was not modified for the heart rate signal, so Ahrv = Ahrv_ex. Model resting respiratory rate is approximately 12 breaths/min, compared to 1.5 * 12 = 18 breaths/min in the exercise model simulation. With reference to the respiration signal, increased frequency is typically associated with decreased amplitude, so the amplitude of the respiration model during exercise is decreased from resting by a factor of 2. The frequencies tested for exercise are listed in Table 3.1.

TABLE 3.1. Index of Simulation Frequency Multipliers for Transition from Rest to Exercise

CARDIAC CYCLE		RESPIRATION	
FREQUENCY MULTIPLIER	HEART RATE [BEATS/MIN]	FREQUENCY MULTIPLIER	BREATHING RATE [BREATHS/MIN]
1.4	85	1.1667	14
1.6	95	1.333	16
2.1	125	1.5	18
2.3333	140	1.6667	20
2.9333	175	1.8333	22

3.2 Cardio-Respiratory Data for COPD Study

All data were collected in a non-invasive manner on human subjects. Although the COPD and presbyopic cardiac data were recorded at different locations, all IRB protocols were strictly enforced for both studies.

3.2.1 Heart Rate Variability

Heart Rate Variability (HRV) requires as an input an inter-beat interval signal that is a measure of milliseconds between successive heartbeats. For this research, a study of normals and patients with Chronic Obstructive Pulmonary Disease (COPD) that was conducted at Columbia University's College of Physicians and Surgeons is the source of heart rate variability data. The testing was performed in the Human Performance Laboratory in Atchley room 327 of the Columbia Presbyterian Hospital in New York City, NY. The protocol included a Pulmonary Stress Test at 30% supplemental Oxygen, as per the NETT protocol. Continuous Respiration, Electrocardiogram (ECG) and Blood Pressure (BP) were acquired during the study.

3.2.2 Subject Population

The subjects that participated in the study included individuals with severe pulmonary disease that were being enrolled in the National Emphysema Treatment Trial (NETT) with the goal of studying lung volume reduction surgery (LVRS) as well as healthy individuals with no known cardiac or pulmonary disease. Data of 10 COPD subjects were analyzed in the course of the research. The data of 5 normal subjects were employed for the research.

3.2.3 Data Acquisition

All exercise stress testing was performed on a bicycle ergometer with a SensorMedics Vmax 229 series workstation. The protocol was a ramp exercise with five minute baseline data collection, followed by a three minute warm-up at no load and then a maximum exercise test with a 5 Watt/min ramp. All exercise was performed on 30% supplemental oxygen. The autonomic biopotentials were obtained through an interface board (BNC 2080, Naitonal Instruments, Austin, TX) and fed into a 12-bit analog-to-digital converter (DAQcard 700, National Instruments, Austin, TX). The data were then recorded by a Pentium computer (Hitachi Vision Book Plus, San Jose, CA). Five minute resting data collections were also done in a counter-balanced order on room air and 30% supplemental oxygen. Post acquisition data analyses were carried out separately.

Various levels of testing were performed. Testing was performed during rest and during exercise, which consisted of three minutes of unloaded warm-up, one minute exercise increments to maximum ventilatory threshold, and then followed by a three minute unloaded recovery period. These are established, non-invasive methods to perturb the autonomic system for analysis of autonomic tone using the variability of the

R-R interval as a result of the perturbations. The laboratory employed an established and validated routine to extricate and interpolate the inter-beat interval (IBI) from the ECG data.

The heart rate variability data were obtained using a Labview program. The program extracts the inter-beat interval (IBI) by recording the time stamp between successive R-wave peaks in the ECG signal. The program then performs a reverse interpolation to ensure that the sampling rate is evenly resampled to 200 Hz. The process is shown in Figure 3.3, and the front panels of the program are included in Appendix A. Note that the height of the square wave is the length of each successive inter-beat interval in milliseconds. The time periods are different between any successive two beats if the heart is healthy. The length of time between beats is called the inter-beat interval (IBI). The time interval becomes the height of a square wave that is generated from these data. The sampling rate of the square wave is 200 Hz and is created by reverse interpolation of the IBI data.

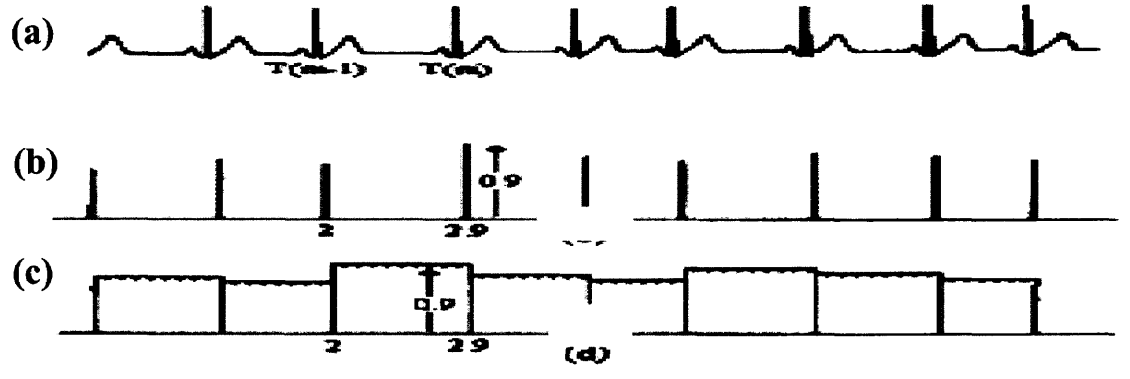

Figure 3.3 ECG Waveform conversion to Interpolated Inter-Beat Interval. a) ECG signal. b) Inter-beat interval (IBI) Signal. The height of each pulse becomes the time between each pulse. c) Interpolated Inter-beat Interval (IIBI) Signal. The pulse train is reverse interpolated to generate an evenly sampled square wave for analysis.
Source: Reisman, S. Lecture Notes, ECE 667, 1999.

3.3 CARDIO-RESPIRATORY DATA FOR PRESBYOPE POPULATION

All data were collected in a non-invasive manner on human subjects. Although the COPD and presbyopic cardiac data were recorded at different locations, all IRB protocols were strictly enforced. The IRB for this study is included in the Appendix.

3.3.1 Heart Rate Variability

For this research, a study of controls and apparently healthy subjects with Presbyopia was conducted at the Laboratory for Visual Processes in the Department of Biomedical Engineering at New Jersey Institute of Technology. Continuous Respiration and Electrocardiogram (ECG) were recorded for three different controlled breathing levels: 8 breaths/min, 12 breaths/min, and 16 breaths/min in an effort to obtain respiration rates in the low and high HRV cardiac autonomic response ranges.

3.3.2 Subject Population

As this was a pilot study, a small data set was collected. The data were collected from 10 subjects, six presbyopic and four control human subjects. The ages of the controls ranged from 18-35. The ages of the presbyopic group ranged from 50 – 75. The presbyopic group was further divided into two groups, those who are able to adapt to wearing integrated lenses and those who are restricted to the use of traditional bifocal lenses.

3.3.3 Data Acquisition

ECG and respiration were recorded using Grass bioamplifiers that fed data through a National Instruments DAQcard. The ECG was measured using passive electrodes that were passed to the Grass-Telefactor model IP511, which is an industry standard isolated physiological pre-amplifier. Measurement of the respiration signal was performed by passing the output from a Grass-Telefactor Respiratory Effort Transducer to the Grass isolated pre-amplifier. The measurement was obtained by placing a band containing a piezo-electric (this type of material generates a very low level voltage when it changes size, either by being stretched or compressed) crystal film around the subject's ribcage. The measurement was obtained by recording the difference in the microvolt level signal that is generated when the piezo film is stretched or compressed due to the expansion/compression of the chest during inhalation/exhalation. The band was directly connected to the pre-amplifier, and no external power supply was required. The connectors are touch-proof safety connectors and the instrument to which it was attached employs both optical and transformer isolation.

Each subject was seated in a dark environment that was created by enclosing an area with black felt to block stray light from entering the area. The subject was instructed to focus on a green light emitting diode (LED) array, which illuminated from a near to a far target at a specific frequency (8, 12 or 16 breaths/min). The subject was then instructed to pace their breathing with the target presentation. The data were then sent to the computer where they were recorded by a custom LabView program at 500 Hz to ensure high frequency resolution.

3.4 Data Analysis

The problem of non-linearity and non-stationarity in a time series is increasingly confounding to biomedical researchers. As more research is performed upon biological systems, it is increasingly apparent that there is a need for an expanded signal processing toolbox. In this research, the data form the two sources discussed above will be analyzed using similar but not identical methods. Adjustments will need to be performed to accommodate for the different physiological systems. For instance, a wavelet kernel that is appropriate for heart rate variability is not appropriate for vergence eye movements. In addition, frequency ranges of interest differ, and thus differing scales of time-frequency distributions will be used as appropriate. All kernels will be orthonormal in order to generate independent time series' that can be analyzed individually.

3.4.1 Critical Variables

Before delving into the algorithms employed in this research, it is important to specify certain parameters and their impact on the analysis. As the research is based upon a wavelet analysis, there are certain parameters that are critical in the application of this technique for the implementation described in the following Sections. This Section specifies these terms and their impact on the analyses. It also provides default values for these terms, which should be adjusted based upon the desired application of the methods.

Threshold. This variable sets the minimum level of correlation between wavelet series. Above this value, a specific mathematical function is applied to the wavelet series. Varies according to patient population and data recording condition. Regarding dynamic

sessions, or diseased populations, this value must be decreased (held constant within a specific study) as the level of correlation between cardiac and respiratory patterns decreases during these times. For COPD, this value was set to 0.6, and may need to be lower, depending on the health of the subject. For healthy normals, it can be set as high as 0.85.

Sampling frequency. Beside the obvious Nyquist requirements, sampling frequency becomes critical when determining the appropriate number of scales to be used in the analysis. For HRV, frequencies of interest range between 0.04 and 0.4 Hz. This requires a certain number of scales to implement. When the sampling frequency changes, the number of scales, as well as the scales of interest, must change, as well. Refer to equation (2.3), or Section 2.2.3 for the mathematical basis of this statement. The default was set to 40 HZ for this study. This allowed for a decent frequency resolution in the frequency range of interest using the coiflet wavelet.

Scale. Tied directly to ***sampling frequency***, this variable must change depending on the wavelet chosen and the frequency resolution. The center frequency of the wavelet used will dictate the pseudo-frequencies employed in the analysis. Again, refer to Section 2.2.3 (in particular, equation 2.3) for details. The resulting signal will contain spurious frequency components if too many scales are employed for the WavS analysis. After a certain number of scales, the information contained in the wavelet series is not valid. That is, after a certain level of decomposition, the calculated coefficients are not long enough to contain any valid information. The program is designed to perform signal extension so that the output will not be affected by spectral wrap-around effects inherent in the wavelet series. This signal extension allows the wavelet analysis to run to

whatever level is specified, even though the information contained is not valid. Using extra levels of invalid information in correlations introduces spurious frequency components into the reconstructed signals. The extra levels of information will typically have a correlation > 0.95 and will cause artifact. Use caution when selecting the maximum scale for the analysis. The wavelet used in this study was coif3, so the scales employed were $2^{[6:10]}$, correlating to frequency values of 0.03 to 0.44 Hz.

Wavelet basis. The value controls the efficacy of the separation. This variable will determine whether a discrete wavelet transform is possible in addition to whether the coefficient sets generated form the analysis will be orthonormal. The order of the wavelet basis chosen, if that is an option within the specific wavelet chosen, will determine how *regular* (smooth) the wavelet is. In terms of filtering, this is equivalent to the filter length of a discrete filter. In digital signal processing, this parameter affects the length of the coefficient set generated and also impacts the phase of the output. The wavelet shape should match closely with the signal being analyzed as the values generated are, in essence, measures of how well the signal correlates with the wavelet at a specific frequency. If the shape is very different from the signal being analyzed, the analysis will not be as powerful and may even introduce artifact.

Window size. This value determines the length of the correlation signal at each scale, ***a***. This parameter is significant because when dynamics are varying quickly, it is critical to be able to capture those changes. For each instant in time, the signal correlations between dynamically recorded signals will be changing.

If this parameter is too large, the correlations will not be high enough to change the signal and the reconstruction vector will pass the original signal through as the output.

Similarly, if the window is too small, the frequencies being analyzed will not have time to manifest change. Specifically, the LF range (0.04 – 0.15 Hz) equates to approximately 1 oscillation every 25 seconds at the low end, and 1 oscillation every 6.7 seconds at the high end of the range. The use of window lengths less than the period of the signal being analyzed will not result in an accurate quantification of the frequency content in these signals at those levels.

In addition, the ***sampling frequency*** becomes and issue with the length of the ***window***, since the number of samples contained in the ***window*** is a direct outcome of this value. The length of the signal decreases by two for each successive scale employed in the analysis. The number of samples may not be sufficient for a useful analysis at lower scales if the ***window*** is not sufficiently large.

Decimation level. This value sets the frequency resolution for the signal being analyzed. When this number is adjusted, it changes the ***sampling frequency***, which in turn requires that the maximum ***scale*** be adjusted. The reason for this variable being used in the study is that by increasing the decimation level, you decrease the time it takes for the analysis in two ways. First, the length of the signal is reduced so there are fewer calculations to be performed, resulting in a decreased processing consumption. The next important aspect is that it creates a lower Nyquist frequency, which is defined in Matlab as half of the sampling frequency, whether or not this is the case. Again, it is important to be WARY of over-decimating the signal and lowering the ***sampling frequency*** too much. The significance of a lowered Nyquist frequency is that the total number of ***scales*** required to attain the autonomic frequencies of interest can be reduced. However, this also means that the resolution will not be as good and potentially means that the high and

low frequency autonomic regions will overlap. The default level is set to 5, so F_s equates to 200 (the original re-sampled rate of the IIBI) divided by 5 (the decimation level), or 40 Hz.

3.4.2 Wavelet Entropy

Wavelet analyses are being used increasingly for biomedical applications, among other adaptive time-frequency methods of analysis [80, 81, 82, 83, 84, 85]. A recent international conference of the IEEE EMBS showcased over 45 papers using wavelets in the anlaysis and classification of biological signals. Of rising interest in various signal processing arenas is the non-linear assessment of the coefficient time series generated by this analysis. Wavelet entropy in specific bands has been used in both classical and quantum mechanics, in communications and, more recently, in biological applications [86, 87,88, 89].

In this research, the wavelet transform is used to decompose the biological signals into sets of independent, orthogonal time series. The wavelet entropy program was written using the wavelet toolbox in Matlab v6.5, employing the continuous wavelet transform (CWT) of the coif3 mother wavelet. The program generates wavelet time series for all data sets and further calculates the entropy of the calculated data sets in accordance with Shannon entropy principles. Figure 3.4 illustrates the algorithm for the wavelet entropy method, which creates a matrix of time-frequency distributions for each scale. Entropy measures are then calculated based on that matrix, as indicated in (3.1).

$$S_{wt} = -\sum[P_a * \ln(P_a)] \tag{3.1}$$

In this equation, S_{wt} represents the Shannon energy of the wavelet transformed data, P_a represents the probability density of the wavelet coefficients at each scale, a. Another measure of wavelet information used in this research will include the normalized Wavelet energy, Q. The normalized energy is calculated based upon (3.2).

$$Q = S_{wt} / \ln(a) \tag{3.2}$$

A heart rate variability measure of entropy was calculated based upon the knowledge of frequency bands of interest, namely the low frequency (LF, 0.04-0.14 Hz) and high frequency (HF, 0.14-0.4 Hz) bands, in addition to the LF/HF ratio, which is believed to

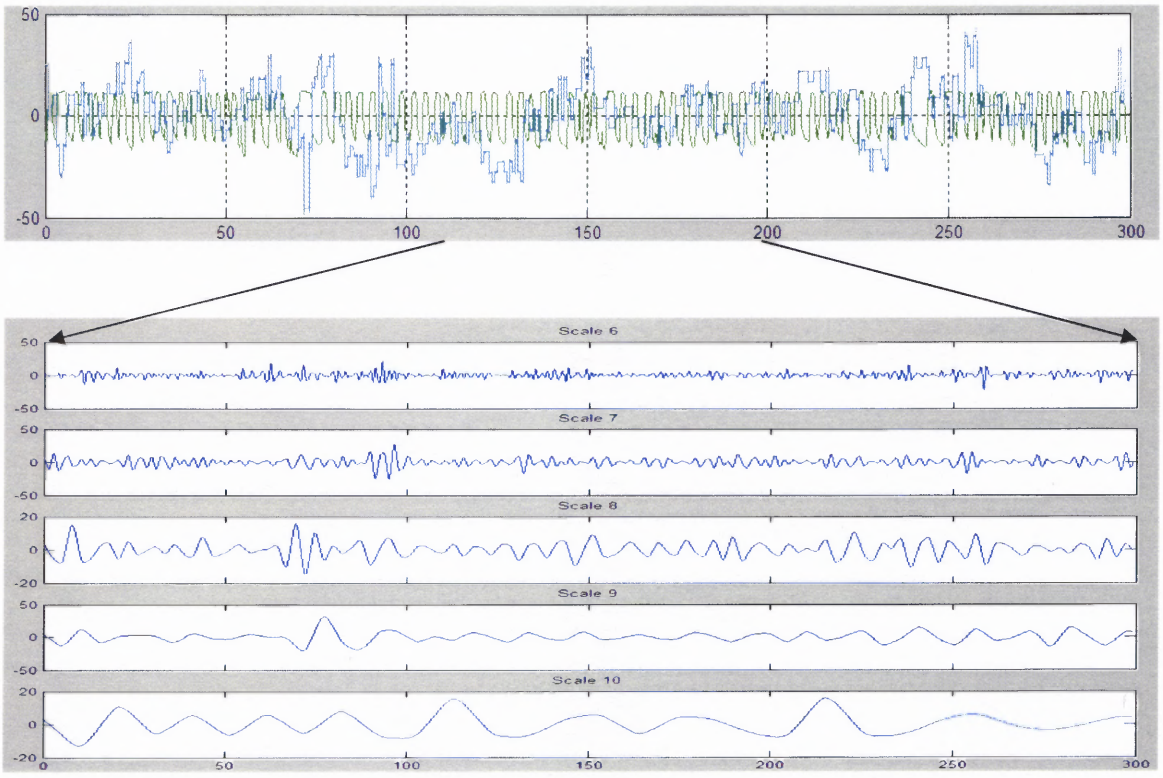

Figure 3.4. Wavelet analysis basis for entropy quantification. The top Figure is the original raw data set, IIBI (blue) and Respiration (green). The bottom Figure is the set of wavelet coefficient series from scales 6:10, the frequencies of interest, over the same course of time.

be indicative of the sympatho-vagal activity. These indices were determined as per (3.3) and (3.4). The use of a different wavelet kernel or sampling frequency (refer to Section 3.3.1) would necessitate modification of (3.3) and (3.4). The frequency bands for this analysis were the low frequency (0.03 – 0.11 Hz) and high frequency (0.11 to 0.44 Hz). The wavelet entropy method provides useful information about neural control of individual systems.

$$S_{wt\_LF} = -\sum_{a=8}^{10} [P_a * \ln(P_a)] \tag{3.3}$$

$$S_{wt\_HF} = -\sum_{a=6}^{8} [P_a * \ln(P_a)] \tag{3.4}$$

3.4.3 K-Means Cluster Analysis

A cluster analysis provides objective classification of varying levels of health of the examined systems. The reason for selection of K-means cluster analysis in lieu of any other clustering technique is that the number population types is known a priori, but the distance between mean values for any given group is unknown. To perform most methods of cluster analysis, it is necessary to have an estimate of the distribution of the statistics of the data set, such as mean value and variance for each group. K-means approaches subject classification without knowledge of statistical parameters, only the number of groups within data sets. The algorithm creates ***k*** groupings of the data, based upon dividing the sample population, ***n***, by the number of groups, ***k***. For example, if there are 100 subjects and it is known that there are 5 groups, the algorithm will seek five mean values around which the data fall, within a certain distance to (or variance from) the

mean value. The method will then seek to minimize within group distance. This method provides a significant, straight forward tool for classification of level of health based upon neural variability. The distance calculation employed in this analysis was the Euclidean least squares distance, which is a basic distance calculation, whereby:

$$d_{Euclid^2} = (x_2 - x_1)^2 + (y_2 - y_1) \tag{3.5}$$

Note that the square root sign is missing for least squares measures in cluster analyses. The centroid is defined by the mean of the distances between all points in the specific cluster. Before the analysis was performed, the entropy matrix was normalized using the z-score normalization technique, as in (3.6):

$$z_{norm} = (x - \bar{x}) ./ \sigma_x \tag{3.5}$$

where z_{norm} is the normalized value, x is the vector being analyzed, $\bar{x}$ is the mean value of the vector x, and σ_x is the standard deviation of the original data set, x.

3.4.4 Wavelet Source Separation

Wavelet Source Separation was performed in several steps, with the variables listed in Section 3.4.1 playing a critical role in the performance of the algorithm. Figure 3.5 is a flow chart overview of the algorithm developed for the analysis. Essentially, this program makes use of the fact that division in the frequency domain is equivalent to a deconvolution in the time domain. Because each of the wavelet time series generated at

each scale is statistically independent, each can be treated as such for further manipulations.

The process began by loading the IIBI and respiration signals into the workspace in Matlab 6.5 (the program has also been validated for Matlab 2006a). The signals are decimated by a factor of 'dec', described in Section 3.4.1. The wavelet analysis is then performed on the two pre-processed signals. The vector representation is presented in (3.6) and (3.7). Figure 3.5 illustrates the actual signals and their correlations. Note that in this Figure, the subject was breathing at a rate of 16 bpm, or a frequency of 0.2667 ($a \approx 8$), the top red and blue image in the wavlet analysis bank Figure. The details matrices are represented as follows in this research:

$$dHRV = \begin{pmatrix} dHRV_{11} & \cdots & dHRV_{1n} \\ \vdots & \ddots & \vdots \\ dHRV_{71} & \cdots & dHRV_{7n} \end{pmatrix} \tag{3.6}$$

$$dRESP = \begin{pmatrix} dRESP_{11} & \cdots & dRESP_{1n} \\ \vdots & \ddots & \vdots \\ dRESP_{71} & \cdots & dRESP_{7n} \end{pmatrix} \tag{3.7}$$

where $dHRV_{11}$ through $dHRV_{1n}$ represent the details vector for scale 1 for the entire length, n, of the analysis, and $dHRV_{71}$ through $dHRV_{7n}$ represent the vactor for scale 7, the lowest frequency band of the analysis.

A range of scales from 1:7 is used in conjunction with the coif3 wavelet for the analysis, which correlates with a frequency range of 0.03 Hz ~ 3.84 Hz. The data were manually phase adjusted to match the first onset of respiration and HRV signal peaks using velocity tracings, due to the offset that results from the generation of the IIBI

signal. Once the data were transformed into the time-scale domain, they were squared and a unity offset was introduced to ensure that neither the respiration nor HRV signals crossed zero, as in Equation 3.9. This ensured that no large, spurious artifact was introduced into the reconstructed series by introducing large numbers into the reconstruction vector as a result of a divide by zero effect. Once the division was performed, the square root of the quotient was obtained and the unity offset was removed.

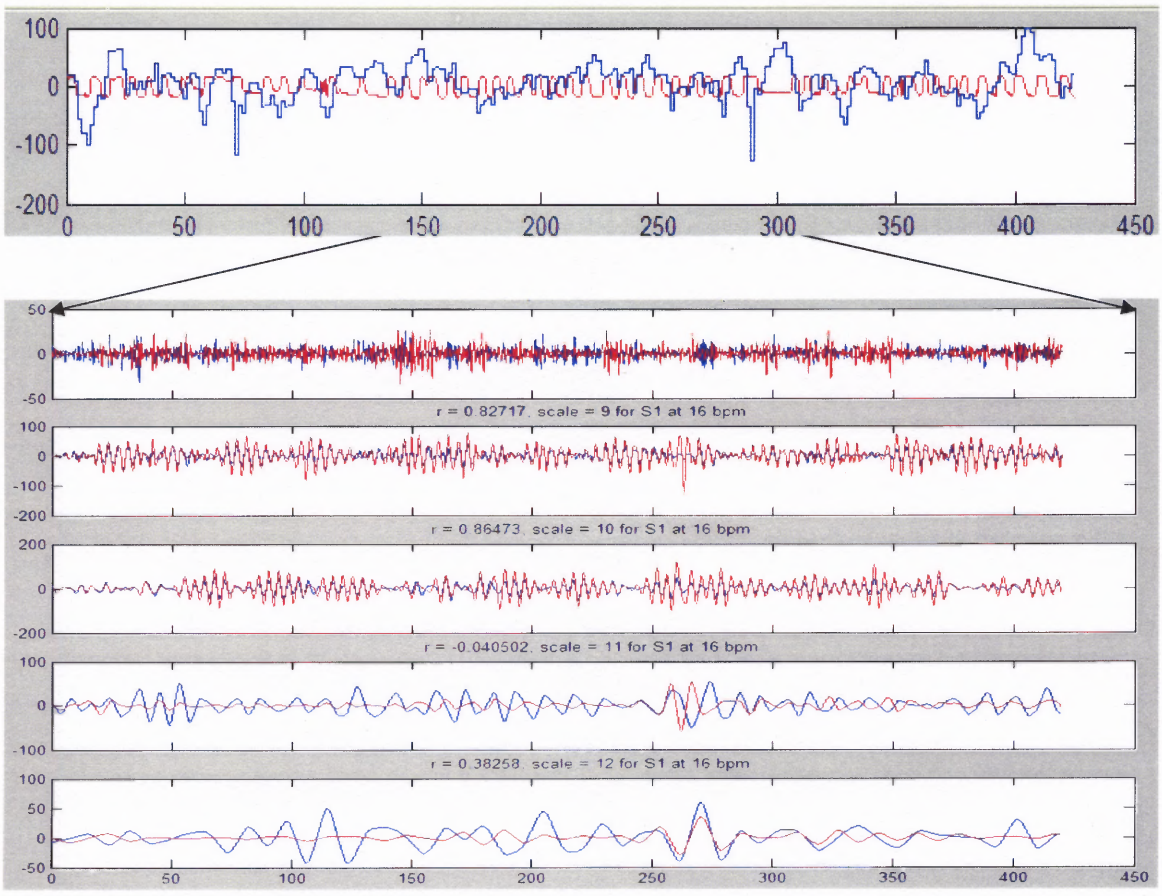

Figure 3.5. Wavelet series correlations of both respiration (red) and HRV (blue) to form basis of WavS analysis. The top Figure is the raw respiration (green) and IIBI (blue) signal. Correlations between the two signals at each scale is displayed.

The data pre-processing step was important for several reasons. First, for optimal wavelet performance, it is necessary to ensure that the signal length is a power of two. There are several mechanisms by which to do this in Matlab. The wavelet toolbox has an extension mechanism called *dwtmode* which extends the signal in specific scales to the appropriate length. There are several methods of extension. For this research, the periodic extension was chosen to ensure that no unnecessary DC component, or abrupt changes were introduced to the signal content.

It is also important to extend the signal to ensure that wavelet domain wrapping does not occur during the analysis. This phenomenon occurs at the edges of the wavelet time series, where information content gets shifted between wavelet subbands, and

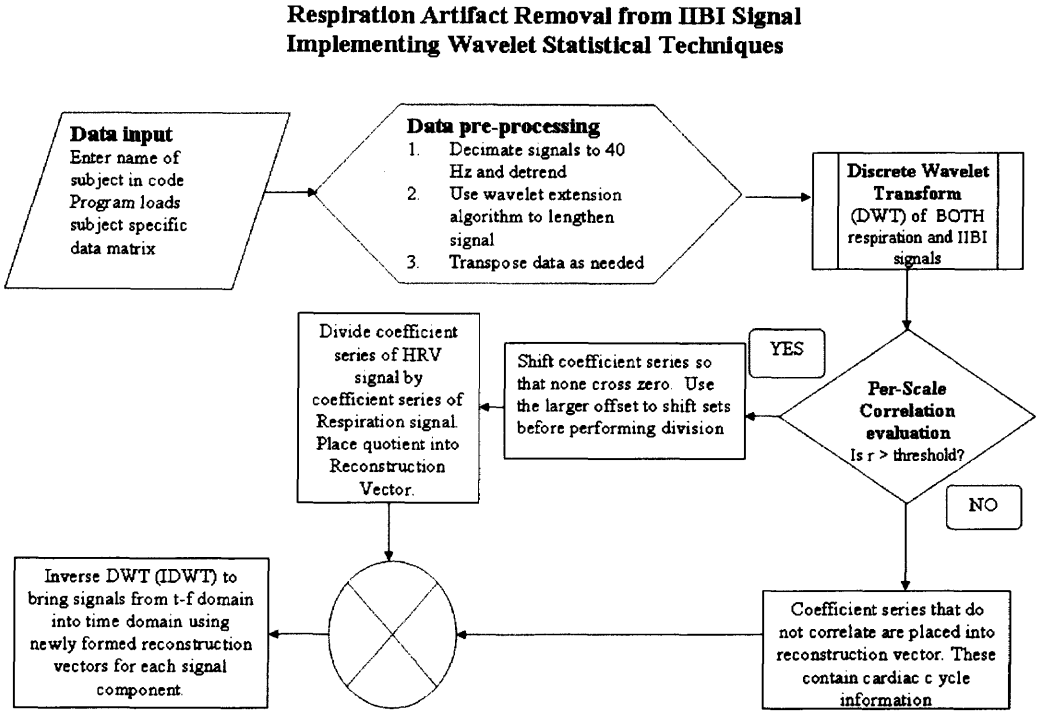

Figure 3.6. Flow chart of WavS algorithm.

introduces a large artifact at these points. This problem can be avoided by using a symmetric (about zero) wavelet and extending the signal when necessary, which will cause the artifact to cancel itself [92]. The coiflet wavelet used in this analysis is symmetric, highly regular, possesses a high number of vanishing moments, and is orthogonal.

Once each signal is decomposed via the DWT into time series of varying resolutions, respiration (***dResp***) and HRV (***dHRV***) signals are correlated at each scale. When a correlation above a specific threshold exists, in this case $r_{HRV,RESP} \geq 0.6 - 0.85$, depending upon subject population, for a given window, *win*, of time as in (3.8) the signals are sent to an array to be divided into each other, as in (3.9). They are first squared and then the HRV is divided by the respiration signal. Division was chosen because the signals are in the frequency domain and division in that domain equates to deconvolution in the time domain. A unity offset is introduced because when ***dHRV*** is divided by ***dResp***, if ***dResp*** is zero (or very close to zero), it creates a spike in the output that is several orders of magnitude greater than the remainder of the data. The offset is removed after the division is performed and before replacing the values into the reconstruction vector, ***dRECONST***, where ***a*** is scale.

$$r_{HRV,RESP} = \frac{\sum_{i=1}^{n}(dHRV_{ai} - \overline{dHRV})(dRESP_{ai} - \overline{dRESP})}{(n-1)\sigma_{HRV}\sigma_{RESP}} \tag{3.8}$$

$$dRECONST_{a(n:n+win)} = \sqrt{(dHRV_{a(n:n+win)}+1)^2./(dRESP_{a(n:n+win)}+1)^2} - 1 \tag{3.9}$$

The reconstruction vector is the vector of wavelet coefficients that will be used to reconstruct the signal. It is a set of numbers that is generated when the discrete wavelet deconstruction is performed. As can be seen in Figure 3.6, if a correlation is below the ***threshold***, it is not manipulated. Rather, the entire wavelet series for that specific scale is passed unaltered directly to the reconstruction vector. If $r \geq$ ***threshold***, the wavelet coefficient series ***dHRV*** and ***dRESP*** for that specific scale is passed to the remainder of the analysis program. $dHRV_a$ and $dRESP_a$ are offset and squared, then the square root of the quotient is offset by -1 and entered into the reconstruction vector ($dRECONST_a$), as in (3.9). Note that this calculation is performed at each scale and for each window, *win*, of time within that scale. Then $dRECONST_a$ is passed to a larger vector, ***dRECONST***, which concatenates the reconstruction vectors at all scales. The variable ***dRECONST*** is then passed to the ***waverec*** function, part of the wavelet toolbox in Matlab, for reconstruction into the time domain. Figure 3.5 displays the flow of decisions for calculations and manipulations performed in the analysis.

CHAPTER 4

RESULTS

4.1 Cardio-Pulmonary Coupling Model

The model results indicated several key findings that were in agreement with the findings from the clinical studies. The first finding is that the WavS method output had an average correlation between the simulated cardiac cycle and extracted cardiac cycle of 0.9975, as in Figure 4.1. The average coherence between the two signals was 0.9988. These values are averaged for the five different model signals that were used in the validation segment of the research. Figure 4.1 illustrates the original cardiac signal used to create the simulated IIBI signal in blue, as well as the signal that was reconstructed as a result of the analysis in red dashes. The correlation value for these specific signals is listed on the Figure. The red signal was extracted from the combined cardiac and respiratory signal, using only the respiration signal as the template for removal.

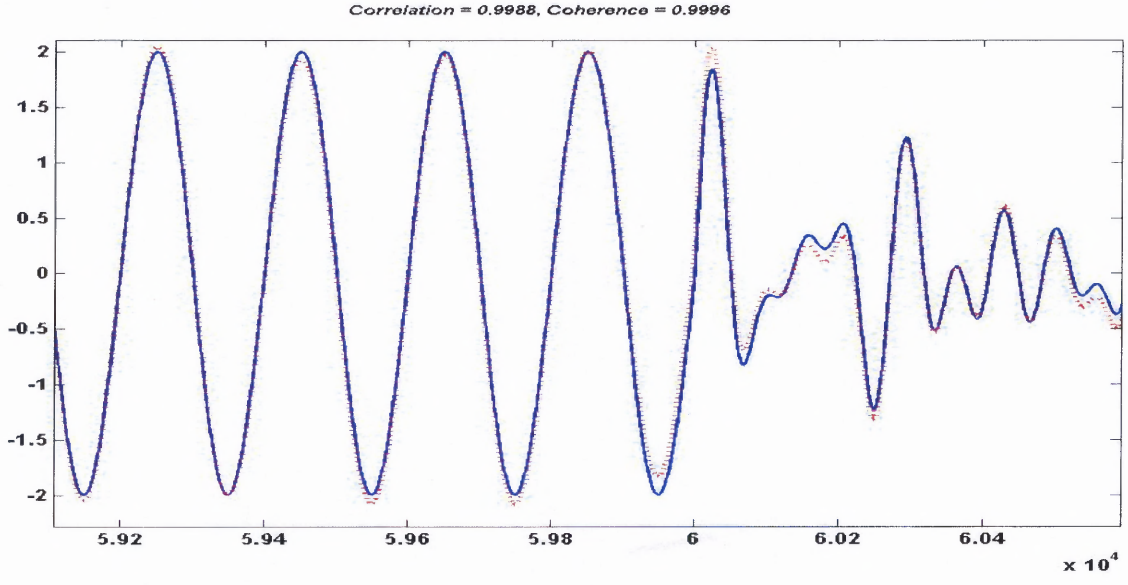

Figure 4.1 Correlation and coherence of input simulated cardiac cycle signal (solid blue) and reconstructed cardiac cycle (red dashed).

The second result of the model data is that although frequency content within a signal can change, this does not necessarily alter the low frequency/high frequency ratio of the signal. Figure 4.2 illustrates the changes in frequency content in each of these sub-bands. It also illustrates that the change in LF/HF ratio is not orders of magnitude, although the spectral power in each component individually change by orders of magnitude. Significant differences were obtained between the LF and HF content of the pre and post processed signal, although the ratio of LF to HF did not yield significantly different values for the data set. The results are presented in Table 4.1. This supports the observation that the LF/HF ratio can be unaffected, although trends may be seen, even when the individual components change by orders of magnitude. The small sample size (n = 6) and large variance suggest that a larger model application may show different values.

Table 4.1 Statistical Changes in Spectral Power between Pre- and Post Model Analysis

Parameter	**HF Spectral Power**		**LF Spectral Power**		**LF/HF Ratio**	
	Original	***Reconst***	***Original***	***Reconst***	***Original***	***Reconst***
Mean	6130	33	0.9521	0.0082	0.0002	0.0005
Variance	0.5	1508	0.0587	6.97e-6	1.59e-9	8.41e-8
P(t < t)	4.2e-10		0.0009		0.0793	

Another significant finding is that when the respiratory wavelet coefficient value is at zero, the output signal approaches infinity, introducing large artifacts. To compensate for this, the program squares $dRESP_a$ and $dHRV_a$, performs the division, takes the square root of the quotient and then reduces the value of the result by 1. On the output, a

spectrum with two distinct peaks at each frequency of the new signal is created when two harmonic sinusoids are combined, as shown in Figure 4.2, below. The top Figure

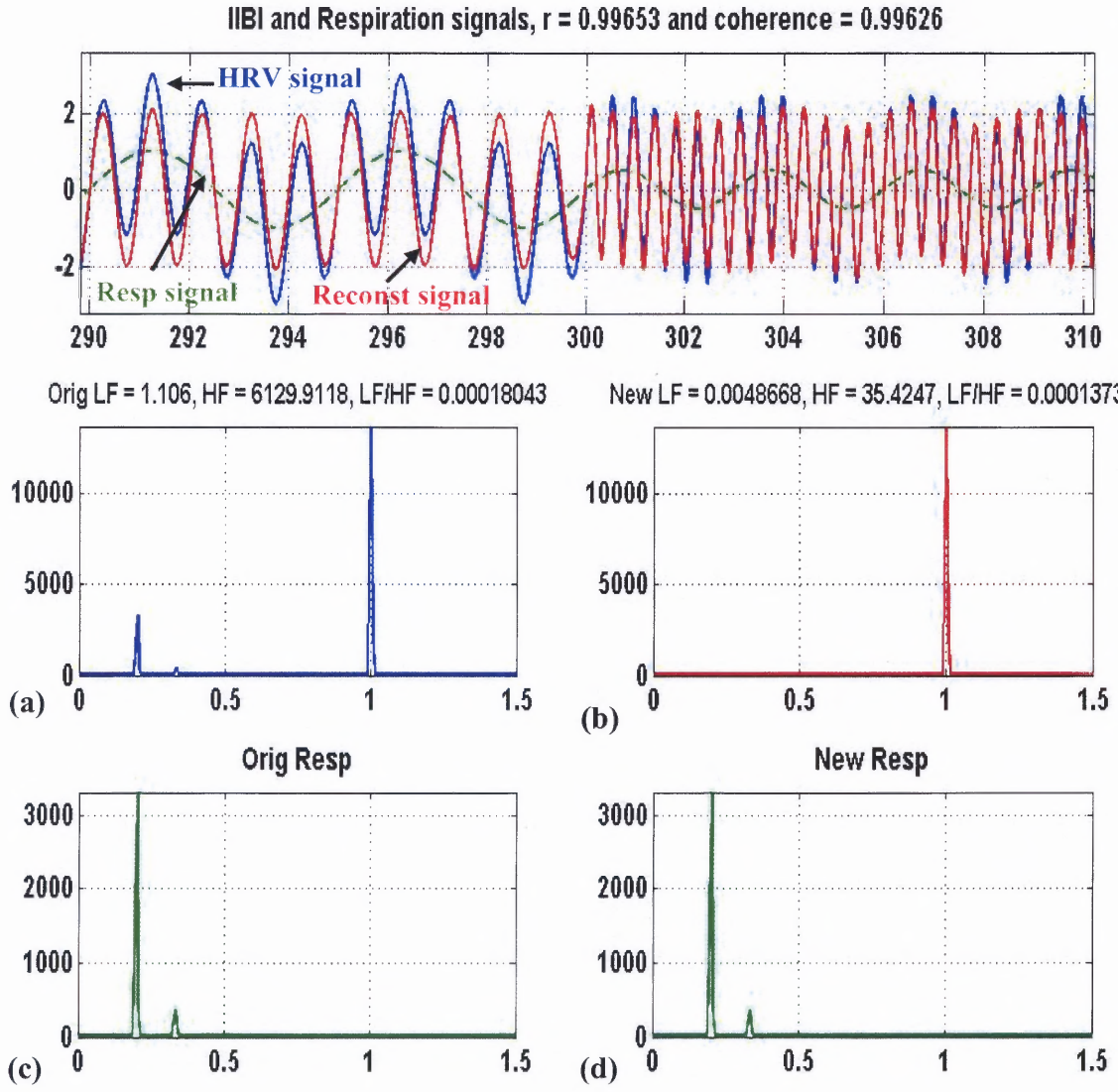

Figure 4.2 WavS output for model data analysis. The top Figure is the sum of the cardiac and respiratory (green) signals to create the simulated IIBI signal (blue). (a) The spectrum of the original HRV signal. (b) The Spectrum of the reconstructed HRV signal. (c) The spectrum of the original respiration signal. (d) The spectrum of the reconstructed respiration.

illustrates the model signals. The dark blue signal is the approximated IIBI signal. The green dashed signal is the simulated respiration signal, and the red is the reconstructed output of the analysis program, simulating the IIBI with the respiration signal removed. The four spectral graphs, color coordinated with the top Figure, plotted below the Figure are discussed clockwise from top left. Listed at the top of images (Figures 4.2a and b) are the values for the LF, HF and LF/HF ratios calculated for those specific spectra. At the top left (Figure 4.2a) is the original spectrum of the simulated IIBI signal. This is the spectrum correlating to the dark blue signal in the top image. Next, the red spectrum in Figure 4.2b is that of the reconstructed signal after the wavelet removal of the respiration from the IIBI. The bottom two green spectra are the respiration spectra, reconstructed 4.2d and original 4.2c. Note that the spectrum of Figure 4.2a has a peak at the respiration frequency of approximately 0.2 Hz, in coordination with the respiration signal in Figure 4.2c. Note also that the respiration peak is missing from the spectrum of the reconstructed signal, shown in Figure 4.2c. The spectral power of the two signals changed dramatically from pre to post processing, as can be seen at the top of Figures 4.2a and 4.2b. The HF and LF values changed, on average, by orders of magnitude.

The local frequency content of the signals became important when assessing the global correlation of the two signals. Because the periods of harmonically related signals would change in a coordinated manner, the wavelet was able to perform a more global correlation analysis of the data. When the signals were not harmonically related, the correlation over large time scales decayed and resulted in a poor signal separation. It is for this reason that the ***window*** becomes important again. This was one of the most significant outcomes of the model analysis. Further, the onset time of the frequency

influenced the correlations. Interestingly, in the model the LF component of respiration is removed from the HRV signal in conjunction with the HF component, causing negligible changes in the LF/HF ratio after removal of the respiration signal. This result is in keeping with the findings of the WavS analysis of the healthy subjects in the COPD study.

4.2 Wavelet Entropy

The wavelet entropy analysis was performed on both the COPD and presbyopic subject populations. Both groups showed trends, but the sample size was quite small, yielding a large variance, and did not yield significant results. To address this, the method of ZSCORE normalization was employed, which normalizes the distribution statistically in an effort to do comparisons between populations with largely different mean values. The results for each study are discussed in this Section. While applying the wavelet entropy method to both sets of heart rate variability data, patterns of control emerged in addition to patterns within the probability distribution and wavelet entropy calculated. It is also of significance that the distribution of entropy differs between control and subject populations.

4.2.1 COPD Wavelet Entropy Results

The wavelet entropy for this patient group contained large variances within populations. However, the zscore normalization algorithm in combination with a PCA component reduction enabled a highly accurate separation of each of the groups, which were control or COPD. For the files taken at rest, the classification rate is 93%, with one control getting classified as a patient. For the files taken during rest-exercise-recovery, the

classification rate is 100%. The confusion plots for the classification scheme are in Tables 4.2a and 4.3b. The high classification rate at rest suggests that there are significant differences in the physiology that are measurable. Differences in populations are evident during exercise with visual inspection. At rest, the differences are more subtle, but still produce significant results.

Table 4.2a Confusion Plot of COPD Study Subjects at Rest Classifcation rate is 93 %

		Actual Class	
		Control	***COPD***
Predicted Class	***Control***	4	0
	COPD	1	10

Table 4.2b Confusion Plot of COPD Study Subjects in Exercise Classifcation rate is 100 %

		Actual Class	
		Control	***COPD***
Predicted Class	***Control***	5	0
	COPD	0	10

Another result of this analysis was the individual components that were found to be major contributors to the separation algorithm. A Principal Components Analysis (PCA) was performed on the matrices for rest and exercise to determine the components that influenced the distribution the most. This type of analysis provides information about which variable provide the largest portion of the variance, and therefore information, within the distribution. Interestingly, during the resting state the variables which contained the most significant amount of information were based upon the entropy values in the low and high frequency ranges, S_{wtHF} and S_{wtLF} , as well as the percentage of

energy contained in scale 3, P_3. During exercise, the percentage of entropy contained in scales 1 and 5, P_1 and P_5, were of significance, as was the percentage of entropy contained within the LF and HF ranges, P_{LF} and P_{HF}.

4.3 Wavelet Source Separation

The WavS method yielded some interesting results for the subject group tested. The main intent of this aspect of the research was to determine if the respiration effect could be removed from the IIBI signal. Further, could the results obtained from analyzing the separated data provide clinical implications for diagnosis? The two subject populations yielded some striking results, but again, the research was a pilot study by design, and the sample sizes were not robust enough to form any statistical determinations. However, interesting trends exist and should be further investigated.

Phase alignment was performed to ensure that the content in the time-frequency distributions were appropriately aligned for the removal of the respiration signal. Because the coefficient series are time-dependant, shifts introduced by the interpolation of the inter-beat-interval signal at the beginning of the signal may not accurately reflect the initial HRV and may result in offsetting the signal by a small amount, depending on where in the cardiac cycle recording of the ECG began. To address this, it is necessary to align the signals initially for the analysis.

The ***window*** applied to the segment ensured that if at points in time during the acquisition the signals lost synchrony, the impact on the correlation remained localized. That is, the program employed a local rather than global correlation. This ensured that if there were parts of the signal that contained large transients, the correlation would only

be affected in that one specific segment of the signal. If this was not implemented, the signal may have a correlation lower than the threshold and the respiratory influence would not be removed, even though the loss of correlation was only in one small part of the signal.

Due to the time-dependant nature of this analysis, even if the frequency activity between the respiration and IIBI signals was highly correlated, the analysis may not have detected a correlation because the onset time of the frequency activity was not the same between the two signals. As can be seen in Figure 4.3, the alignment of the signals in time is quite important to the analysis. Figure 4.3a is the signal analysis result before the phase alignment. Figure 4.3b is the signal analysis output after phase alignment. The top

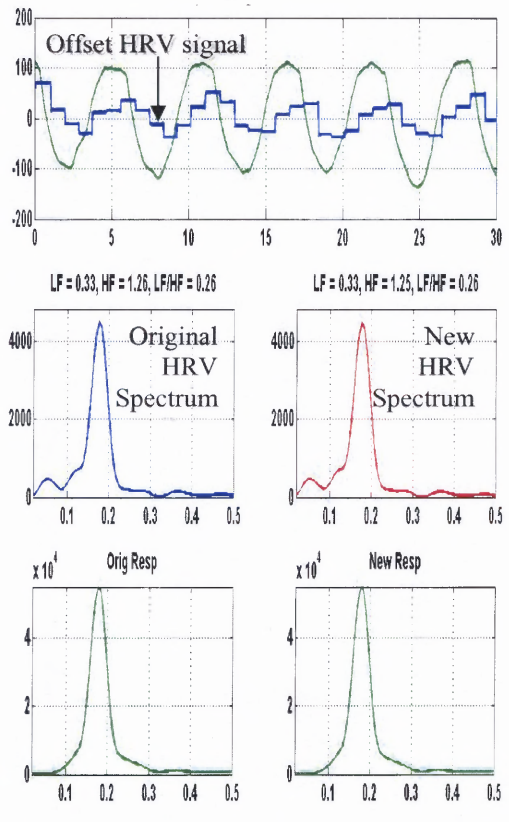

Figure 4.3a Unmatched signals in time.

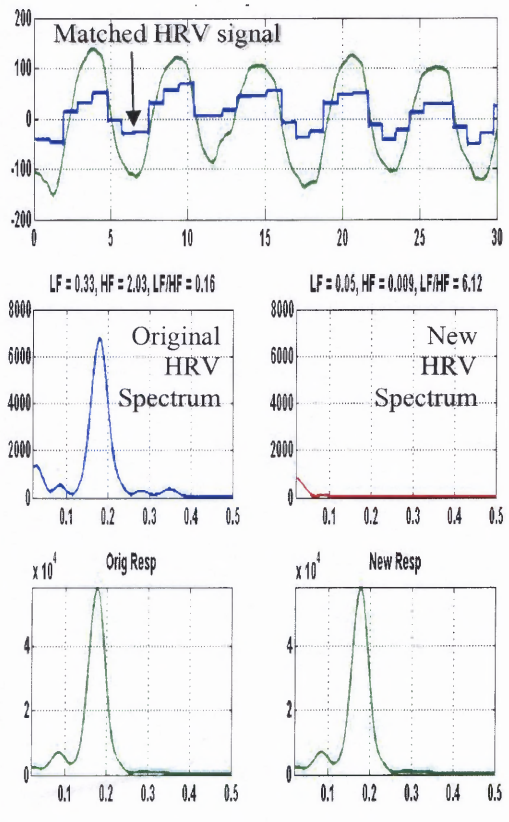

Figure 4.3b Signals matched in time.

image in each Figure illustrates the change in onset time of the signal. Note the relationship between the matched signals at the top of Figure 4.3b in contrast to the offset between the two unmatched signals at the top of Figure 4.3a. There is a significant impact on the separation algorithm when the two signals are not correlated in time. This effect can be seen in the differences in the original and reconstructed HRV spectra of Figures 4.3a, where the respiration is not removed, in contrast to 4.3b, where the respiration peak is removed.

A gain was applied to the amplitude of the respiration and HRV signals to ensure that the maximum amplitude of each was equivalent. As can be seen in Figures 4.4a and 4.4b, the amplitudes of the respiration and HRV signals differed from subject to subject due to the gain on the amplifier. Because a unity ratio between HRV and respiration is desired if the two signals are correlated, the amplitudes of the two signals should be equivalent. The gain value was a constant for the entire signal.

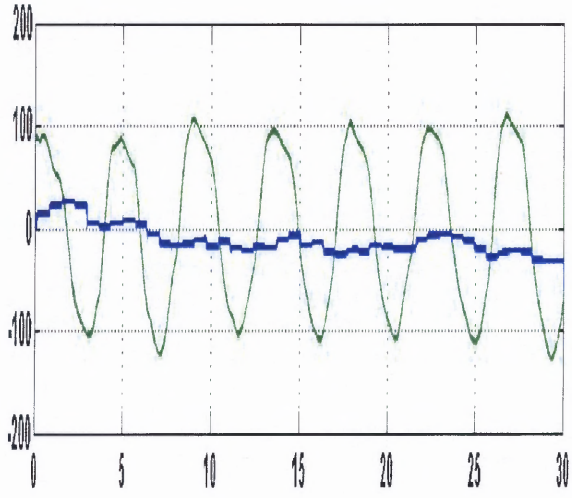

Figure 4.4a Gain of Respiration is much higher than cardiac gain.

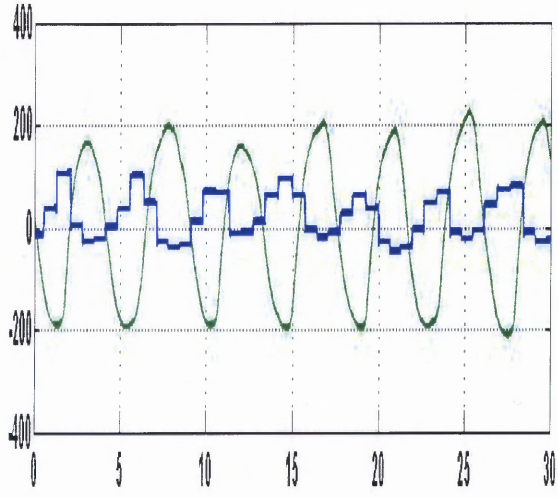

Figure 4.4b Gain of Respiration is more proportional with cardiac gain.

4.3.1 COPD Population

This population was characterized by a significant difference in values of HF and LF between the two groups, particularly after the separation of the respiration influence. After separation, the LF spectral content of the control subjects was decreased by approximately 50%. This was in contrast to the COPD population, where the HF values decreased disproportionately with the LF values. This resulted in the LF/HF ratio increasing for the COPD population and decreasing for the control population after the source separation.

The minimum correlation threshold necessary to separate the signals varied according to subject population. As a result, the lower end of the correlation range was used for both sets of data. The correlation for the COPD subjects often went as low as 0.5 and the healthy subjects were able to employ an average separation threshold of least 0.8. The windowing of the signal made it possible to detect correlations even when the system was subjected to stimuli because the transients that would typically cause the analysis to fail were overcome by the time-varying nature of the frequency analysis.

The LF and HF values changed from pre to post analysis, and the results are tabulated in Tables 4.2 and 4.3. Figures 4.5 and 4.6 are a sample of the COPD study WavS output at rest and exercise, respectively. The values changed significantly from pre to post processing, and there were smaller or larger changes in the signal from pre to post processing during different times within the signals. Note the difference in respiration spectra between rest and exercise for both samples. At rest, the control and COPD spectra are not significantly different. However, during exercise there is a

difference in the distribution of the spectral content of the signal that is particularly evident during the smaller windows of time illustrated in Figures 4.6 c and d.

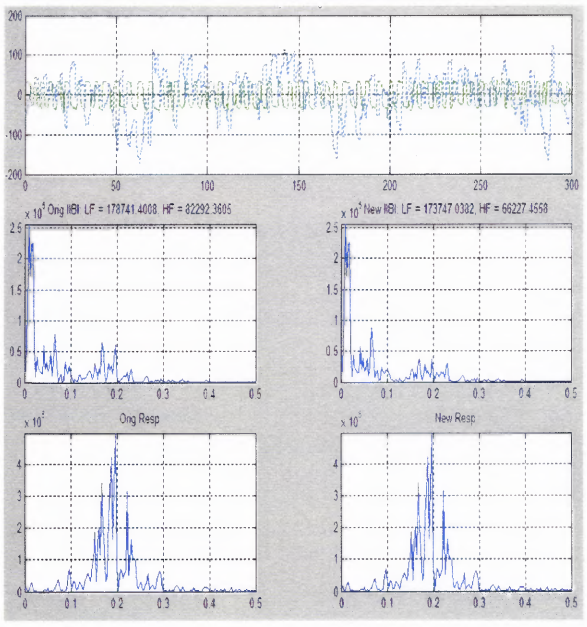

Figure 4.5a Output of WavS for Control subject at rest.

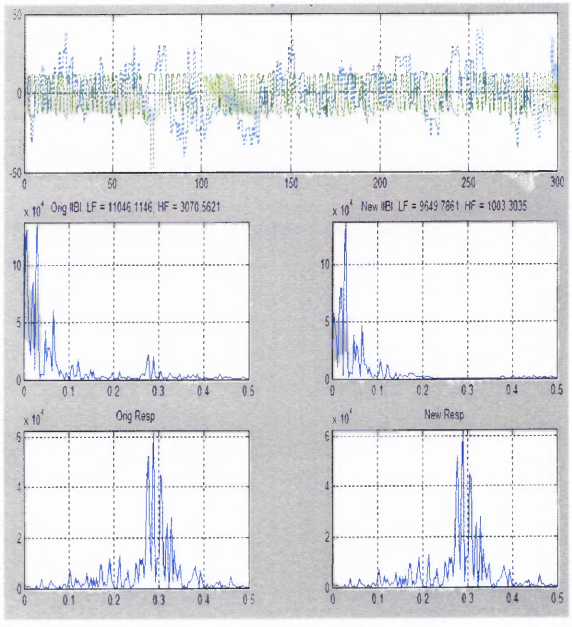

Figure 4.5b Output of WavS for COPD patient at rest.

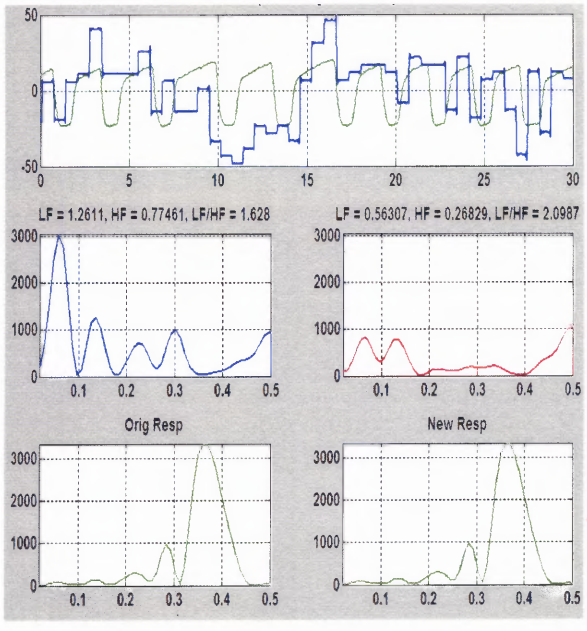

Figure 4.5c Output of WavS for control subject at rest, for a 30 second window of time.

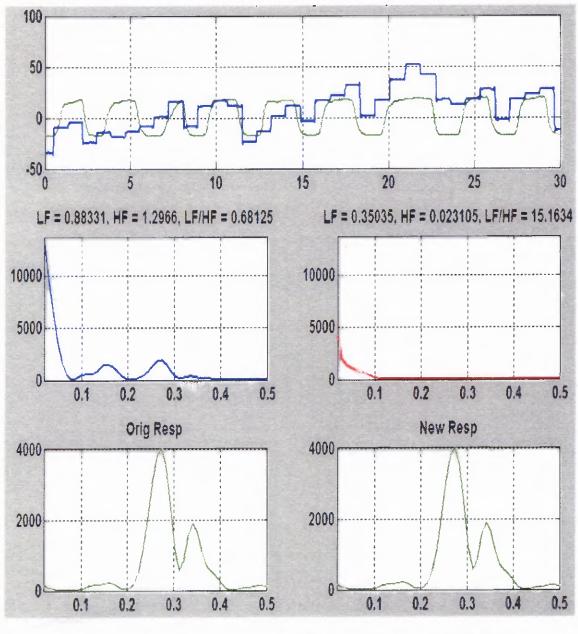

Figure 4.5d Output of WavS for COPD subject at rest, for a 30 second window of time.

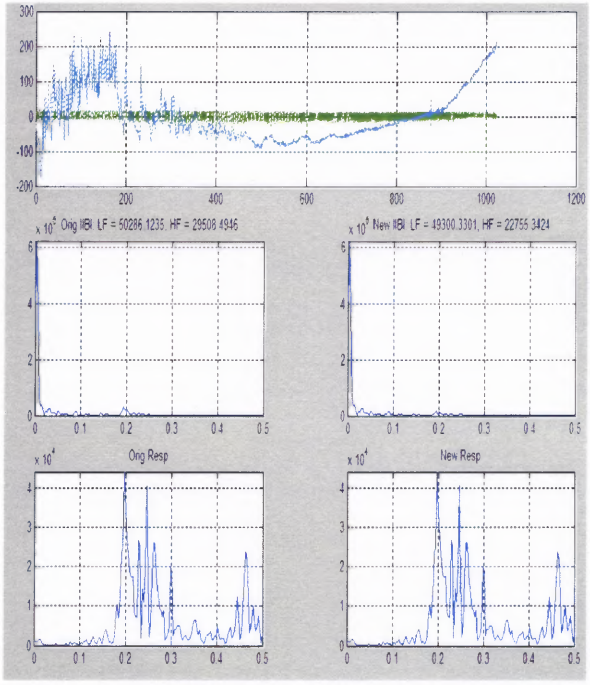

Figure 4.6a Output of WavS for Control subject during exercise.

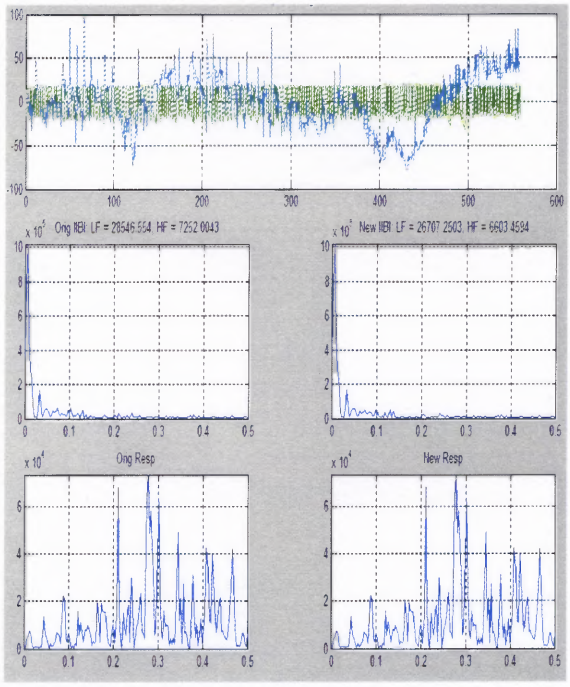

Figure 4.6b Output of WavS for COPD patient during exercise.

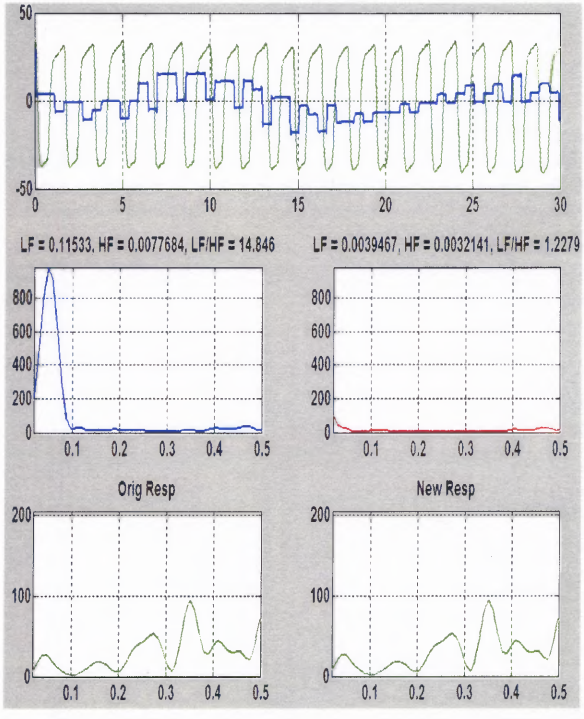

Figure 4.6c Output of WavS for control subject during exercise, for a 30 second window of time.

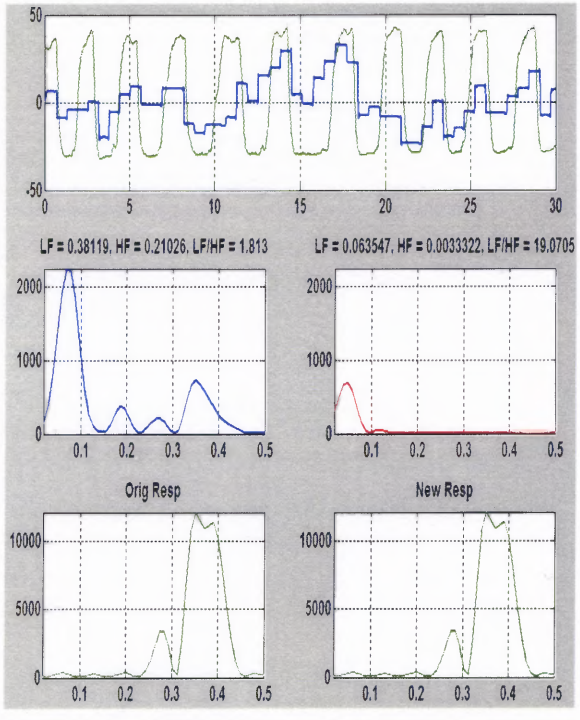

Figure 4.6d Output of WavS for COPD subject during exercise, for a 30 second window of time.

The variance of the data sets decreased by orders of magnitude between pre- and post-processing. More data are needed to perform statistically robust tests on this data set. This trend suggests that smaller changes in activity may be detected in the time series after it has been processed. If the variance is smaller between samples, then the statistical power analysis suggests that changes in the mean values will become more significant for the same number of samples. Table 4.3 lists the mean, variance and t-statistic values for the data. Note the change in the variance in all samples. Table 4.4 is the same statistics, but separated for the individual control and COPD patient populations.

Table 4.3 Statistical Changes of Spectral Power between Overall Pre- and Post-Processing During Exercise

Parameter	**HF Spectral Power**		**LF Spectral Power**		**LF/HF Ratio**	
	Original	*Reconst*	*Original*	*Reconst*	*Original*	*Reconst*
Mean	8.96	5.77	11.44	6.52	1.97	1.32
Variance	106.38	19.13	98.61	18.30	1.29	.20
P(t < t)	0.21		0.08		0.07	

Table 4.4 Statistical Changes of Spectral Power Between Control and COPD Data Pre- and Post- Processing During Exercise

	HF pre		**HF post**		**LF pre**		**LF post**		**LF/HF pre**		**LF/HF post**	
	Norm	*COPD*	*Norm*	*COPD*	*Norm*	*COPD*	*Norm*	*COPD*	*Norm*	*COPD*	*Norm*	*COPD*
Mean	10.23	7.68	6.83	4.71	15.82	7.07	8.87	4.16	2.25	1.68	1.51	1.13
Var	179.3	64.61	21.74	19.88	150.7	28.31	17.09	10.87	1.14	1.66	0.19	0.17
P(t < t)	0.81		0.66		0.37		0.21		0.63		0.42	

The specific HRV indices become more similar after the analysis has been performed, as per the decreased level of variance, although the changes in discrete windows of time are significantly different, as in Figure 4.6. The results may suggest that the respiration may have been driving a significant portion of the frequency activity that has been studied for so long in HRV. This would imply that sinus arrhythmia (SA) at rest and during stress or exercise, may be of the greatest significance in the study of HRV. However, the fact that the LF and HF frequency content is not completely removed with the respiration may indicate that another physiological mechanism is at work in the variability exhibited in the heart rate.

Within the BE (rest) data set, the LF values overall changed from a mean of 194.20 to 67.20, variance changing from 31403.60 to 4702.33, with P(T<=t) of 0.015. HF values overall changed from a mean of 123.57 to 58.21, var from 13063.33 to 4723.96, p value of 0.039. Within the ME (exercise) data set, the LF frequency content changed from a mean value of 11.44 to 6.52, var from 98.61 to 18.30, p = 0.08. HF content changed from a mean value of 8.96 to 5.77, var from 106.38 to 19.13, p value 0.21. The ratio changed from a mean value of 1.97 to 1.32, var of 1.29 to 0.20, p value of 0.07. Recall the small sample size. Larger sample sizes may likely yield significant changes in these areas. Values are tabulated in Tables 4.5 and 4.6.

Table 4.5 LF, HF and LF/HF Ratio Values Before and After the WavS Analysis for the Resting Segment of the COPD Study

	BE					
Subject	*LF pre*	*LF post*	*HF pre*	*HF post*	*Ratio pre*	*Ratio Post*
S1	199.03	58.20	59.69	31.84	3.33	1.83
S2	87.61	55.74	93.99	58.88	0.93	0.95
S3	488.94	168.75	227.15	37.55	2.15	4.49
S4	424.15	174.22	255.72	91.56	1.66	1.90
S5	91.51	6.47	44.39	10.80	2.06	0.60
S6	213.27	59.80	286.24	213.26	0.75	0.28
S7	35.29	7.45	16.96	16.65	2.08	0.45
S9	13.82	6.99	4.41	5.12	3.14	1.36

Table 4.6 LF, HF and LF/HF Ratio Values Before and After the WavS Analysis for the Exercise Segment of the COPD Study

	ME					
Subject	*LF pre*	*LF post*	*HF pre*	*HF post*	*Ratio pre*	*Ratio Post*
s1	11.34	7.78	9.17	5.82	1.24	1.34
s2	15.90	11.86	5.34	7.61	2.98	1.56
s3	12.58	9.58	3.80	5.42	3.31	1.77
s4	2.62	2.83	1.59	1.56	1.65	1.82
s5	3.54	2.24	2.75	2.12	1.29	1.06
s6	32.18	11.19	30.18	12.73	1.07	0.88
s7	11.89	6.00	18.39	10.48	0.65	0.57
s9	1.51	0.64	0.42	0.42	3.57	1.53

4.3.2 Presbyope Population

The presbyope population saw changes in the frequency content between pre and post processing, as well as the COPD group. Tables 4.7, 4.8 and 4.9 display the results from the analysis of this data set. Note that the separation of each group cannot be considered statistically significant due to the small sample size, and must be increased in future studies. Figure 4.7 is the output of one of the normal subjects breathing at 12 [bpm]. Note the correlation between the respiration and IIBI signals, and the corresponding clean

separation of the spectral components. This correlation of respiration and IIBI and the subsequent separation of the respiration from the IIBI was similar for all breathing rates, and for all subjects. The differences existed between the autonomic markers of the groups, as indicated in Tables 4.5, 4.6 and 4.7.

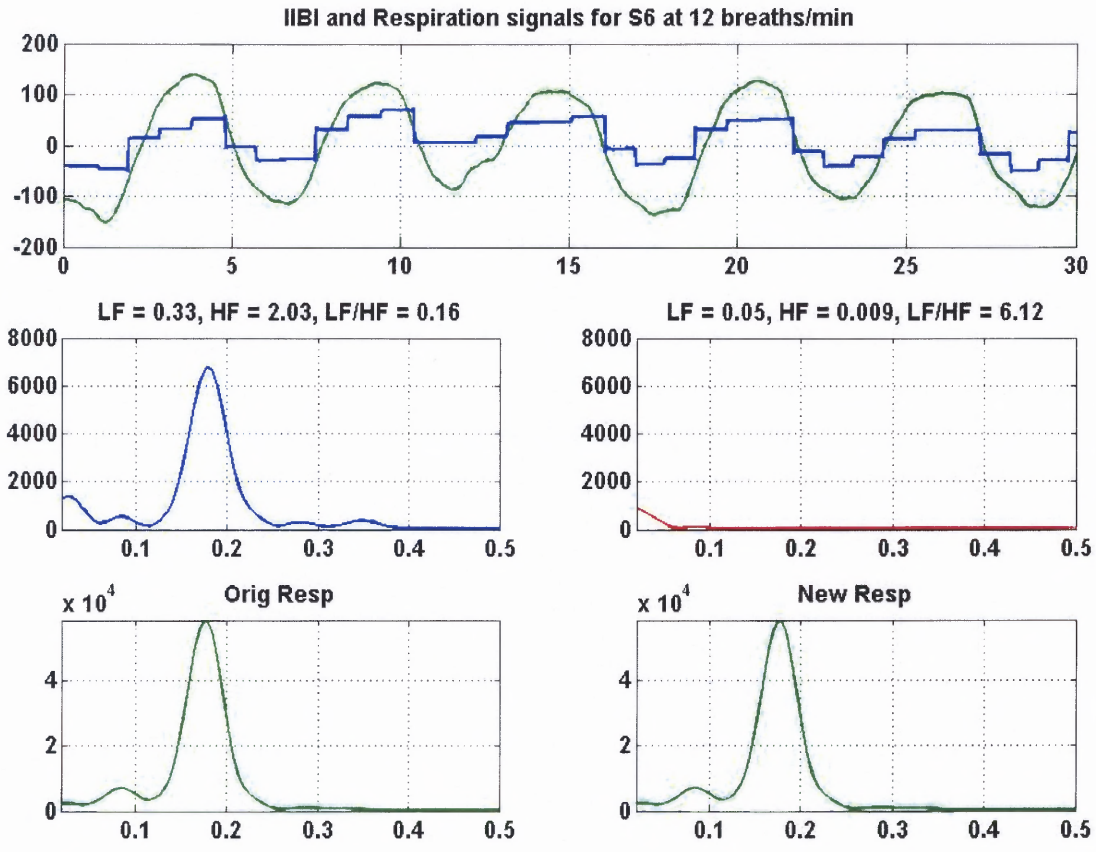

Figure 4.7 Output of the WavS analysis of adaptive presbyope subject breathing at 12 [bpm].

As a clinical validation of the WavS method in addition to the model the LF value changed nearly significantly during controlled breathing at 8 breaths/min [bpm], as listed in Table 4.7, and the HF content changed nearly significantly during controlled breathing at 12 and 16 [bpm], as indicated in Table 4.8.

Table 4.7 Presbyope LF data.

n = 10	8		12		16	
	Pre	Post	Pre	Post	Pre	Post
Mean	486.46	127.00	78.52	50.83	45.15	44.79
Var	197604.8	19778.95	15629.75	7379.62	1498.54	1334.81
P(T≤t)	0.016		0.14		0.89	

Results for 8, 12 and 16 breaths/min.

In terms of standard deviation, differences between the control and presbyope groups were evident not only in the standard deviations, but in the frequency content of the signals. Figure 4.6 illustrates the differences in IIBI signals by group. Figure 4.7 groups the differences in values by age, indicating that the differences are specific to the category of the visual adaptability, not the age, of the subject.

Table 4.8 Presbyope HF Data

n = 10	8		12		16	
	Pre	Post	Pre	Post	Pre	Post
Mean	47.44	44.27	182.38	41.31	117.08	31.66
Var	2028.18	1706.48	34957.91	3055.4	18499.28	1694.28
P(T≤t)	0.50		0.04		0.06	

Results for 8, 12 and 16 breaths/min.

Table 4.9 Presbyope LF/HF Ratio Data

n = 10	8		12		16	
	Pre	Post	Pre	Post	Pre	Post
Mean	19.49	4.53	0.75	1.27	1.26	2.20
Var	833.07	14.31	0.644	0.47	1.47	2.32
P(t>t)	0.15		0.11		0.02	

Results for 8, 12 and 16 breaths/min.

Table 4.10 summarizes the standard deviations statistically. Note that the trends indicate that at higher breathing rates, the controls and presbyopes who like the lenses approach the same behavior, while the presbyopes who are unable to adapt to the use of the lenses deviate from the group.

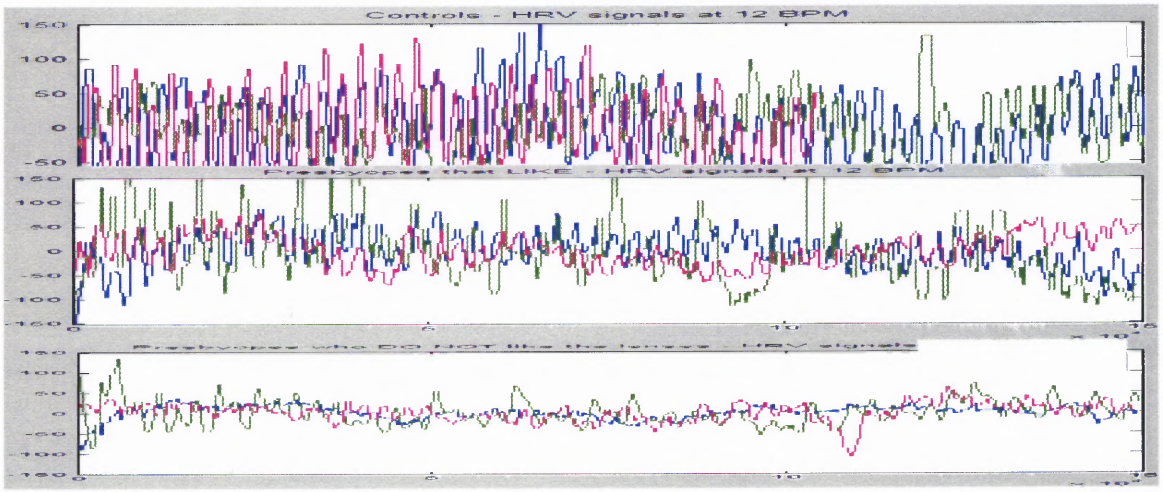

Figure 4.6 Presbyope IIBI data grouped by level of visual adaptability.

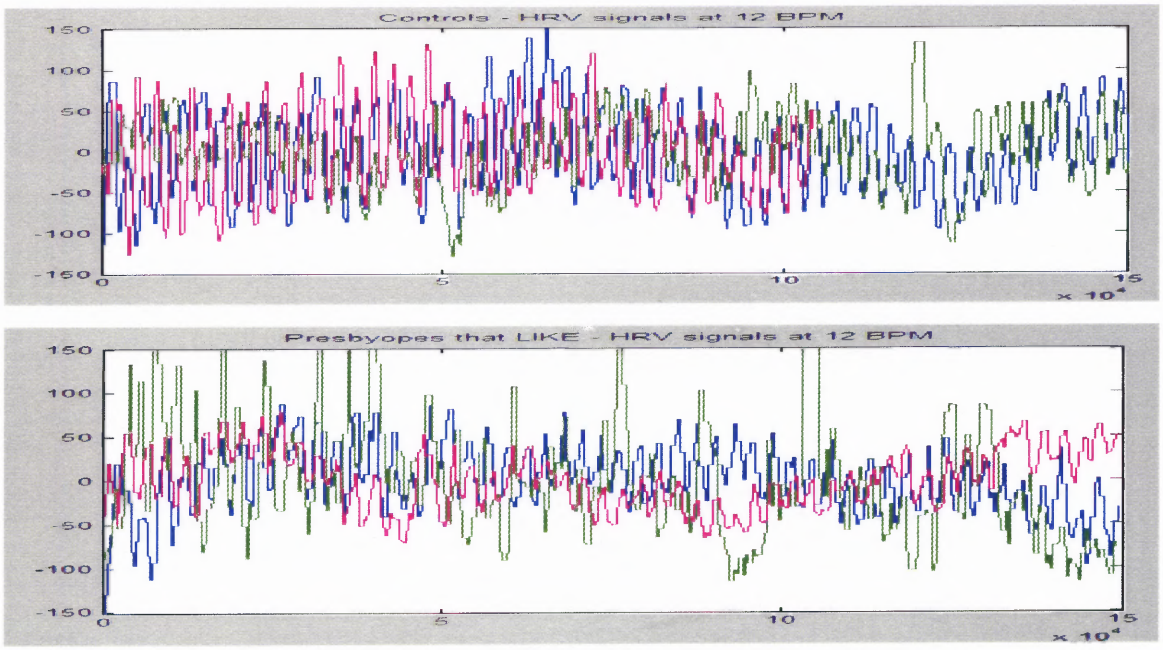

Figure 4.7 Presbyope IIBI data grouped by age.

Table 4.10 Standard Deviations of IIBI Signals of Presbyope Study Populations

Mean Values	*8 breaths/min*	*12 breaths/min*	*16 breaths/min*
Controls	67.29	50.19	47.72
Likes	49.19	47.20	43.73
Dislikes	33.73	23.41	16.90

The results indicate many possibilities for the application of these analyses, with important clinical implications. The next phase of this study must include larger data sets to statistically validate the trends witnessed with all data sets. The two data sets displayed similar trends in terms of the frequency content changes when the respiration removal algorithm was employed. Further, the implications for differences in autonomic function correlating with oculomotor function is significant in that it has not been reported in this way in the literature.

CHAPTER 5

CONCLUSIONS

There were three main hypotheses of this research. First, the research sought to examine changes in central autonomic influence during pulmonary disease. Next, links between central and peripheral autonomic control were investigated. Finally, the research sought to provide tools to enable the clinical quantification of level of disease and classification of subject through these objectives, and to provide new insight into those mechanisms with novel wavelet statistical measures.

5.1 Central Autonomic Influences

The first goal of the research was to provide new insights into the ***central*** autonomic influence over cardio-pulmonary interactions (COPD population). It was hypothesized that different information content, or entropy, existed in specific frequency ranges depending on the subject's level of health. Also, this distribution of entropy varies with subject population and can be classified statistically, enabling computer-aided separation of clinical populations. It was hypothesized that HRV markers would be altered during aging and disease. It was further hypothesized that the Wavelet Source Separation method would alleviate the need to perform controlled measures like paced breathing during clinical assessments of health. This would in turn allow researchers to investigate the dynamics of the system during activity without concern for respiratory effect.

The results indicate that wavelet entropy can be used effectively to characterize central autonomic influences and objectively separate clinical populations with a high level of

accuracy. This is supported by the impressive performance of 93% classification accuracy of COPD study participants at rest and 100% classification accuracy of COPD study participants during exercise using the both the wavelet entropy values and the distribution of that entropy across frequency sub-bands as the input to the cluster analysis.

Changes in COPD and control autonomic markers are, in fact, evident after respiration is removed. LF/HF ratio slightly decreased on average from pre to post reconstruction for controls, increased (sometimes significantly) on average for COPD. In healthy controls, respiration frequency seems to vary, causing large decreases in LF and HF autonomic markers. This results in the LF/HF ratio decreasing significantly after the removal of the respiration artifact from the data. With respiration effect removed from COPD population data, LF dominates autonomic response. Subsequently, this results in a significant increase in LF/HF ratio in COPD due to the concurrent decrease in HF content as a result of respiration removal.

A decrease in variance by orders of magnitude after the removal of the respiration increases the probability that smaller changes can be detected in values. This can have a significant impact on data sets where the intra-subject variability is quite high, confounding the data sets and reducing the likelihood of significant findings in a study. It may also indicate that the physiological response to respiration, in terms of mechanical and chemical alterations, may be a large contributing factor of differences in levels of health rather than direct sympatho-vagal influence.

It is hypothesized that the signal content that remains after the removal of direct pulmonary influence may be indirect indicators of the indirect influence of respiration

through mechanical and chemical pathways on HRV. The link between chemoreceptors and mechanoreceptors in modulation of heart rate cannot be overlooked. Sections 2.1.4 and 2.1.5 provide the physiological basis of this statement. The outcome of this study suggests that the direct influence of respiration is not the only component driving the high frequency or, interestingly, low frequency content of the HRV signal which serve as the markers of cardiac autonomic response. The collective outcome of this segment of the research suggests that the direct influence of respiration may mask other indirect indicators of respiratory influence occurring through chemical and mechanical pathways and new insights into autonomic function in disease may be obtained with these methods.

5.2 Central and Peripheral Autonomic Linkage

The second goal of the research was to provide new insights into the links between *central* and *peripheral* autonomic influence. It was hypothesized that peripheral autonomic influence over the visual system is linked to the central autonomic influence over cardio-pulmonary interactions, and that this link would be evidenced by a decrease in HRV in people with lower levels of oculomotor adaptability.

As a result of the assessment of pilot data obtained from the presbyopic population, there is strong evidence in favor of a correlation between peripheral and central autonomic influences on HRV, as evidenced by oculomotor adaptability. There are several results that support the linkage hypothesis.

The first result is the standard deviation of the data sets across populations. Differences between populations were quantified, not between age group as is the typical assumption, but rather by level of oculomotor adaptability. The standard deviation of the

adaptive presbyope and control data sets displayed similar trends at increasing frequencies of controlled breathing. The non-adaptive presbyopes showed significantly lower values at the higher respiratory frequency of 16 [bpm]. This suggests that controls and adaptive presbyopes have similar sympathetic responses. The question that remains to be answered is in what way the sympathetic response of non-adaptive presbyopes varies from that of the adaptive presbyopes and controls.

Not unlike the COPD data set, the presbyopic population displayed different autonomic markers before and after the respiration was removed from the IIBI signal. As with the COPD population, the frequency content did not completely disappear in the reconstructed IIBI data sets with the effect of respiration removed. This suggests that a mechanism other than pure sinus arrhythmia is driving the variability at all breathing rates. Of significance is that the autonomic markers for each breathing rate were different from each other after the removal of respiration. If they were the same, this would indicate that the primary influence of the variability is the respiration. The fact that they are different supports, once again, the hypothesis that there may be something more than respiration driving HRV. A larger data set must be employed to validate whether the differences in autonomic markers after respiration extraction are significantly different between various controlled breathing rates.

The subjects in the presbyope group displayed some interesting, and in some cases significant, trends in the WavS methods, although the sample size must be larger to accurately assess the results obtained. In addition, it would be of interest to assess entropy levels after the influence of the respiration is removed. This would address questions regarding the influence of respiration in the level of variability in cardiac

oscillations. Based upon the findings of this research, it is hypothesized that the levels of entropy would be greatly reduced after removal of the respiration. However, the variance in the series would also be reduced and would likely yield significant results regarding even small changes in the vagal modulation of HRV.

5.3 Wavelet Statistical Methods

The final goal of this research was to assess the utility of novel Wavelet Statistical Methods with respect to cardio-pulmonary dynamics. This included the development and application of wavelet statistical measures to aid in assessment of autonomic health. This was accomplished in two ways:

a. Development and application of wavelet entropy measure specifically with application to HRV, and combination of this with k-means cluster analysis for separation of level of health of clinical populations. Entropy and density distribution of energy within and between specific bandwidths can be used to separate clinical groups.

b. Specific frequency of respiration and HRV signal components correlate highly in time. This correlation can be used to remove the confounding influence of respiration from central autonomic neural control signals.

This research indicates that there is significant potential for wavelet based statistical measures applied to cardio-pulmonary dynamics to provide information that can be implemented clinically for computer-aided assessments of autonomic health.

The wavelet entropy method possesses potential for classification of level of health because it employs not only the complexity measure of entropy, but also incorporates the distribution of complexity in different bandwidths into the classification. This resulted in a highly accurate classification scheme.

The model illustrates the power of the WavS analysis. As a result of the model analysis, many considerations important in the development of the WavS algorithm, as discussed in Chapter 3, were evaluated for significance in the algorithm. The model served as a validation that the analysis could be performed, with a high level of accuracy, on dynamic signals to separate a known component from a signal.

The first validation of the WavS method came from the model, where the correlation between the input and the reconstructed signals was 0.9988. The method was able to capture changes in frequency content due to changing respiration with a high level of accuracy. The second validation of the WavS method came from the presbyope population in the differences between autonomic markers at different breathing rates. WavS reduced frequency content in ranges concurrent with breathing rate, indicating a robust analysis. The WavS method reduced frequency content in ranges concurrent with breathing rate, indicating a robust analysis. Specifically, at 8 [bpm], which is a content in the LF range, the LF autonomic marker is the only one that showed significant changes after the removal to the respiration signal. Further, at 12 and 16 [bpm], which are evidenced in the HRV spectrum as content in the HF range, the HF autonomic marker is the only one that showed significant, or nearly significant, changes after the removal to the respiration signal. This suggests that the WavS method successfully removes the influence of respiration from clinically obtained data.

The main intent of this aspect of the research was to determine if the respiration effect could be removed from the IIBI signal. The model results indicate that this can be done. However, what clinical implications for diagnosis does this method possess? The two subject populations yielded some striking results, but again, the research was a pilot

study by design, and the sample sizes were not robust enough to form any statistical determinations. However, interesting trends exist and should be further investigated via the use of a larger sample size.

A significant outcome of the model, as well as in both subject populations, is that even with a spread spectrum respiration signal, the analysis was able to separate the respiratory from the cardiac fluctuations. The respiration spectra were illustrated in Chapter 4, including the standard Fourier content measures as numerical validation, and it is clear that the overlap was removed for small and large band peaks in the spectra. Of particular interest is the fact that some frequency activity is still evident at specific frequencies that must be attributed to the cardiac cycle, as the bulk of the respiration spectral activity is removed from the IIBI spectra. Further investigation should be performed in the assessment of changes in the ratio, as the values for each group are now much closer together. The algorithm performed in a normalizing capacity by removing large fluctuations induced by the pulmonary system and revealing underlying cardiac autonomic function. With a smaller variance, smaller changes in mean value can be detected and therefore, a smaller sample size can be used for analysis.

The COPD population was characterized by a significant difference in values of HF and LF between the two groups. The minimum correlation threshold necessary to separate the signals varied according to subject population. As a result, the lower end of the correlation range was used for both sets of data. The correlation for the COPD subjects often went as low as 0.6 and the healthy subjects were able to employ an average separation threshold of least 0.8. Specifically, the larger removal of LF content in the control population than in the COPD population leads to questions of whether

sympathetic stimulation occurs in COPD patients with each breath, as opposed to the LF content being an artifact of the noise. Interestingly, Min et al. found that acute hypoxia in fetal lambs increased low-frequency and LF/HF ratio content, suggesting an increased sympathetic activation compared with baseline [105]. The results of this research indicate that the LF content may represent true sympathetic content in the COPD population, where it may be more driven by sinus arrhythmia in controls.

The WavS method showed some interesting trends in terms of the Presbyope population data. Of significance is the change in each of the cardiac response parameters. Although the samples size was not large enough for statistical significance, there are some noTable results. It is of significance that the separation algorithm employed a correlation value of 0.85 for each subject as it was assumed that they were all ostensibly of the same general level of health. There were different levels of signal separation for each group based upon the level of correlation, which is evident in the varying degree of change in frequency content values from one breathing rate to another. It may also be appropriate to investigate non-linear correlation measures to more fully capture trends over larger windows of time.

In addition, the onset adjustment varied from population to population, suggesting the existence of some intrinsic factor that differs among populations, which resulted in a delay the cardiac loop. The same differences in both onset time and level of correlation were seen for both presbyopic and COPD populations. Although a certain degree of that is due to the change in signals from ECG to IIBI, there is a certain degree that is unaccounted for. Alterations in the cardio-pulmonary tissue may account for the change

in onset time as the system ages or is diseased and should be investigated as a possible source for the variation.

There are points within the signals of both populations during which the respiration and ECG lose coordination, even during steady state. Although the signals typically return to the coordinated state, there are significant points during which control and subject populations have a decrease in the level of correlation of their cardio-pulmonary dynamics. Perhaps the threshold must be adaptive to account for this. Perhaps this loss of coordination, and the extent to which this loss occurs, may yield significant information regarding autonomic control.

It is also evidenced that if the signals are out of phase with each other, the signals are not separated in the WavS algorithm, although the program performs well for respiration signals that are 180 degrees out of phase. This occurs even if there is a significant peak in the HRV spectrum that correlates with the respiration peak in the Fourier domain. When the signals are aligned, the separation accuracy increases. It is possible that a wavelet spectral alignment occurring before the analysis would improve the robustness of this analysis.

CHAPTER 6

FUTURE WORK

This work was primarily a pilot study. The most important consideration for future work is the expansion of the data sets employed in these analyses. The analyses had some significant results with the small sample size. It is hypothesized that with larger data sets, more significant relationships can be established between central and peripheral autonomics, as well as between healthy and diseased populations.

6.1 Cardio-Pulmonary Coupling Model

The model can be expanded for testing the adaptability of the analysis in quantifying activity of signals which contain frequency content that is not harmonic. First the phase matching must be performed. Then, the analysis must be performed in small windows to capture the changes accurately. This may prove a valuable way to assess methods of implementing adaptive windowing of the signal for correlations.

6.2 Wavelet Entropy

The wavelet entropy analysis was performed on both the COPD and presbyopic subject populations. Both groups showed trends, but the sample size was quite small, yielding a large variance, and did not yield significant results.

The subjects in the presbyope group displayed some interesting, and in some cases significant, trends in the WavS methods, although the sample size must be larger to accurately assess the results obtained. In addition, it would be of interest to assess

entropy levels after the influence of the respiration is removed. This would address questions regarding the influence of respiration in the level of variability in cardiac oscillations. It is hypothesized that the levels of entropy would be greatly reduces after removal of the respiration. However, the variance in the series would also be reduced and would likely yield significant results regarding the vagal modulation of HRV.

6.3 Wavelet Source Separation

The main intent of this aspect of the research was to determine if the respiration effect could be removed from the IIBI signal. The model results indicate that this can be done. However, what clinical implications for diagnosis does this method possess? The two subject populations yielded some striking results, but again, the research was a pilot study by design, and the sample sizes were not robust enough to form any statistical determinations. However, interesting trends exist and should be further investigated via the use of a larger sample size.

What was seen in the model, as well as in both subject populations, is that even for spread respiration spectra, the analysis was able to separate the signals fairly well. The respiration spectra were illustrated in Chapter 4, including the standard Fourier content measures as numerical validation, and it is clear that the overlap was removed for small and large band peaks in the spectra. Of particular interest is the fact that some frequency activity is still evident at specific frequencies that must be attributed to the cardiac cycle, as the bulk of the respiration spectral activity is removed from the IIBI spectra. Further investigation should be performed in the assessment of changes in the ratio, as the values for each group are now much closer together. The algorithm

performed in essentially a normalizing capacity. With a smaller variance, smaller changes in mean value can be detected and therefore, a smaller sample size can be used for analysis.

The COPD population was characterized by a significant difference in values of HF and LF between the two groups. The minimum correlation threshold necessary to separate the signals varied according to subject population. As a result, the lower end of the correlation range was used for both sets of data. The correlation for the COPD subjects often went as low as 0.6 and the healthy subjects were able to employ an average separation threshold of least 0.8. Specifically, the larger removal of LF content in the control population than in the COPD population leads to questions of whether sympathetic stimulation occurs in COPD patients with each breath, as opposed to the LF content being an artifact of the noise. Interestingly, Min et al. found that acute hypoxia in fetal lambs increased low-frequency and LF/HF ratio content, suggesting an increased sympathetic activation compared with baseline in hypoxia [105]. The effects of hypercapnia were not discussed in that study. The results of this research indicate that the LF content may represent true sympathetic content in the COPD population, where it may be more driven by sinus arrhythmia in controls.

The WavS method showed some interesting trends in terms of the Presbyope population data. Of significance is the change in each of the cardiac response parameters. Although the samples size was not large enough for statistical significance, there are some notable results. It is of significance that the separation algorithm employed a correlation value of 0.85 for each subject as it was assumed that they were all ostensibly of the same general level of health. There were different levels of signal separation for

each group based upon the level of correlation, which is evident in the varying degree of change in frequency content values from one breathing rate to another. It may also be appropriate to investigate non-linear correlation measures to more fully capture trends over larger windows of time.

In addition, the onset adjustment varied from population to population, suggesting the existence of some intrinsic factor that differs among populations, which resulted in a delay the cardiac loop. The same differences in both onset time and level of correlation were seen for both presbyopic and COPD populations. Although a certain degree of that is due to the change in signals from ECG to IIBI, there is a certain degree that is unaccounted for. Alterations in the cardio-pulmonary tissue may account for the change in onset time as the system ages or is diseased and should be investigated as a possible source for the variation.

There are points within the signals of both populations during which the respiration and ECG lose coordination, even during steady state. Although the signals typically return to the coordinated state, there are significant points during which control and subject populations have a decrease in the level of correlation of their cardio-pulmonary dynamics. Perhaps the threshold must be adaptive to account for this.

It is also evidenced that if the signals are out of phase with each other, the signals are not separated in the WavS algorithm, although the program performs well for respiration signals that are 180 degrees out of phase. This occurs even if there is a significant peak in the HRV spectrum that correlates with the respiration peak in the Fourier domain. When the signals are aligned, the separation accuracy increases. It is

possible that a wavelet spectral alignment occurring before the analysis would improve the robustness of this analysis.

APPENDIX

PRESBYOPE STUDY IRB CONSENT FORM

This appendix contains the Institutional Internal Review Board (IRB) approved consent form that was administered when the Presbyope study was performed at the Laboratory for Visual Processing at NJIT.

NEW JERSEY INSTITUTE OF TECHNOLOGY
323 MARTIN LUTHER KING BLVD.
NEWARK, NJ 07102

CONSENT TO PARTICIPATE IN A RESEARCH STUDY

TITLE OF STUDY:
Autonomic Influences on the Body: Examining the Link Between Cardio-Pulmonary Interactions and Vergence Eye Movements

RESEARCH STUDY:
I,_____, have been asked to participate in a research study under the direction of Dr. Tara Alvarez and Anne Marie Petrock. Other professional persons who work with them as study staff may assist to act for them.

PURPOSE:
The purpose of this study is to understand how the body changes when I look at different targets and breathe in a controlled way by recording my eye movements, ECG and respiration.

DURATION:
My participation in this study will last for 1 to 3 experimental sessions which are approximately 1.5 hours long.

PROCEDURES:
I have been told that, during the course of this study, the following will occur:

An eye movement monitor (which meets the ANSI and OSHA specifications as well as an independent ophthalmologist safety recommendations) will be placed on my head. Three electrodes will be placed on my left and right arms to record my ECG. I will be shown how to place a respiration recording band on my ribcage and I will place that on myself to record my breathing signal. I will be handed a button, which will control the experiment. Once I feel comfortable, I will push the button and follow the target movement and try to pace my breathing as closely as possible to the movement of the lights. This will take a maximum of 5 minutes to complete. At that point, I may rest until I am ready to look at a new target movement.

PARTICIPANTS:
I will be one of about 10 participants to participate in this trial.

EXCLUSIONS:
I will inform the researcher if any of the following apply to me.

- During experiments any stress or fatigue is experienced.
- My eyes feel dry.
- I have had LASIK surgery or any other types of eye surgery.
- I have worked around metal where potential metal files may be within my eyes.
- I have consumed caffeine or another stimulant in the past two hours.
- I am currently taking any medications.
- I am under the age of 18.

RISKS/DISCOMFORTS:
I have been told that the study described above may involve the following risks and/or discomforts.

I may experience fatigue during the experiments and possibly drying of my eyes. If drying of my eyes occurs, I should blink. If I get tired, I can ask for a rest period.

I may experience lightheadedness during this experiment due to control of breathing rate. If this occurs, I should stop and start breathing at a normal rate.

I will not wear my contact or glasses during an experiment. I will be given a lens that matches my prescription if needed.

There also may be risks and discomforts that are not yet known.

I fully recognize that there are risks that I may be exposed to by volunteering in this study which are inherent in participating in any study; I understand that I am not covered by NJIT's insurance policy for any injury or loss I might sustain in the course of participating in the study.

CONFIDENTIALITY:
I understand confidential is not the same as anonymous. Confidential means that my name will not be disclosed if there exists a documented linkage between my identity and my responses as recorded in the research records. Every effort will be made to maintain the confidentiality of my study records. If the findings from the study are published, I will not be identified by name. My identity will remain confidential unless disclosure is required by law.

PAYMENT FOR PARTICIPATION:
I have been told that I will not receive compensation for my participation in this study.

RIGHT TO REFUSE OR WITHDRAW:
I understand that my participation is voluntary and I may refuse to participate, or may discontinue my participation at any time with no adverse consequence. I also understand that the investigator has the right to withdraw me from the study at any time.

INDIVIDUAL TO CONTACT:
If I have any questions about my treatment or research procedures, I understand that I should contact the principal investigator at:

Tara Alvarez, Ph.D.
Assistant Professor
Department of Biomedical Engineering
New Jersey Institute of Technology
University Heights, Newark, NJ 07102
Phone: (973) 596-5272 Fax: (973) 596-5222
Email: tara.l.alvarez@njit.edu

If I have any addition questions about my rights as a research subject, I may contact:

Dawn Hall Apgar, PhD. IRB Chair
New Jersey Institute of Technology
323 Martin Luther King Boulevard
Newark, NJ 07102
(973) 642-7616
dawn.apgar@njit.edu

SIGNATURE OF PARTICIPANT

I have read this entire form, or it has been read to me, and I understand it completely. All of my questions regarding this form or this study have been answered to my complete satisfaction. I agree to participate in this research study.

Subject Name:_____ Signature:_____

Date:_____

SIGNATURE OF READER/TRANSLATOR IF THE PARTICIPANT DOES NOT READ ENGLISH WELL

The person who has signed above. _____, does not read English well, I read English well and am fluent in (name of the language) _____, a language the subject understands well. I have translated for the subject the entire content of this form. To the best of my knowledge, the participant understands the content of this form and has had an opportunity to ask questions regarding the consent form and the study, and these questions have been answered to the complete satisfaction of the participant (his/her parent/legal guardian).

Reader/Translator Name:_____

Signature:_____

Date:_____

SIGNATURE OF INVESTIGATOR OR RESPONSIBLE INDIVIDUAL

To the best of my knowledge, the participant, _____, has understood the entire content of the above consent form, and comprehends the study. The participants and those of his/her parent/legal guardian have been accurately answered to his/her/their complete satisfaction.

Investigator's Name:_____ Signature:_____

Date:_____

REFERENCES

[1] J.M. Lee, C.J. Park, Y. Lee, I. Shin, and K.S. Park. "Characterizing EEG during Mental Activity using Non-linear Measures: the More Concentration, the Higher Correlation Dimension," *Proc. 22nd Ann. EMBS Int. Conf.*, pp. 1326-1328, 2000.

[2] C. Giller and M. Mueller. "Linearity and non-linearity in cerebral hemodynamics," *Med. Eng. & Phys.*, vol. 25, pp. 633-646, 2003.

[3] K.H. Chon, J.K. Kanters, R.J. Cohen and N.-H. Holstein-Rathlou. "Detection of chaotic determinism in time series from randomly forced maps," *Physica D*, vol. 99, pp. 471 – 486, 1997.

[4] P. Van Leeuwen and H. Betterman. "The status of nonlinear dynamics in the analysisof heart rate variability," *Herzschr Elektrophys*, vol. 11, pp. 127-130, 2000.

[5] C.K. Peng, J. Mietus, Y. Liu, et al. "Quantifying Fractal Dynamics of Human Respiration: Age and Gender Effects." *Ann. of Biomedical Engineering*, vol. 30, pp. 683-692, 2002.

[6] A.C.-C. Yang, S.-S. Hseu, H.-W. Yiemn, A.L. Goldberger and C.-K. Peng. "Linguistic Analysis of the Human Heartbeat Using Frequency and Rank Order Statistics," *Physical Review Letters*, vol. 90, no. 10, pp. 108103-1 – 108103-4, 2003.

[7] D. Hoyer, U. Leder, H. Hoyer, B. Pompe, M. Sommer, and U. Zweiner. "Mutual information and phase dependencies: measures of reduced nonlinear cardiorespiratory interactions after myocardial infarction," *Med. Eng. & Phys.*, vol. 24, pp. 33-43, 2002.

[8] S. Havlin, L.A. Amaral, Y. Ashkenazy, et al. "Application of statistical physics to heartbeat diagnosis," *Physica A*, pp. 99-110, 1999.

[9] A.L. Goldberger, V. Bhargava, B. West and A.J. Mandell. "Nonlinear dynamics of the heartbeat: II. Subharmoninc bifurcations of the cardiac interbeat interval in sinus node disease," *Physica D: Nonlinear Phenomena*, vol. 17, no. 2, pp. 207-214, 1985.

[10] P. Guillen, M. Vallverdu, D. Jugo, H. Carrasco and P. Caminal. "Non-linear dynamics in heart rate variability of normal subjects and chagasic patients," *Proc. 22nd EMBS Int. Conf.*, pp. 2414-2415, 2000.

[11] P. Guillen, M. Vallverdu, F. Claria, D. Jugo, H. Carrasco and P. Caminal. "Complexity Analysis of Heart Rate Variability Applied to Chagasic Patients and Normal Subjects," *Comp. in Cardiol.*, vol. 27, pp. 469-472, 2000.

[12] T. Batu, S. Dasgupta, R. Kumar and R. Rubinfeld. "The complexity of approximating the entropy," *Proc. 17th IEEE Ann. Conf. on Computational Complexity*, 2002.

[13] Y.C. Tzeng, P.D. Larsen and D.C. Galletly. "Cardioventilatory coupling in resting human subjects," *Exp. Physiol.*, vol. 88, no. 6, pp. 775-782, 2003.

[14] N. Montano, C. Cogliati, V.J. daSilva, T. Gnecchi-Ruscone and A. Malliani. "Sympathetic rhythms and cardiovascular oscillations," *Autonomic Neuroscience: Basic and Clinical*, vol. 90, pp. 29-34, 2001.

[15] A. Malliani. "Neural regulation of cardiovascular function explored in the frequency domain," *Autonomic Neuroscience: Basic and Clinical*, vol. 90, pp. 1-2, 2001.

[16] A. Malliani. "Heart rate variability: from bench to bedside," *European J. Int. Med.*, vol. 16, pp. 12-20, 2005.

[17] S. Akselrod, J. Arbel, O. Oz, V. Benary and D. David. "Spectral analysis of HR Fluctuations in the Evaluation of Autonomous control During Acute Myocardial Infarctions," *Computers in Cardiiology*, pp. 315-318, 1985.

[18] P.S. Addison. "Wavelet Transforms and the ECG: A review," *Physiol. Meas.*, vol. 26, no. 5, 2005.

[19] A. Malliani, F. Lombarto, M. Pagani and S. Cerutti. "The neural regulation of circulation explored in the frequency domain," *J. Autonomic Nervous System*, vol. 30, supp. 1, pp. S103-S108, 1990.

[20] F. Lombardi, G. Sandrone, S. Pernpruner, et al. "Heart rate variability as an index of sympathovagal interaction after acute myocardial infarction," *Am. J. Cardiol.*, vol. 60, no. 16, pp. 1239-1245, 1987.

[21] E. Pyetan, E. Toledo, O. Zoran and S. Akselrod. "Parametric description of cardiac vagal control," *Autonomic Neuroscience: Basic and Clinical*, vol. 109, pp. 42-52, 2003.

[22] A. Vander, J. Sherman and D. Luciano. *Human Physiology: The Mechanisms of Body Function*. 8th ed. New York: McGraw-Hill, 2001.

[23] L.R. Squire, F. Bloom, S.K. McConnell, J. Roberts, N. Spitzer and M. Zigmond. (eds.) *Fundamental Neuroscience*, 2nd ed., Florida, Academic Press, 2003.

[24] E. Toledo, S. Akselrod, I. Pinhas and D. Aravot. "Does synchronization reflect a true interaction in the cardiorespiratory system?," *Med. Eng. & Phys.*, vol. 24, pp. 45-52, 2002.

[25] P. Grossman, F.H. Wilhelm and M. Spoerle. "Respiratory sinus arrhythmia, cardiac vagal control, and daily activity," *Am. J. Physiol. – Heart*, vol. 287, pp. 728-734, 2004.

[26] J.A. Taylor, C.W. Myers, J.R. Halliwell, H. Seidel and D. Eckberg. "Sympathetic restraint of respiratory sinus arrhythmima: implications for vagal-cardiac tone assessment in humans," *Am. J. Physiol, - Heart Circ. Physiol.*, vol. 280, pp. H2804 - H2814, 2001.

[27] American Lung Association, http://www.lungusa.org/site/pp.asp?c=dvLUK9O0E&b=35020, 10/31/2005.

[28] L.E. Mays, J.D Porter, P.D. Gamlin, and C.A. Tello. "Neural Control of Vergence Eye Movements: Neurons Encoding Vergence Velocity," *J. Neurophysiol.*, vol. 56, pp. 1007-1021, 1986.

[29] L.E. Mays and P.D. Gamlin. "Neuronal Circuitry Controlling the Near Response," *Curr. Opin. Neurobiol.*, vol. 5, pp. 763-768, 1995.

[30] R. Merletti, L. Conte and C. Orzio. "Indices of Muscle Fatigue." *J. Electromyographic Kinesiology,* vol. 1, pp. 20-33, 1991.

[31] S. Mallat. *A Wavelet Tour of Signal Processing*. San Diego: Academic, 1998.

[32] P. Maass, G. Tescheke, W. Willmann, and G. Wollmann. "Detection and Classification of Material Attributes – A Practical Application of Wavelet Analysis." *IEEE Trans. on Signal Processing,* vol. 48, no. 8, pp. 2432-38, 2000.

[33] A. Poularikas, ed. *Transforms and Applications Handbook*. London: CRC Press, January 1996.

[34] E. Serrano and M. Fabio. "Application of Wavelet Transform to Acoustic Emission Signal Processing." *IEEE Trans. on Signal Processing,* vol. 44, no. 5, pp. 1270-75, 2001.

[35] N. Martin, J. Mars, J. Martin, and C. Chorier. "A Capon's Time-Octave Representation Application in Room Acoustics." *IEEE Trans. on Signal Processing,* vol. 43, no. 8, pp. 1842 - 1854, 1995.

[36] L. Shang, G. Herold, and J. Jaeger. "A New Approach to High-Speed Protection for Transmission Line Based on Transient Signal Analysis Using Wavelets." *IEEE Developments in Power System Protection, Conference Publication* 479, pp. 173-76, 2001.

[37] C. Pattichis and M. Pattichis. "Time-Scale Analysis of Motor Unit Action Potentials." *IEEE Trans. on Biomedical Engineering,* vol. 46, no. 11, pp. 1320-29, 1999.

[38] P. Dolan, A. Mannion, and M. Adams. "Fatigue of the Erector Spinae Muscles. A Quantitative Assessment using "frequency banding" of the Surface Electromyography Signal." *Spine* 20 (1995): 149-159.

[39] Mathworks, Incorporated. *Matlab Wavelet Toolkit*. Rev. 2. http://www.mathworks.com/access/helpdesk/help/pdf_doc/wavelet/wavelet_ug.pdf (September 2001)

[40] C. Valens. "A Really Friendly Guide to Wavelets." 1999. http://perso.wanadoo.fr/polyvalens/clemens/wavelets/wavelets.html. (August 2002)

[41] D. Newandee. "Time-frequency investigation of heart rate variability and cardiovascular system modeling of normal and chronic obstructive pulmonary disease (COPD) subjects," *Doctoral Dissertation*, New Jersey Institute of Technology, 2003.

[42] L. Keselbrener and S. Akselrod. "Time-frequency analysis of transient signals – application to cardiovascular control," *Physica A*, vol. 249, pp. 482-490, 1998.

[42] A.M. Reza. "Wavelet Characteristics: What Wavelet Should I Use?," *White Paper*, Spire Lab, UWM, October 19, 1999.

[43] S. Akselrod, Y. Barak, Y. Ben-Dov, L. Keselbrener and A, Baharav. "Estimation of autonomic response based on individually determined time axis," *Autonomic Neuroscience: Basic and Clinical*, vol. 90, pp. 13-23, 2001.

[44] M. Akay and R. Fischer. "Fractal analyses of HRV signals: A comparative study," *Methods of Information in Medicine*, vol. 36, no. 4-5, pp. 271-273, 1997.

[45] D. Clifton, P.S. Addison, M. Styles et al. "Using wavelet transform reassignment techniques for ECG characterization," *Computers in Cardiology*, 2003.

[46] E. Toledo and O. Gurevitz. "Wavelet Analysis of instantaneous heart rate: A study of autonomic control during thrombolysis," *Am. J. Physiol. – Regulatory Integrative and Comparative Physiology*, vol. 284, no. 4, pp. 53-54, 2003.

[47] A.L. Goldberger, L.A. Amaral, L. Glass, J.M. Hausdorff, P.Ch. Ivanov, R.G. Mark, J.E. Mietus, G.B. Moody, C.-K. Peng and H.E. Stanley. PhysioBank, PhysioToolkit, and PhysioNet: Components of a New Research Resource for Complex Physiologic Signals. *Circulation* **101**(23):e215-e220 [Circulation Electronic Pages; http://circ.ahajournals.org/cgi/content/full/101/23/e215]; 2000 (June 13)

[48] C.L. Bolis and J. Licinio, eds. *The Autonomic Nervous System.* Geneva: World Health Organization, 1999.

[49] A. Voss, J. Kurths, H.J. Kleinerm et al. "The application of methods of non-linear dynamics for the improved and predictive recognition of patients threatened by sudden cardiac death," *Cardiovascular Res.*, vol. 31, pp. 419-433, 1996.

[50] N. Wessel, A. Voss, A. Witt and K.J. Osterziel. "24 Hour Heart Rate Variability Analysis Based on New Methods of Non-Linear Dynamics," *Computers in Cardiology*, pp. 693-696, 1995.

[51] F. Claria, M. Vallverdu, P. Martinez, et al. "Autonomic Function Evaluated by Entropy Measures of the Heart Rate Variability," *Computers in Cardiology*, vol. 27, pp. 461-464, 2000.

[52] B. Aysin, L.F. Chaparro, I. Grave and V. Shusterman. "Detection of Transients in Heart Rate Variability Signals Using a Time-Varying Karhunan-Loeve Expansion," *IEEE*, pp. 3586-3588, 2000.

[53] G. Krstacic, M. Martinis, E. Vargovic et al. "Non-Linear dynamics in Patients with Stable Angina Pectoris," *Computers in Cardiology*, vol. 28, pp. 45-48, 2001.

[54] A.M. Kowalski, M.T. Martin, A. Plastino, A. Proto and O.A.. Rosso. "Wavelet Statistical Complexity Analysis of the Classical Limit," Phys. Lett. A, vol. 311, no. 2-3, pp. 180-191, 2003.

[55] A.M. Petrock, S. Reisman and I. Dardik. "Total wavelet entropy analysis of cyclic exercise protocol on heart rate variability," *Proc. IEEE NE Bioengineering Conf.*, pp.91-92, 2004.

[56] M. Costa, A.L. Goldberger and C.-K. Peng. "Multiscale Entropy Analysis of Physiologic Time Series," *Physical Review Letters*, vol. 89, no. 6, pp. 068102-1 - 068102-4, 2002.

[57] M. Costa, A.L. Goldberger and C-K. Peng. "Multiscale entropy analysis of biological signals," *Phys. Rev. E*, vol. 71, pp. 021906-1 - 18, 2005.

[58] F. Claria, M. Vallverdu,M., A. Martinez et al. "Sympatho-Vagal Activity Described by the Complex and Deterministic Behavior of Heart Rate Variability," *Computers in Cardiology*, vol. 28, pp. 473-476, 2001.

[59] N. Wessel, A. Voss, J. Kurths, P. Saparin, A. Witt, H.J. Kleiner And R. Dietz. "Renormalized Entropy: A New Method of Non-Linear Dynamics for the Analysis of Heart Rate Variability," *Computers in Cardiology*, pp. 137-140, 1994.

[60] J.J. Gonzalez, J.J. Cordero, M. Feria and E. Pereda. "Detection and sources of nonlinearity in the variability of cardiac R-R intervals and blood pressure in rats," *Am. J. Physiol. Heart Circ. Physiol.*, vol. 279, pp. H3040-H3046, 2000.

[61] J. Kurths, A. Voss, P. Saparin, A. Witt, H.J. Kleiner and N. Wessel. "Quantitative analysis of heart rate variability," *Chaos*, vol.5, no. 1, pp. 88-94, 1995.

[62] C.-K.Peng, S. Havlin, H.E. Stanley and A.L. Goldberger. "Quantification of scaling exponents and crossover phenomena in nonstationary heartbeat time series," *Chaos*, vol. 5, no. 1, pp. 82-85, 1995.

[63] X.-R. Cao and R-w. Liu. "General Approach to Blind Source Separation," *IEEE Trans. Sig. Proc.*, vol. 44, no. 3, pp. 562-571, 1996.

[64] Y. Yao and G.B. Giannakis. "On Regularity and Identifiability of Blind Source Separation Under Constant-Modulus Constraints," *IEEE Trans. Sig. Proc.*, vol. 53, no. 4, pp. 1272-1281, 2005.

[65] G-j. Chen, J. Liang, and J-x Qian. "A Method of Process Monitoring Based on Blind Source Separation with Denoising Information by Wavelet Transform and its Application to Chemical Process," *Proc. IEEE Int. Conf. on Systems, Man and Cybernetics*, pp. 2724-2729, 2004.

[66] C.J. Ku and T.L. Fine. "Testing for Stochastic Independence: Application to Blind Source Separation," *IEEE Trans. Sig Proc.*, vol. 53, no. 5, pp. 1815-1826, 2005.

[67] J-F. Cardoso. "Blind Signal Separation: Statistical Principles," *Proc. IEEE*, vol. 86, no. 10, pp. 2009-2025, Oct. 1998.

[68] P. Comon. "Independent component analysis: A new concept?," *Signal Process. Special Issue on Higher Order Statistics*, vol.36, pp. 287-314, 1994.

[69] A. Hyvarinen. "Survey on Independent Component Analysis," *Neural Computing Surveys*, vol. 2, pp. 94-128, 1999.

[70] J-F Cardoso. "High-Order Contrasts for Independent Component Analysis," *Neural Computation*, vol. 11, pp. 157-192, 1999.

[71] E.-W. Bai, Q. Li, and Z. Zhang. "Blind Source Separation/Channel Equalization of Nonlinear Channels With Binary Inputs," *IEEE Trans. Sig. Proc.*, vol. 53, no. 7, pp. 2315-2323, 2005.

[72] Y. Li and K. Liu. "Adaptive Blind Source Separation and Equalization for Multiple-Input/Multiple-Output Systems," *IEEE Trans. Inf. Theory*, vol. 44, no. 7, pp. 2864-2876, 1998.

[73] J. Semmlow, W. Yuan, and T. Alvarez. "Short-term adaptive control processes in vergence eye movement," *Current Psychology of Cognintion*, vol. 21, no 4-5, pp. 343-375, 2002.

[74] T. Alvarez, J. Semmlow and C. Pedrono. "Divergence eye movements are dependant upon initial stimulus position," *Vis. Res.*, vol. 45, pp. 1847-1855, 2005.

[75] L. Shang, Z. Hussain, and R. Harris. "Performance of quadratic time-frequency distributions in blind source separation of speech signals," *ISSSTA 2004*, pp. 905-908, 2004.

[76] M. Pensky. "Density deconvolution based on wavelets with bounded supports," *Stat. and Prob. Lett.*, vol. 56, pp. 261 – 269, 2002.

[77] A. Bronstein, M. Bronstein, and M. Zibulevsky. "Quasi Maximum Likelihood MIMO Deconvolution: Super- and Sub-Gaussianity versus Consistency," *IEEE Trans. Sig. Proc.*, vol. 53, no. 7, pp. 2576-2579, 2005.

[78] J. LeCaillec, and R. Garello. "Nonlinear system identification using autoregressive quadratic models," *Sig. Proc.*, vol. 81, pp. 357-379, 2001.

[79] M. Pitzalis, F. Mastropasqua, F. Massari, et al. "Effect of respiratory rate on the relationships between RR interval and systolic blood pressure fluctuations: a frequency-dependent phenomenon," *Cardiovascular Research*, vol.38, pp. 332-339, 1998.

[80] L. Senhadji, G. Carrault, J. Bellanger, and G. Passariello. "Comparing Wavelet Trasnforms for Recognizing Cardiac Patterns." *IEEE Eng. In Med. And Biol.*, pp. 167-173, Mar/Apr 1995.

[81] L. Gamero, M. Risk, J. Sobh, A. Ramirez, and J. Saul. "Heart rate variability analysis using wavelet transform," in *Proc. Computers in Cardiology*, pp. 177–180, 1996.

[82] U. Wiklund, M. Akay, and U. Niklasson. "Short-term analysis of heart-rate variability by adapted wavelet transforms," *IEEE Eng. Med.Biol. Mag.*, vol. 16, no. 5, pp. 113–118, 1997.

[83] U. Wiklund, M. Akay, S. Morrison, and U. Niklasson. Wavelet Decomposition of Cardiovascular Signals for Baroreceptor Function Tests in Pigs. *IEEE Trans. Biomed. Eng.* Vol. 49, no. 7, pp. 651-661, 2002.

[84] V. Pichot, J. Gaspoz, S. Molliex, A. Antoniadis, T. Busso, F. Roche, F. Costes, L. Quintin, J. Lacour and J. Barthelemy. "Wavelet transform to quantify heart rate variability and to assess its instantaneous changes," *J. Appl. Physiol.*, vol. 86, pp. 1081–1091, 1999.

[85] S. DeGauna, A. Lazkano, J. Ruiz, and E. Aramendi. Discrimination between Ventricular Tachycardia and Ventricular Fibrillation Using the Continuous Wavelet Transform. *Comp. in Cardiol.*, vol. 31, pp. 21-24, 2004.

[86] A. Hossen. "A soft decision algorithm for obstructive sleep apnea patient classification based on fast estimation of wavelet entropy of RRI data," *Technology and Health Care*, vol. 13, pp. 151-165, 2005.

[87] O. Rosso, M. Martin, and A. Plastino. "Evidence of self-organization in brain electrical activity using wavelet-based informational tools," *Physica A*, vol. 347, pp. 444-464, 2005.

[88] O. Rosso, W. Hyslop, R. Gerlach, R. Smith, J. Rostas and M. Hunter. "Quantitative EEG analysis of the maturational changes associated with childhood epilepsy," *Physica A*, vol. 356, pp. 184-189, 2005.

[89] I. Provaznik, J. Bardonova, M. Novakova, Z. Vesely and M. Blaha. "Analysis of Optical Recording Stability Using Wavelet Entropy of Action Potentials," *Proc. 26th Ann. Int. Conf. of the IEEE EMBS*, pp. 377-379, 2004.

[90] G. Zouridakis, and D. Iyer. "Comparison between Independent Components Analysis and Wavelet-based denoising of single trial evoked potentials," *Proc. 26th Int. Conf. of IEEE EMBS*, pp. 87-90, 2004.

[91] E. Kandel, J. Schwartz, and T. Jessell. (eds.) *Principles of Neuroscience.* 4th ed. New York: McGraw-Hill, 2000.

[92] Reza, Ali. "Wavelet Characteristics: What wavelet should I use?" *White paper.* Spire Lab, UWM, October 1999.

[93] Blatter, Christian. *Wavelets: A Primer.* Natick: A. K. Peters Limited, 1998.

[94] S. Huang, and C. Hsieh. "Coiflet Wavelet Transform Applied to Inspect Power System Disturbance-Generated Signals." *IEEE Transactions on Aerospace and Electronic Systems*. Vol 38, No. 1, Jan 2002.

[95] R. Khot, R. Lav and S. Panigrahi. "Wavelet transform, Data compression, Denoising, Pattern classification and prediction,' *ASABE/CSBE North Central Intersectional Meeting*, 2006.

[96] I. Turkoglu, A. Arslan and E. Ilkay. "A Wavelet based network for the detection of heart valve diseases." *Expert Systems*. Vol 20, No. 1, 1-7. 2003.

[97] D. Lemire, C. Pharand, J.-C. Rajoanah, B. Dube, and A.-R. LeBlanc. "Wavelet time entropy, T wave morphology and myocardial ischemia." *IEEE Transactions in Biomedical Engineering*, Vol. 47, No. 7, July 2000.

[98] O.A. Rosso, M.T., Martin and A. Plastino. "Brain electrical activity analysis using wavelet-based informational tools (II): Tsallis non-extensivity and complexity measure." *Physica A: Statistical Mechanics and its Applications*. Vol. 320, pp. 497-511, 2003.

[99] O.A. Rosso, et al. "Wavelet entropy: a new tool for analysis of short duration brain electrical signals." *J. Neurosci. Meth.*, Vol 105, No. 1, pp. 65-75, 2001.

[100] J. Yordovana, et al. "Wavelet entropy analysis of event-related potentials indicates modality-independent theta dominance." *J. Neurosci. Meth.*, Vol. 117, No. 1, pp. 99-109, 2002.

[101] O.A. Rosso, S. Blanco, and A. Rabinowicz. "Wavelet analysis of generalized tonic-clonic epileptic seizures." *Signal Processing*, Vol. 83, No. 6, pp. 1275-1289, 2003.

[102] K. Kotani, M. Tachibana, and K. Takamasu. "Investigation of the influence of swallowing, coughing, and vocalization on heart rate variability with respiratory-phase domain analysis." *Proceedings of the Fifth International Workshop on Biosignal Interpretation*, Tokyo, 2005.

[103] M. Yildiz, et al. "Model based and experimental investigation of respiratory effect on the HRV power spectrum." *Physiol. Meas.*, Vol. 27, pp. 973-988. 2006.

[104] T. Nagata, M. Mochizuki, and H. Minamitani. "Assessment of autonomic function and mental condition on cardio-respiratory variability and thermal regulation by using neural networks." *Proceedings of the 20th Annual International conference of the Engineering in Medicine and Biology Society*, pp. 364-366. 1998.

[105] S.-W. Min, H. Ko, and C.-S. Kim. "Power spectral analysis of heart rate variability during acute hypoxia in fetal lambs." *Acta Obstetrica et Gynecologica Scandinavica*, Vol. 81, No. 11, pp. 1001-1005, 2002.

[106] U. Wiklund, U. Niklasson, and P. Bjerle. "Adaptive cancellation of respiratory sinus arrhythmia." *Computers in Cardiology*, pp. 259-262, 1990.

[107] A.M. Bianchi, U. Scholz, , L. Mainardi, P. Orlandini, G. Pozza, and S. Cerutti. "Extraction of respiration influence from heart rate variability signal by means of lattice adaptive filter." *Proceedings of the 16th Annual International Conference of the IEEE Engineering in Medicine and Biology*, pp. 121-122, 1994.

[108] R. Barbieri, et al. "Continuous quantification of respiratory and baroreflex control of heart rate: use of time-variant bivariate spectral analysis." *Computers in Cardiology*, pp. 765-768, 1994

[109] E. Byrne, and S. Porges. "Data-dependent filter characteristics of peak-valley sinus arrhythmia estimation: A cautionary note." *Psychophysiology*, Vol. 30, No. 4, pp. 397-404, 1993.

[110] X.-P. Zhang, and M. Desai. "Nonlinear adaptive noise suppression based on wavelet transform." *Proceedings of the IEEE International conference on Acoustics, Speech and Signal Processing*, pp. 1589-1592, 1998.

[111] S.-P. Song, and P.-W. Que. "Wavelet based noise suppression technique and its application to ultrasonic flaw detection." *Ultrasonics*, Vol. 44, No. 2, pp. 188-193, Feb. 2006.

[112] R. DeMeersman, et al. "Deriving respiration from pulse wave: a new signal-processing technique." *Am. J. Physiol. Heart Circ. Physiol.*, Vol. 270, pp. 1672, 1996.

[113] M. Bartels, S. Jelic, P. Ngai, R. Basner, and R. E. DeMeersman. "High-freqeuncy modulation of heart rate variability during exercise in patients with COPD," *Chest*, Vol. 124, pp. 863-869, 2003.

[114] M. Bartels, J. Gonzalez, W. Kim, and R. E. DeMeersman. "Oxygen supplementation and cardiac-autonomic modulation in COPD." *Chest*, vol. 118, pp. 691-696, 2000.

[115] A. Bellouchrani, and M. Amin. "Blind Source Separation based on time-frequency signal representations," *IEEE Trans. Sig. Proc.*, vol. 46, no. 11, pp. 2888-2897, 1998.

[116] Y. Zhang, and M. Amin. "Blind separation of nonstationary sources based on Spatial Time-Frequency Distributions," *EURASIP J. Appl. Sig. Proc.*, Vol. 2006, pp. 1 – 13, 2006.